Universidad de Valladolid

DOCTORAL PROGRAMME IN PHYSICS

DOCTORAL THESIS:

Free and graphene supported metallic nanoparticles and their interaction with hydrogen

Thesis submitted by:

Alejandra Granja del Río

as part of the requirements for the degree of Doctor in Physics

Supervised by:

Julio Alfonso Alonso Martín
María José López Santodomingo

Valladolid, October 2018

Universidad de Valladolid

PROGRAMA DE DOCTORADO EN FÍSICA

TESIS DOCTORAL:

Nanopartículas metálicas libres y soportadas en grafeno y su interacción con hidrógeno

Presentada por:

Alejandra Granja del Río

para optar al grado de Doctora en Física por la Universidad de Valladolid

Dirigida por:

Julio Alfonso Alonso Martín
María José López Santodomingo

Valladolid, octubre 2018

A mis padres, a mis abuelos y a Manchi.
Gracias por fomentar la curiosidad
por el mundo que nos rodea,
por poner los medios para llegar
a construir todo esto
y por dejarme ser yo.

Abstract

Contamination is one of the most important environmental problems in the present days. Changing from fossil-based energy sources to renewable energy sources is one of the challenges of this century. Hydrogen is a potential fuel for motive power or for stationary power generation. Hydrogen is the most abundant chemical element in the universe (around 75%). Under normal conditions hydrogen is a diatomic gas, H_2, and it is necessary to find an efficient way to store it in a tank to use it in hydrogen fuel-cell powered electric cars. One of the most promising avenues for hydrogen storage is focused on light solid materials, such as nanoporous carbons. They show high hydrogen storage capacities at low temperature ($\sim$77 K), but at room temperature, this capacity drops to values which are below the acceptable threshold. The hydrogen storage capacity of carbon nanoporous materials can be enhanced by doping them with transition metal atoms and nanoparticles, for example with palladium. Therefore, understanding the physical and chemical mechanisms responsible for the Pd contribution to the enhancement of storage capacity is of great importance. Pd atoms and clusters strongly attach to defects on the walls of nanoporous materials. The aim of this thesis is to investigate the mechanisms of interaction and adsorption of hydrogen on Pd-doped nanoporous carbons by means of DFT simulations. Moreover, the spillover mechanism has been proposed to be the explanation for the enhancement of hydrogen storage on nanoporous carbon materials doped with Pd, but this mechanism is not well demonstrated and it is necessary to evaluate it. In particular, this work has focused on the hydrogen adsorption and desorption on Pd_6 clusters anchored on a graphene mono-vacancy in order to investigate the steps of the spillover mechanism. To summarize, the main conclusions after this work are:

i) For low hydrogen content, the dissociative adsorption channel is preferred over the molecular channel.

ii) We have found the saturation limits for free and anchored Pd_6 clusters. More hydrogen can be adsorbed on free Pd clusters than on the supported clusters.

iii) We have discovered that the supporting surface has two main effects on the adsorption of hydrogen on the Pd clusters: a steric effect which does not allow

hydrogen to fully surround the anchored Pd cluster and a chemical effect induced by the vacancy that prevents hydrogen to interact with the Pd atom which saturates the vacancy.

iv) We have investigated the reactivity of the vacancy and the competition between hydrogen and palladium to saturate the defect. We have concluded that: 1) palladium is bonded more strongly than hydrogen to graphene vacancies and 2) hydrogen adsorption mechanisms and energies do not depend on whether the vacancy was decorated on one or two sides with Pd atoms and clusters.

v) There is no evidence of transfer of hydrogen atoms from the nanoparticle onto the supporting carbon surface (spillover mechanism).

Therefore, this thesis contributes to unravel the hydrogen storage mechanisms on palladium-doped nanoporous carbon materials. The effects of the palladium nanoparticles and of the graphitic substrate on the adsorption of hydrogen are clarified.

The research of this doctoral thesis was conducted in the Nanostructures Group at the University of Valladolid.

Resumen

La contaminación medioambiental es uno de los problemas más importantes a los que se enfrenta la humanidad actualmente. Pasar de fuentes de energía basadas en combustibles fósiles a fuentes de energía renovables es uno de los retos a alcanzar en este siglo. El hidrógeno es un combustible con gran potencial para la generación de potencia motriz o de potencia estacionaria. El hidrógeno es el elemente químico más abundante en el universo (sobre un 75%). Bajo condiciones normales es un gas diatómico (H_2) y es necesario encontrar una manera eficiente de almacenarlo en un tanque para usarlo en coches eléctricos basados en la celda de hidrógeno. Una de las vías más prometedoras para el almacenamiento de hidrógeno consiste en usar materiales sólidos ligeros, tales como los carbones nanoporosos. Estos materiales muestran gran capacidad para almacenar hidrógeno a bajas temperaturas ($\sim$77 K), pero a temperatura ambiente, la capacidad de almacenar hidrógeno es más pequeña que el mínimo acordado. Por otro lado, la capacidad de almacenar hidrógeno de los carbones nanoporosos puede ser mejorada al doparlos con átomos y agregados de metales de transición, como por ejemplo, de paladio. Por lo tanto, es de gran importancia comprender los mecanismos físicos y químicos responsables de la contribución del paladio a la mejora de la capacidad de almacenamiento. Los átomos y las nanopartículas de paladio se adhieren fuertemente a los defectos de las paredes de los materiales nanoporosos. El propósito de esta tesis es investigar la interacción y la adsorción de hidrógeno en carbones nanoporosos dopados con paladio empleando simulaciones de DFT. Por otro lado, el mecanismo del "spillover" ha sido propuesto como explicación para la mejora del almacenamiento de hidrógeno en los materiales nanoporosos de carbono dopados con paladio, pero dicho mecanismo no está bien demostrado y es necesario comprobarlo. En particular, este trabajo se ha centrado en la adsorción y desorción de hidrógeno en nanopartículas de seis átomos de paladio (Pd_6) ancladas en una monovacante de grafeno con el fin de investigar las etapas del mecanismo de "spillover". En resumen, las conclusiones más importantes que se obtienen de este trabajo son:

i) Para pequeñas cantidades de hidrógeno, la vía de adsorción preferida es la disociativa sobre la molecular.

ii) Hemos encontrado los límites de saturación por hidrógeno de agregados de

seis átomos de paladio libres y soportados en grafeno. Se puede adsorber más hidrógeno en las nanopartículas libres que en las soportadas.

iii) Hemos descubierto que la superficie tiene dos efectos principales en la adsorción de hidrógeno en los agregados de paladio: un efecto estérico que no permite al agregado de paladio anclado rodearse completamente de hidrógeno y un efecto químico inducido por la vacante que no permite al hidrógeno interactuar con el átomo de paladio que satura la vacante.

iv) También hemos investigado la reactividad de la vacante y la competición entre el hidrógeno y el paladio para saturar el defecto. Podemos concluir que: 1) el paladio se une más fuertemente a la vacante que el hidrógeno y 2) que los mecanismos y las energías de adsorción de hidrógeno no dependen de si la vacante estaba decorada por uno o por los dos lados con átomos y/o agregados de paladio.

v) Finalmente, no hemos encontrado evidencia de que ningún átomo de hidrógeno se transfiera desde la nanopartícula de paladio a la lámina (mecanismo de "spillover").

Por lo tanto, esta tesis trata de descifrar los mecanismos del almacenamiento de hidrógeno en carbones nanoporosos dopados con paladio. También trata de clarificar los efectos de las nanopartículas de paladio y del sustrato grafítico en la adsorción de hidrógeno.

El trabajo de esta tesis doctoral se ha llevado a cabo en el Grupo de Nanoestructuras de la Universidad de Valladolid.

Contents

List of Figures

List of Tables

Acronyms

AC activated carbon. 9
AE all-electron. 44, 46
AM1 Austin model 1. 25
APW Augmented plane waves. 40
ASE Atomic Simulation Environment. 47

B3LYP Becke's 3 parameter exchange-correlation functional. 25, 36–38
B88 Becke 1988. 36, 37
B97 Becke 1997. 37
BJ Becke-Johnson. 37, 38, 90, 102, 109–111
BJM Becke-Johnson modified. 38, 90, 102, 109–111
BO Born-Oppenheimer Approximation. 23

CASPT2 complete active space perturbation theory. 25
CDC carbide-derived carbon. 8, 9
CHG Chai-Head-Gordon or zero. 37, 109–111
CNDO complete neglect of differential overlap. 25

DFT Density Functional Theory. iii, v, 1, 18, 21, 24–27, 30, 33, 36–40, 42, 46, 47, 67, 82, 90, 109–111
DOE Department of Energy. 4, 9, 11, 12

EAM embedded-atom method. 25
EHT extended Hückel theory. 25
EMT effective medium theory. 25

FBZ First Brillouin Zone. 41, 42, 44, 48
FD Fermi-Dirac. 48

GGA Generalized Gradient Approximation. 18, 25, 35, 36, 38, 40, 47, 48
GM General Motors. 2
GTO Gaussian's type orbitals. 40
GW Green's function G and the screened Coulomb interaction W. 25, 40

HF Hartree-Fock. 25, 36
HK Hohenberg-Kohn. 26, 28–30
HMO Hückel molecular orbital. 25
HSE Heyd-Scuseria-Ernzerhof. 36, 37

iPB incomplete pentagonal bipyramid. Sometimes, also referred as ICO structure. 73, 74, 82–84, 86, 102, 104–106

KS Kohn-Sham. 30, 32, 34, 37, 46

LDA Local Density Approximation. 25, 33–36, 40, 47
LYP Lee-Yang-Parr. 36, 37

Meta-GGA Meta Generalized Gradient Approximation. 36
MMP Modified Monkhorst-Pack. 44
MOF metal organic framework. 5, 9
MP Monkhorst-Pack method. 44
MPn Møller Plesset perturbation theory nth order. 25
MX M is meta-GGA functional. X is the last two digits of the year. 37

NC norm-conserving. 45
NEB nudged elastic band. 49, 50, 67, 82

OCT octahedral structure. 62, 64, 65, 67–69, 71, 82–87, 113

PBE Perdew-Burke-Ernzerhof. 35–38, 48, 49, 90, 102, 109–111
PP pseudopotentials. 45
PW plane waves. 39, 40, 44
PW91 Perdew-Wang 1991. 35–37, 48, 49, 90, 109–111

STO Slater's type orbitals. 40

TF Thomas-Fermi model. 26, 27
TFD Thomas-Fermi-Dirac. 27
TPSS Tao-Perdew-Staroverov-Scuseria. 36, 37

USPP Ultrasoft Pseudopotentials. 45

VS98 Voorhis-Scuseria 1998. 37
VWN Vosko-Wilk-Nusair. 37

zerom zero modified. 38, 102, 109–111

Chapter 1

Introduction

If you really want to do something, you will find a way. If you don't, you will find an excuse.

Jim Rohn.

Everything is related to energy. Energy is the exchange "coin" for all processes in Nature. Energy sources and the storage of these sources are of vital interest in an energy based world, as well as the achievement of an *environmentally sustainable* economy. The storage of energy sources can be studied at macroscopic scale or at nanometric scale. Nano-world is a relatively new field and nanomaterials are regarded as promising materials to solve different issues, such as hydrogen storage, by taking advantage of the new properties that these materials provide.

Hydrogen might be the next promising non-polluting fuel to replace gasoline, but it is crucial to find an efficient material to storage it. Nanoporous carbons have been proposed as a suitable material for hydrogen storage. In this work, we study hydrogen storage process in nanoporous carbons using **simulation techniques** based on the Density Functional Theory (DFT).

1.1 Energy sources

In our current way of live, energy is needed for everything. Thus, finding efficient non-polluting energy sources is the challenge of this century. Contamination is one of the most important environmental problems since it seriously affects and destroys our planet and it is very dangerous for human health. The principal origins of environmental emissions are: (i) combustion in the production and transformation of energy, (ii) **transport**, (iii) industry or (iv) farming. About 40% of the total consumed energy is used for transport and the 60% is used to produce electricity.

The world dependence on fossil-fuels is about 81% [1, 2]. Petroleum, coal and natural gas are still the principal energy sources in our planet [1, 3–9]. These energy sources cause an important global contamination, global warming, greenhouse effect and, in the case of petroleum, political problems as well.

Despite efforts to reduce de amount of harmful emissions, the current economy based on non-renewable energy sources is not sustainable and generates an important environmental impact. The rapid increase of population (and thus, the energy request) and the limitation of traditional fossil energy sources have led to the urgent need for clean and renewable energy sources and for clean and ecological vehicle industry. Several solutions have been proposed:

- Fuel-efficient vehicles: they use less fuel to travel the same distance than their less efficient counterparts. When we burn less or more efficiently fuel, fewer emissions are generated.
- Cleaner fuels: they produce less emissions when they are burned. Some fuels such as the ones made from cellulosic biofuels can reduce emissions by 80% compared to gasoline.
- Electric cars and trucks: which use electricity as fuel. The energy is typically stored in rechargeable batteries.
- Hydrogen-based cars: they use hydrogen as fuel for motive power. One of the most important parts of these cars is the hydrogen fuel cell.

Transport burns the majority of the petroleum produced in the world. This creates a considerable amount of air pollution. As a consequence, **hydrogen** is regarded as a promising candidate to replace gasoline, since it is said to be clean, renewable and efficient. And thus, a **hydrogen-based economy** would be a non-polluting long-term solution. However, hybrid-cars, electric cars and fuel-cell cars are still being developed [9, 10].

1.2 Hydrogen-based Economy

Hydrogen-based economy is a proposed system for supplying energy using hydrogen [11]. Hydrogen economy term was explained by John Bockris during a talk he gave in 1970 at General Motors (GM) Technical Centre, in Vienna. Advocates of a hydrogen-based economy defend hydrogen as a potential fuel for motive power (cars, boats), for stationary power generation (supplies the energetic requirements of buildings) and for energy storage media (conversion of the excess electric power generated in hydrogen) [12].

Hydrogen is the most abundant chemical element in the universe (around 75%). Under normal conditions, hydrogen is a diatomic gas, H_2. Hydrogen in gas form is

very rare in the Earth's atmosphere because of its light weight which enables it to escape from gravity. However, hydrogen is the third most abundant element on the Earth's surface since it forms part of chemical compounds, for instance hydrocarbons and water [13, 14].

Hydrogen is not a primary energy source like petroleum or coal, but it is considered an energy vector. This is, hydrogen has to be produced in gas form and then, we can extract the energy stored in its molecules to use it later as electric energy, for example. Its entire energy conversion chain when produced from renewable electricity is environmentally and climatically clean. It also would diminish political problems since is more widely distributed than oil. No nation is excluded as hydrogen producer, trader or user. The biggest challenge is to find the best answers to the three principal issues: hydrogen production, **hydrogen storage** and hydrogen distribution [15].

1.2.1 Hydrogen Production

Hydrogen is considered the "forever fuel" since it can be produced from any primary energy fuel: coal, oil, natural gas, nuclear, *all kind of renewable energy producers*, etc. Hydrogen and electricity are interchangeable via electrolyzer and fuel cell. Electrolyzer produces hydrogen from electricity and hydrogen fuel cell produces electricity from hydrogen. At the present, hydrogen is produced from fossil fuels (steam reforming of natural gas and gasification of coal), from biomass and where the electricity is cheap, through the electrolysis of water.

Obtaining hydrogen from renewable energies is a task for electrochemists, with the goal of not breaking the hydrogen's inherent character of being clean over the entire of its conversion chain. Thus, renewable hydrogen production is the most interesting way to generate hydrogen. Some examples are the gasification of biomass or using photosynthetic living organisms which produce hydrogen, such as some seaweeds. These hydrogen sources are not developed enough for producing hydrogen cheaply and efficiently. However, we can introduce as "renewable" hydrogen producers solar and wind powers. They produce clean electricity which can be used to produce hydrogen through electrolysis. Solar and wind powers usually generate large peaks of electricity that sometimes are lost because electricity requirements are satisfied in that moment and, in general, electricity can not be stored. Thus, instead of loosing that excess electricity, it could be used to produce hydrogen [16–19].

1.2.2 Hydrogen Storage

Energy density, cost, weight and size of on-board storage are important characteristics of fuels and tanks for automotive applications. Fuels that require large, heavy or expensive storage could reduce the space available or make it too expensive, even including cheaper fuels.

Hydrogen has one of the highest energy density values per mass unit (142 MJ/kg) and it is three times more energetic than gasoline (46.4 MJ/kg) [20]. However, since in normal conditions hydrogen is gas, the energy content of hydrogen per unit volume (less than 10 MJ/L) is very small. Moreover, its gaseous form creates storage difficulties. Thus, it is required the development of advanced storage methods that have potential to reach higher energy densities by volume and mass of storage system (container plus hydrogen) [5, 21–24].

Investigating hydrogen storage is the key to make possible the development of a hydrogen-based economy and hydrogen fuel cell technologies. Hydrogen storage for transport has the inconvenient that the space for the tank in a car is limited. Thus, developing a tank which fits in a car and has the same autonomy than oil-based cars is needed. Moreover, for transport applications, the U.S.A. Department of Energy (DOE) has set three main targets for efficient hydrogen storage by 2020 (a) a gravimetric capacity[1] of 4.5% or 0.045 kg(H_2)/kg(system), (b) volumetric density[2] of 0.03 kg(H_2) per litre of storage material and (c) a reversible uptaking and releasing of the gas at ambient conditions [26, 27]. These targets are very demanding and none of the current technologies meets the three requirements.

There are two main ways of storing hydrogen:

- Physical-based: physical-based storage is the most well established hydrogen storage technology. It can be subdivided in:

    1. Compressed gas: hydrogen is compressed from 300 up to 700 bar of pressure. The principal disadvantages are (i) the large tank volume required, (ii) the high cost of compressing the gas (approximately 500 \$/H_2kg) and (iii) to develop a tank which would be able to withstand very high pressures.
    2. Cold[3]/Cryo[4] compressed: cryo-compressed hydrogen storage technologies have the potential to satisfy all on-board hydrogen storage 2020 DOE targets, including energy density. This method is still being investigated due to the high hydrogen densities that can be achieved at reduced temperatures.

- Material-based or solid materials: the storage of hydrogen in solid materials has the potential to become a safe and efficient way to store energy for both, stationary and mobile applications. These materials might be able to store hydrogen at normal conditions of temperature and pressure. Solid materials are classified in three main groups: metal hydride materials, chemical hydrogen

[1] The gravimetric storage capacity of a hydrogen-absorbing material is typically calculated from the ratio of the mass of hydrogen stored within the material to the total weight of the system (hydrogen+container) [25].

[2] Volumetric density is the amount of hydrogen stored (mass) per volume unit of storage material.

storage and *sorbent or physisorption-based materials* such as **carbon-based** and *other large surface area* materials.

The goal is to reach the highest volumetric density possible by using as little material for making the tank as possible. Hydrogen storage implies the reduction of an enormous volume of gas or the increase of mass/volume ratio [26–28]. In order to rise hydrogen density, work must be focused on compressing the gas or on reducing the repulsion interaction of hydrogen with the storage material. Hydrogen storage is the main problem which this thesis is about.

Carbon-based Materials

An efficient material for hydrogen storage must have high volumetric and gravimetric capacities, fast sorption kinetics at room conditions, to be recycled and low cost. Thus, materials with large surface areas and porosities are good candidates for hydrogen storage. Some examples of porous materials are zeolites, metal organic frameworks (MOFs) and **carbon-based materials**.

- Zeolites: are complex microporous aluminosilicates used as commercial sorbents, catalysts and for hydrogen storage [29, 30].
- Metal organic frameworks (MOFs): are made of metal atoms or clusters linked by organic structures. Their special feature is that they are usually porous and used for gas storage, catalysts, sensors or drug storage [31, 32]. A very common example is ZnO structures bridged with benzene rings.
- Carbon-based materials: carbon is one of the most abundant elements in the universe and plays an important role in the biochemical processes in life. They are capable to store high H_2 amounts because of its porosity [28, 33, 34]. Hydrogen also maintains its chemical nature during all the storage process. Hydrogen can be stored in molecular and dissociated (atomic) form. Molecular hydrogen is physisorbed but the adsorbed hydrogen amount it is only significant at cryogenic temperatures. Atomic hydrogen is chemisorbed but it is only liberated at very high temperatures (more than 400°C). The reason is that atomic hydrogen is very reactive and it is attached to the substrate atoms through covalent bonds. Thus, it is required a new bonding mechanism with energies between physisorption and strong covalent chemisorption. Theoretical studies of H adsorption on carbon surfaces will determine if there is any new C-H bonding mechanism possible and, if so, how to achieve it in practice.

[3] This means sub-ambient temperatures but greater than 150 K.
[4] Temperatures about 150 K and lower than this.

1.2.3 Hydrogen Fuel Cell

Hydrogen fuel cell is a device that converts chemical energy (energy stored in molecular bonds) into electrical current to do work. They can be used in industry, **transport** and in living places and houses.

There are several kinds of fuel cells, but they all work in a same general way. They have a cathode, an anode and an electrolyte[5]. Hydrogen molecules enter in the fuel cell at the anode where a catalyst (generally platinum or palladium) oxidizes the hydrogen. The oxidation reaction produced is:

$$2H_2 \rightarrow 4H^+ + 4e^-. \tag{1.1}$$

Electrons go to the cathode through an external circuit establishing an electric current. The protons go to the cathode as well, but through the electrolyte. At the cathode, protons are bound to the electrons and oxygen to produce energy (heat) and water. The reduction reaction at the cathode is:

$$4H^+ + 4e^- + O_2 \rightarrow 2H_2O + \text{Energy (heat)}. \tag{1.2}$$

As long as a fuel cell is supplied with hydrogen and oxygen, it will continue generating electricity see Figure 1.1.

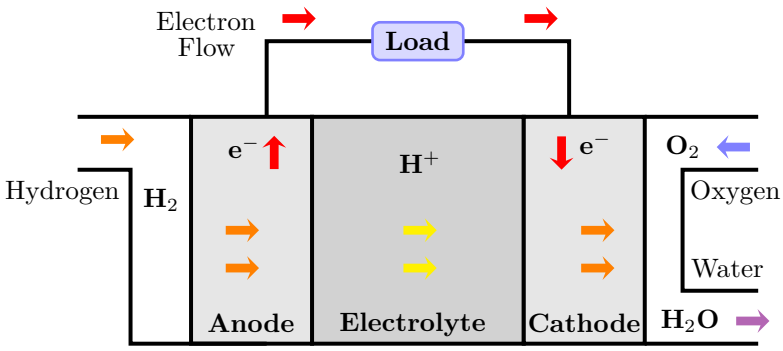

Figure 1.1: Schematic representation of a hydrogen fuel cell.

1.3 Nanomaterials

The "nano-world" is a very popular and relatively new topic in physics. A material is considered in the nanometric scale (*nanomaterial*) when any of its dimensions is the size of nanometers[6]. Macroscopic solid materials usually have constant physical

[5]It is a special substance which protons can pass through it but electrons can not. The electrolyte plays a key role. It must permit only the appropriate ions to pass between the anode and cathode. If free electrons or other substances could travel through the electrolyte, they would disrupt the chemical reaction.

[6]1nm=10^{-9}m.

properties regardless of its size, but at the nano-scale, size-dependent properties are often observed. The properties of nanomaterials strongly depend on the size and number of atoms.

Nanomaterials are applied to different fields in science, for example, they can be applied **to store hydrogen**, in electronics, buildings, pharmaceutical industry, new fuels development, transport, etc. Nanomaterials can be classified as:

- 0D materials or nanoparticles: their three dimensions are in the nano-scale. They are aggregates of atoms made up of a few to tens of millions of atoms with sizes varying from one to a few hundred nanometres [35]. They are generally used to dope other materials, as catalysts, to deliver drugs in biological systems or as storage devices. An example of 0D materials are **metal clusters**.

- 1D materials: such as nanotubes or nanowires. Two of the three dimensions are of nanometers, namely, the diameter is much smaller than its length.

- 2D materials or thin films: are crystalline materials of one atom of thickness. **Graphene** was the first 2D material and plays an important role in this thesis. It is a single layer of graphite. After graphene, several 2D materials have been discovered. Graphyne, silicene or 2D alloys are other examples of 2D materials.

Nanoparticles are halfway between bulk materials and atomic or molecular structures. There are basically two types of size-dependent effects: (i) smoothly scalable ones which are related to the fraction of atoms at the surface, and (ii) quantum effects which show discontinuous behaviour due to completion of shells in systems with delocalized electrons

- Surface-volume ratio: in a periodic bulk system the properties are repeated along the three dimensions. But the symmetry and properties are broken at the edges. If we consider a sphere of radius r, the surface of the sphere is $S_s = 4\pi r^2$ and the volume $V_s = \frac{4}{3}\pi r^3$. Therefore the surface-volume ratio is $ratio = \frac{4\pi r^2}{\frac{4}{3}\pi r^3} = \frac{3}{r}$. This means that the surface-volume ratio increases when the radius decreases. We can conclude that, as the size of a particle decreases, a greater portion of atoms are at the surface compared to those inside. Thus, nanoparticles have greater surface per unit volume than larger particles. Interestingly, some materials which are inert in their bulk form become reactive when produced in their nano-scale form. As nanomaterials present size-dependent features, we can tune in and tailor the properties of a nanomaterial to specific applications [36].

- Quantum-size effect: unusual properties arise from confinement of electron to small regions of space in one, two or three dimensions (1D, 2D or 3D

nanomaterials). The size of the materials is small enough (in 1D, 2D or 3D) to be comparable with the order of the excitation wavelength of the electrons of the material. In the bulk form, the energy bands are continuous. But at the nano-scale the quantization of energy appears, namely, the energy spectrum turns to discrete [37, 38], leading to different properties.

1.4 Hydrogen Storage in Nanoporous Carbons

One important disadvantage of hydrogen is that it is gaseous under ambient conditions, with a very low density (at ambient temperature and atmospheric pressure, 1 kg of the H_2 gas has a volume of 11 m^3). This leads to severe storage difficulties. To overcome these problems metallic hydrides and porous materials have been proposed as potential systems to store hydrogen. Metal hydrides store atomic hydrogen dissolved in the crystal lattice of the metal. But the hydrogen atoms are strongly bound to the metal atoms and thus, the process is not reversible at room temperature and high temperatures are required to release the hydrogen [25, 28, 39].

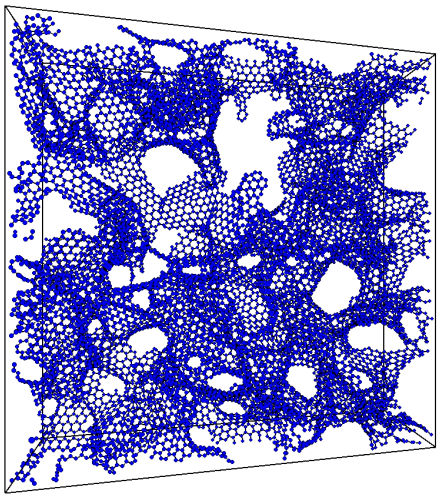

Figure 1.2: Structure of a carbide-derived carbon (CDC) obtained in a molecular dynamics simulation as a nanoporous material example. The cell has a length of 117.45 Å in each direction, but a depth of only 25 Å is shown for clarity. Image retrieved from [40].

Nanoporous-carbon materials are like sponges made of nanometric pores interconnected among them, see Figure 1.2. The pores occupy a very important fraction of the total volume of these materials. Theoretical and experimental studies have shown that the size of the pores in carbon-based materials affects the hydrogen uptake

and storage [33, 41–47]. Nanopores of an average width of 5.6 Å can reach DOE 2020 such as satellites in space, activated carbons (ACs), metal organic frameworks (MOFs) or carbide-derived carbons (CDCs) could be promising materials [48–52]. To reach the volumetric target for 300 K and at least 10 MPa, the average width should be 6 Å. Thus, the size of the pore at given conditions, influences in the hydrogen storage [41].

Nanoporous carbons present a very high specific surface area[7]. The walls of the pores are made of carbon and its width is one atom sized. Thus, **graphene** is a good model to study these walls which are going to interact with hydrogen. Graphene is a two-dimensional structure made of carbon atoms which form a hexagonal lattice [53]. It can be considered as the basic unit to form graphite, fullerenes or carbon nanotubes (see Fig.1.3).

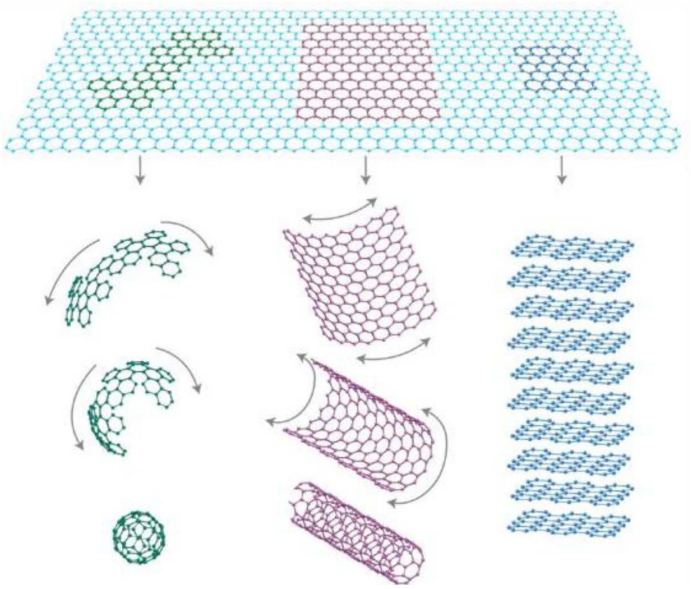

Figure 1.3: Graphene as origin of carbon-based nanomaterials. From a graphene layer we can build fullerenes (green), nanotubes (pink) and graphite (blue). Picture retrieved from [54].

Although carbon materials still do not achieve 2020 DOE targets for hydrogen storage, they are considered promising candidates to store this gas [28, 48–52] since they have important properties, such as high specific surface area, tunable pore structure, low density, stability for large scale production and fast kinetics.

[7]Specific surface area is defined as the total surface area per mass unit of the material.

1.4.1 Hydrogen Adsorption

Adsorption is the process in which atoms or molecules are retained on the surface of a material. In this thesis, the gas employed is hydrogen and can be adsorbed in two different ways [25, 55]:

- Chemisorption: in this process, hydrogen molecules are dissociated to be adsorbed and bonded to the material. Chemisorption implies breaking bonds (hydrogen molecule dissociation) and making new ones with the substrate. This implies high energetic cost since chemisorption of molecular hydrogen presents high barriers around 1.5 eV. Thus, it is necessary to use catalyzers to dissociate the hydrogen molecule in order to make H_2 molecule dissociation favourable. Once the molecule is dissociated, the chemisorption of atomic hydrogen is a favourable process as the adsorption energies are around 0.7 eV and the barriers are about only 0.3 eV [25, 56, 57].

- Physisorption: physisorption occurs in porous solids, in which hydrogen molecules are adsorbed through dispersion forces, namely, through weak interactions of the molecules and the surface. The molecule preserves its identity as the energy is not large enough to break the chemical bond, although the geometry could be distorted. For example, sometimes the H-H distance in the molecule is stretched and the H-H bond weakened but not broken. This is de so-called "activated state". The H-H distance is greater than the molecule distance, 0.754 Å, but smaller than 0.9 Å. Physisorption depends on the nature of the material/surface[8], on the size of the pores and on the pores accessibility[9]. Graphite and carbon nanotubes have been investigated for hydrogen storage during more than 30 years. The H_2 binding energies are in the range 0.035-0.110 eV [58]. Physisorption of molecular hydrogen is very weak and requires therefore low temperatures and high pressures to ensure reasonable storage stability. It has been shown that for these conditions, H_2 can form an uniform compact mono-layer on the graphene sheet with a gravimetric density of 3.3% (doubled if the two sides are considered) [57].

1.5 Hydrogen Storage on Graphene-Based Materials

Hydrogen adsorption in nanoporous materials (activated carbons, graphene, carbon nanotubes...) has been lower than expected to be used for commercial applications [25,

[8]The nature of the material defines the number of interactions between the molecule and the surface (hydrogen and graphene in our case).

[9]The size and the accessibility of the nanocavities define the storage capacity of the material.

59, 60]. The reason is that hydrogen-carbon interactions are too weak. Nevertheless, in the bibliography very large adsorption values have been reported. This is due to these values are obtained under contamination of the materials or by the error in the measurements [61, 62].

Graphene-based materials (see Fig.1.4) shows good potential to be an efficient hydrogen-storage medium [25,63]. Graphene is probably the material with the largest surface to mass ratio. This property is optimal to produce high gravimetric density. Hydrogen can interact with graphene layers by physisorption or chemisorption [63]. Physisorbed hydrogen presents very fast kinetics but is thermodynamically not very stable due to the small binding energies with the graphene layer [64]. The advantages of hydrogen atoms chemisorption rely on much higher stability of the adsorbates which makes the system very suitable for long time storage or transportation. The drawback is related to the chemical nature of the interaction. The chemisorption and the desorption of hydrogen have energetic barriers the order of a few eV. This means that for desorption, temperatures of 650 K need to be reached. It seems that large storage capacity values meeting the DOE targets are only reached under very impractical environmental conditions. However, in contrast to other solid-state systems, graphene offers the possibility of exploring new strategies. For example, sheet deformations, control hydrogen storage with changes of the curvature, corrugated graphene, using graphene oxide, doping with alkali atoms or **catalyzing the hydrogen adsorption by transition metals**. The functionalization of graphene with Pd has been observed to produce chemisorption of H_2 in terms of **spillover mechanism** [25, 64–66].

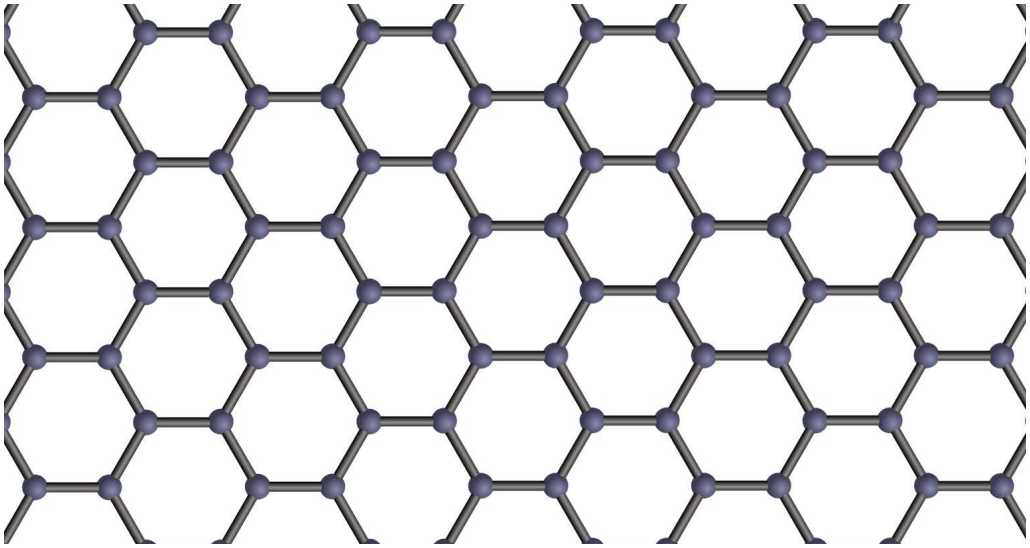

Figure 1.4: The structure of graphene is a two-dimensional hexagonal carbon lattice. Image recovered from [67].

1.6 Enhancement of Hydrogen Storage on Graphene-Based Materials

One approach investigates the chemical decoration of graphene with alkali atoms (Li, Na or K). It was shown that graphene doped with Li adsorbs more hydrogen molecules than clean (without Li) graphene and thus, the gravimetric density is increased [68, 69]. A different approach is based on the Kubas interaction[10] [70–73] to bind hydrogen on transition metal clusters deposited on graphene surface. Some cases for Sc, V or Ti have been studied as well [74, 75].

Experimental results have shown that doping with palladium enhances the hydrogen storage capacity of porous materials [76, 77]. The increase of hydrogen storage was reported and associated with the **spillover mechanism** (see Section below) [78, 79].

Doping is relevant since atomic hydrogen adsorption/desorption on porous carbon materials can be controlled offering new strategies for hydrogen storage [66].

1.6.1 Spillover Mechanism

Experimental and theoretical studies have revealed that hydrogen can be adsorbed onto graphene either by physisorption or by chemisorption [25, 65, 80–82]. But the hydrogen amount does not satisfy the 2020 DOE targets.

Other experimental and theoretical results have shown that doping graphene with transition metal enhances considerably the hydrogen uptake. The mechanism proposed for the enhancement of the storage capacity is the so-called spillover [64, 65, 76, 82–84, 84–88].

Spillover is defined as the transport of a molecule adsorbed on a first surface onto a second surface which does not adsorb the molecule under the same conditions without the first surface [89]. The first surface is typically a metal which works as catalyst and dissociates the hydrogen molecule. The second surface is usually the metal doped support [90]. The steps of the hydrogen spillover mechanism are: (i) firstly, molecular hydrogen is activated and dissociated on a metal catalyst which is in contact with the substrate, (ii) secondly, H atoms migrate from the catalyst particles to the substrate, (iii) finally, hydrogen atoms are spread through the substrate.

The spillover phenomenon has been considered promising for efficient hydrogen storage on nanoporous carbons [86, 91]. The details involved in the different steps

[10] In Kubas interaction, the H-H bond is extended to 0.81-0.82 Å, which is about a 10% extension relative to the H-H bond in free H_2 (0.754 Å). It is suggested that distances smaller than 1.00 Å indicates significant dihydrogen character and separations bigger than 1 Å are better described as dihydride complexes. This class of compounds represent intermediates in metal-catalysed reactions involving hydrogen.

of this process are still not well-known. To exploit spillover for storage, besides the knowledge of each step of the mechanism, there are two important questions: if spillover is reversible at ambient temperature and if the desorption rates at room conditions are fast enough for automotive applications. The important technological and scientific reasons to study hydrogen spillover on Pd clusters supported on carbon surfaces are thus evident.

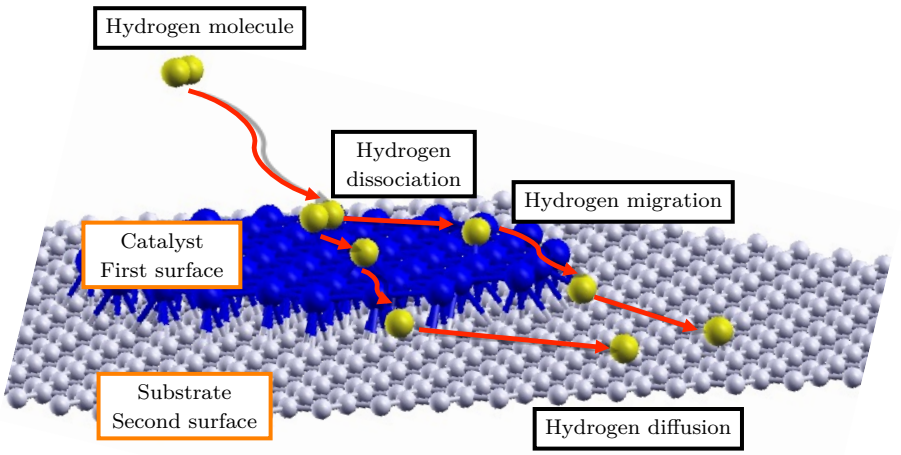

Figure 1.5: Steps of spillover mechanism from hydrogen (yellow) molecule through palladium nanoparticles (blue) to graphene (grey). Hydrogen molecule is dissociated on Pd metal cluster, then hydrogen atoms are spilled over onto the graphene layer and finally, hydrogen atoms are spread through graphene layer.

1.6.2 Palladium to Enhance Hydrogen adsorption on Graphene

Pristine graphene does not adsorbs enough hydrogen under environmental conditions to use it for long storage or transport. To overcome this problem several solutions have been proposed, but the one we are interested in is to decorate the graphene layer with metal atoms and clusters, principally **palladium** [80, 92]. Doping the porous graphitic materials with metallic atoms is a promising strategy to enhance hydrogen uptake [65, 93]. These dopant metals might have the effect of increasing hydrogen adsorption to the pore walls.

Clustering is energetically favourable and kinetically possible for transition metal atoms supported on carbon nanostructures (fullerenes, nanotubes, graphene). The reason is that carbon-metal interactions are weaker (around 1 eV/Pd single atom on graphene surface) than metal-metal interactions (around 3.75 eV/Pd in the bulk) and deposited-metal atoms migration barriers are in a range of 0.2-0.8 eV [25, 93–95]. This explains the tendency of adsorbed transition metals to migrate and form clusters rather than remain as isolated atoms on the pristine graphene surface, leading to

a considerable reduction in the metal efficiency to enhance the hydrogen storage capacity [96–101]. The effect of the dopant metal to enhance hydrogen adsorption would be larger for maximum dispersion of the metal (adsorption of metal atoms or very small clusters). Thus, it is necessary to find a way to prevent cluster growth as only the cluster surface is relevant in hydrogen storage [95].

Palladium is a special metal since it can form interstitial hydrides at room temperature and low H_2 pressures. This means that carbon materials containing palladium have higher H_2 capacities at ambient conditions [76, 102]. However, in Pd doped carbon materials, an increase in the hydrogen uptake that exceeds the amount due to hydride formation was reported. This difference was attributed to a cooperative effect between palladium and carbon support initiated by hydrogen spillover [76, 93, 102].

In our case of interest (the adsorption of hydrogen onto the graphene layer using palladium as a catalyst[11] (Fig. 1.6a)), an important problem which can spoil the spillover mechanism and thus hydrogen storage, was discovered. Cabria et al. showed that for different sizes of the palladium nanoparticles (from Pd_2 up to Pd_6) the desorption of the whole $Pd_n - H_2$ complex might compete with the desorption of molecular and dissociated hydrogen. This would reduce the contribution of supported Pd_n to the reversible hydrogen storage of nanoporous carbon materials [80]. For example, in the case of Pd_1H_2 (Fig. 1.6b), the desorption energy of hydrogen molecule is around 0.96 eV and the desorption energy of the Pd-H complex about 0.93 eV. In the case of Pd_5-H_2 the values for hydrogen molecule and the complex desorption energies are 0.69 eV and 0.60 eV, respectively.

To avoid the desorption of Pd-H complexes, the increase of metal dopant binding energy to the supporting carbon substrate has been proposed. This can be achieved, for example, using graphene oxide [103] or attaching the metal nanoparticles to defects of the graphene layer. These defects can be the replacement of carbon atoms by boron or nitrogen [104–106] or the removal of one or more carbon atoms, the so-called **graphene vacancies** [107, 108]. A comparison between pristine and defective graphene can be found in Figure 1.7.

1.6.3 Anchoring Palladium on Graphene

Two principal difficulties have been found about doping graphitic materials. First one is the migration and aggregation of the dopant metal atoms supported on the pristine graphene surface. The second problem is that in these systems the desorption

[11] In a general way, a catalyst is a substance which modifies the velocity and the energy in a chemical/physical reaction for the same temperature. They provide a different mechanism which leads to a distinct transition state and a lower activation energy. Some examples of catalysed reactions are the production of amonia or methanol, the purification of car exhaust gases or **the break of the hydrogen molecule bond into two hydrogen atoms** to store them.

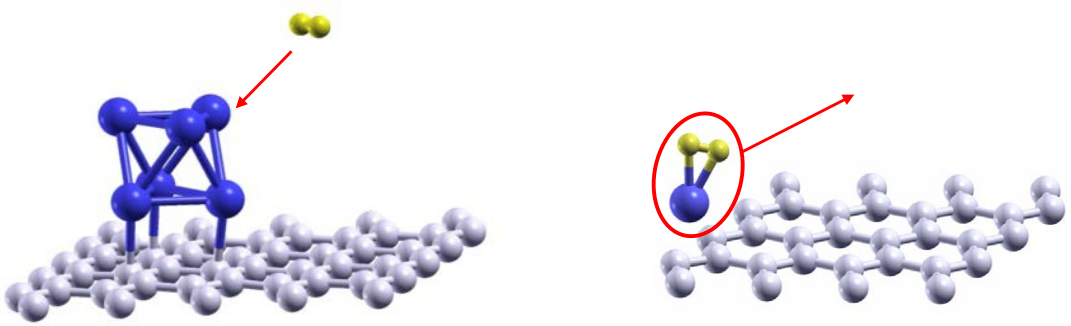

(a) (b)

Figure 1.6: Competition between hydrogen molecule and Pd-H complexes adsorption. **(a)** Adsorption of H_2 on Pd_6 supported on graphene. **(b)** Desorption of Pd_1-H_2 complex.

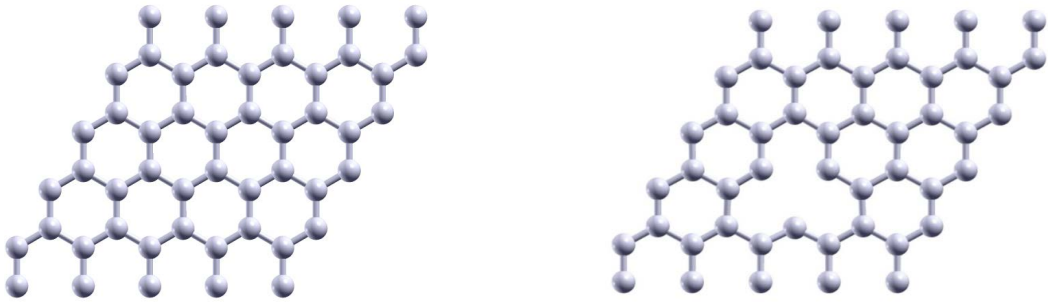

(a) (b)

Figure 1.7: **(a)** Structure of a pristine graphene layer. **(b)** Defective graphene layer. The defect is a mono-vacancy which has been created by removing one carbon atom.

of metal-hydrogen complexes often also competes with the H_2 desorption. Both problems can be reduced by increasing the binding energy of metal atoms or small metal clusters to the supporting carbon material. This can be solved by many ways as described above, but the most interesting for us is **anchoring the metal atoms or small clusters to defects** of the carbon pore walls.

It has been shown that defects in graphene such as mono-vacancies increase the adsorption energy of small metal clusters to the graphene layer. The binding energy of Pd atoms and clusters to defects on graphene substrate (see Fig.1.8a) rises up to 5 eV whereas the adsorption energy on a carbon substrate with no defects is below 1.5 eV [81]. For example, a Pd_6 octahedron is adsorbed on a graphene mono-vacancy with an energy 5.62 eV which is five times higher than the energy required to adsorb the cluster on pristine graphene, 1.14 eV (see Fig.1.9). Thus, Pd clusters attach strongly to vacancies in graphene, but the interaction with the vacancy does not affect very much the Pd-Pd interaction, for instance, the energy required to remove one Pd atom from Pd_6 anchored on a vacancy is 2.77 eV, and the energy required for extracting a Pd atom from free Pd_6 cluster is 2.69 eV.

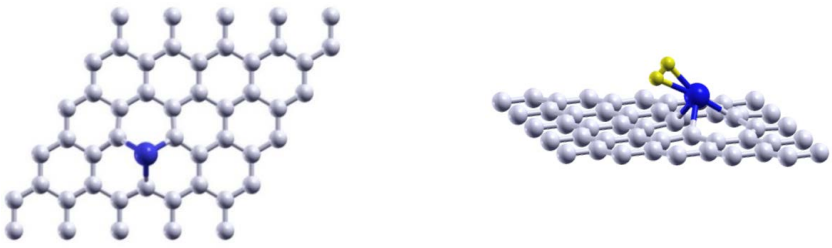

(a) (b)

Figure 1.8: **(a)** One single atom is anchored on a graphene vacancy with an energy of 5.13 eV. **(b)** Hydrogen molecule is adsorbed on a single Pd atom anchored on a graphene mono-vacancy with an energy of 0.21 eV.

Cabria et al. have shown that the adsorption energy of a molecular hydrogen on a single Pd atom anchored on a graphene mono-vacancy is only 0.21 eV (see Fig.1.8b), which contrasts with the H_2 adsorption energy on Pd-doped pristine graphene, 0.96 eV, and also contrasts with the binding energy of H_2 on a free Pd atom, 1.12 eV [80,81]. The desorption of the Pd_1-H_2 complex anchored on a graphene vacancy requires an energy of 4.2 eV and therefore, it does not compete with the desorption of molecular hydrogen. These results show the strong influence of the graphene defects on the molecular hydrogen adsorption. When the Pd atom employs a substantial part of its bonding capacity on interacting with graphene mono-vacancy, the interaction with the hydrogen molecule is weaker than the interaction between H_2 and Pd supported on pristine graphene.

To sum up, the interaction of Pd with graphene vacancies is very strong. It

doubles the strength of the Pd-Pd interaction and is about five times larger than the interaction of Pd with pristine graphene. Thus, Pd atoms dispersed on a graphene surface with defects will tend to saturate first all of the vacancies, and then aggregates will grow on the Pd-saturated vacancies. Anchoring Pd metal dopant on a graphene vacancy, prevents (i) the migration of Pd atoms to nucleate and form big aggregates and (ii) the desorption of the Pd-H complexes.

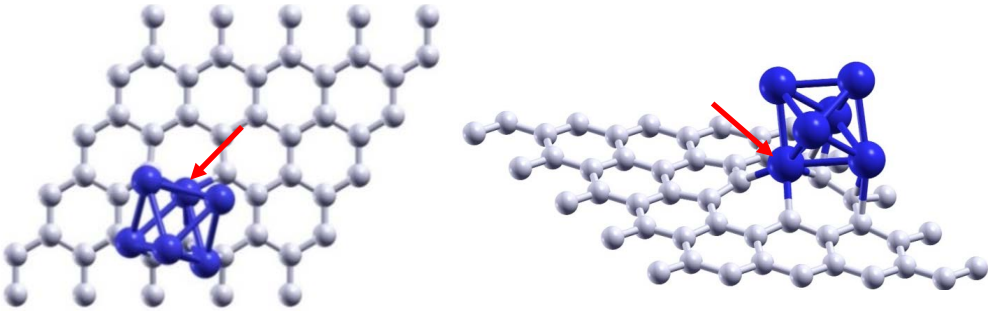

Figure 1.9: Top and side views of the Pd_6 octahedral. The metal cluster is anchored on a graphene mono-vacancy with an energy of 5.62 eV. Red arrows indicate the Pd atom which saturates the graphene mono-vacancy.

1.7 Purpose and Structure of This Work

The ability of carbon materials to store large quantities of hydrogen is still under question. This is due to difficulties in the accuracy of the experimental measurements, impurities in the carbon samples, difficulties in obtaining reproducible adsorption capacities from different laboratories and poor understanding of the hydrogen adsorption process. Thus, it is imperative to understand how hydrogen adsorption takes place in nanoporous carbon materials and specifically, if spillover mechanism describes hydrogen adsorption in these materials. In particular, one may ask if hydrogen is adsorbed and transported in molecular or dissociated form and what is the state and the location of hydrogen are after spilling over into the carbon surface. In addition, spillover depends on the characteristics of the surface, and in our case of interest, spillover might depend on the structure of the carbon support (degree of graphitization, defects, etc.) and the amount of hydrogen present.

A theoretical description of the spillover process is highly challenging since the computational model must account for the effects of the metal catalyst used to split hydrogen molecules into H atoms, the substrate on which the H atoms should be able to diffuse freely on the carbon surface and the interplay at the catalyst-substrate interface. Many of the spillover mechanism steps have been studied but it seems that the picture might not be as simple at it appears [85, 109].

The principal purpose of this thesis is to contribute to the understanding of hydrogen storage steps (spillover mechanism) which are still not well understood. We also investigate the Pd-doping effects, hydrogen saturation effects and the role of the vacancy on the hydrogen adsorption, by using *ab initio* calculations based on Density Functional Theory methods. These simulations are necessary in order to know the behaviour and interactions in graphene-metal-hydrogen systems. Graphene is the simplest carbon surface and graphene doped with a cluster formed by six Pd atoms anchored on a mono-vacancy is a reasonable starting point to model the hydrogen spillover on doped carbon materials. The main objectives are:

1. To provide a detailed description of hydrogen adsorption and saturation on Pd_6 cluster anchored on a defective graphene layer. That is, to analyse the preferred hydrogen adsorption channel, molecular physisorption or dissociative chemisorption on the palladium nanoparticle. Pd_6 is a representative size for which most interesting properties appear and it is not too expensive for computational simulations. This represents the first step of spillover mechanism which is the hydrogen adsorption on the metallic nanoparticle.

2. To investigate the sterical and chemical effects of the carbonaceous surface in the hydrogen adsorption on the Pd_6 cluster and in the hydrogen saturation level of the metal nanoparticle.

3. To explore the competition between hydrogen and palladium atoms and aggregates for saturating the graphene vacancy. This will give detailed insights into hydrogen-graphene-palladium interactions, as well as, into the saturation of the vacancy.

4. To study (i) the diffusion of the adsorbed hydrogen from the nanoparticle to the graphene layer depending on the hydrogen saturation level of the Pd nanoparticle and, (ii) the migration of hydrogen atoms through the graphene layer. These are the last steps of the spillover mechanism.

1.7.1 Structure of This Work

The majority of the results are presented as three published articles corresponding to Chapters 4, 5 and 6. The work is structured as follows:

- Chapter 2: we describe the basis and origin of DFT, its fundamental theorems, the exchange and correlation problem and the most important approximations, with special mention for Generalized Gradient Approximation (GGA).

- Chapter 3: this Chapter includes the computational details, such as a description of the code and approximations used for developing this work. It also contains some useful definitions and approximations of periodic systems.

- Chapter 4: this is the first Chapter of results. We study the competition between molecular and dissociative adsorption ways to saturate a Pd_6 cluster anchored in a graphene mono-vacancy. Some additional results to the published article are presented. Moreover, based on the results obtained, we have studied the energy barriers of different processes: the structural interconversion of the Pd_6 cluster, the hydrogen molecule adsorption and hydrogen diffusion through the Pd nanoparticle.

- Chapter 5: we study the preferred hydrogen adsorption channel on free Pd_6 clusters. We also analyse the effect of the surface on the adsorption and the hydrogen saturation of the free Pd_6 clusters. Energy barriers have been also studied for free Pd_6 systems. In this case, the processes for which the energy barriers have been calculated are: structural transition and hydrogen diffusion within the Pd nanoparticle.

- Chapter 6: this is the last Chapter for published results. We investigate the competition between hydrogen and palladium atoms and clusters to saturate the graphene vacancy. It is also shown that vacancies decorated with Pd just on one side of the graphene layer are not fully saturated. The other side of the vacancy still remains significantly reactive and therefore Pd atoms and clusters can be attached, simultaneously, to both sides of the vacancy.

- Chapter 7: This is the Chapter of unpublished results. Hydrogen atoms spillover from the Pd cluster onto the graphene surface and the diffusion through the graphene surface are investigated. These results correspond to the last two steps of the spillover mechanism.

- Finally, the conclusions and highlights are summarized.

Chapter 2

Methodology

There are people so ugly that it does not matter how they are on the outside.

One of the most important scientific advances of the twentieth century was the development of quantum mechanics and the many experimental observations which confirmed this theory [110, 111]. The translation of quantum and statistical-mechanics of molecular and solids systems into efficient numerical algorithms have allowed us to accurately study many systems computationally. This enables a deeper understanding of the physics behind experimental observations.

In the last two decades, the Density Functional Theory (DFT) has become one of the most popular and widely used methods to solve the many-body problem in physics and chemistry. The reason is that DFT is able to treat many problems with a sufficiently high accuracy.

In this Chapter, we introduce some concepts related to quantum physics to set the basis to explain briefly the standard time-independent DFT. Several approximations, such as, Born-Oppenheimer, Local Density and Generalized Gradient approximations are described. We only try to make a brief exposition with no attempt to discuss the underlying mathematics.

2.1 The Many-Body Problem and the Schrödinger equation

In general, the majority of the systems and problems in physics and chemistry are "many-body problems". At the nano-scale, quantum mechanics is usually used to provide an accurate description and solution for these kind of issues. In our field of study, we try to describe the structure, energy and dynamic properties of many-electrons systems, for instance, single atoms, nuclei, molecules, clusters, dimers and solids [112–114].

Many properties such as conductivity, structural stability, magnetic moments, real space geometry, bond lengths, atomic arrangement, etc. are determined by electronic structure in crystals/solids. If we know the system's electronic ground-state, we can calculate all these properties. For dynamic properties such as electronic excitation spectrum, optical properties, ionization or vibrations, we need to study excited stationary states or time-dependent states [114].

In condensed matter physics, the main problem is to know the motion and the energy of electrons in a system where electrons and nuclei interact. In addition, we would like to know how the energy changes if we move atoms around. In quantum mechanics, the operator associated to the energy is the Hamiltonian ($\hat{H}$). When $\hat{H}$ is applied to the wave function or eigenstate (Ψ) which has all the information we can obtain from a given system, it is called the *many-body Schrödinger equation*. In stationary (time-independent) and non-relativistic terms this is written as:

$$\hat{H}|\Psi\rangle = (\hat{T} + \hat{V})|\Psi\rangle = E|\Psi\rangle \tag{2.1}$$

where E is the eigenvalue corresponding to the eigenstate Ψ when the Hamiltonian is applied. $\hat{T}$ and $\hat{V}$ are the kinetic energy and potential operators, respectively. The Hamiltonian has to include both the nuclei and the electrons for each system. The principal interaction to be considered is the electrostatic or Coulomb interaction, since gravitational interaction is very weak and we can omit it. The electrons must be described by quantum mechanics, while the more massive nuclei can be treated as classical particles. In general, if only the valence electrons are considered, as they move at speeds much less than the speed of light, we can neglect relativistic effects [113]. In absence of external electromagnetic fields, the Hamiltonian operator can be split into two terms: the electronic and the nuclear terms:

$$\hat{H}_{tot} = \hat{H}_{eN} = \underbrace{\hat{T}_e + \hat{V}_{ee} + \hat{V}_{eN}}_{\hat{H}_e} + \underbrace{\hat{T}_N + \hat{V}_{NN}}_{\hat{H}_N} \tag{2.2}$$

and thus, Schrödinger equation can be written as:

$$\hat{H}_{eN}|\Psi\rangle = (\underbrace{\hat{T}_e + \hat{T}_N}_{\hat{T}} + \underbrace{\hat{V}_{ee} + \hat{V}_{eN} + \hat{V}_{NN}}_{\hat{V}})|\Psi\rangle = E|\Psi\rangle \tag{2.3}$$

$\hat{T}_e$ and $\hat{T}_N$ are the kinetic energy operators of electrons and nuclei, respectively. The other terms are the electrostatic interactions among electrons and nuclei. If we consider a system of N nuclei each one with mass M_I, n electrons each one with mass m_e and we label the nuclear coordinates ($\vec{R}_I, ...\vec{R}_N$) and the electron coordinates

$(\vec{r}_1, ...\vec{r}_n)$, the terms of the Hamiltonian (2.2) are:

Kinetic energy of electrons[1]
$$\hat{T}_e = -\frac{\hbar^2}{2m_e}\sum_{i=1}^{n}\vec{\nabla}_i^2. \tag{2.4}$$

Electron-electron interaction[2]
$$\hat{V}_{ee} = \frac{1}{2}\sum_{i=1}^{n}\sum_{i\neq j}^{n}\frac{q_e^2}{4\pi\epsilon_0|\vec{r}_i - \vec{r}_j|}. \tag{2.5}$$

Electron-nuclei interaction
$$\hat{V}_{eN} = -\sum_{i=1}^{n}\sum_{I=1}^{N}\frac{q_e^2 Z_I}{4\pi\epsilon_0|\vec{r}_i - \vec{R}_I|}. \tag{2.6}$$

Kinetic energy of nuclei
$$\hat{T}_N = -\frac{\hbar^2}{2}\sum_{I=1}^{N}\frac{1}{M_I}\vec{\nabla}_I^2. \tag{2.7}$$

Nuclei-nuclei interaction
$$\hat{V}_{NN} = \frac{1}{2}\sum_{I=1}^{N}\sum_{I\neq J}^{N}\frac{q_e^2 Z_I Z_J}{4\pi\epsilon_0|\vec{R}_I - \vec{R}_J|}. \tag{2.8}$$

Where i and j are the subscripts for electrons, I and J are the subscripts for nuclei, -q_e and Zq_e are the charges of electron and nuclei respectively. For a system with N nuclei and n electrons, there are $3N + 4n$ degrees of freedom, $3N$ and $3n$ for the spatial coordinates of the nuclei $(\vec{R}_1, ...\vec{R}_N)$ and the electrons $(\vec{r}_1, ...\vec{r}_n)$ respectively, and for electrons also the spin coordinates [115].

The Eq.(2.3) is too complex to be solved exactly in the majority of the cases, except for the hydrogen atom. In this field of study, an important challenge is to find approximate solutions for the time-independent many-body Schödinger equation, to an acceptable degree of accuracy.

2.2 The Born-Oppenheimer Approximation

The first approximation to simplify this problem is the Born-Oppenheimer Approximation (BO) [116]. The principal idea of this approximation is to decouple electron and nuclear motion. This is possible since the nuclei are significantly more massive than electrons (around 1800 times more massive). According to this, electrons are much faster than nuclei (about $10^2 - 10^3$ times faster) for the same kinetic energy [117]. For typical time-scale of nuclear motion, the electrons will follow the nuclei configuration instantaneously. This allows us to set the nuclear kinetic energy $\hat{T}_N$ to zero and to consider the repulsion between nuclei $\hat{V}_{NN}$ as a *constant*[3]. As a consequence of BO approximation, nuclei are considered as fixed at coordinates $\vec{R}$.

[1] This operator is valid for any non relativistic system. For relativistic systems Dirac equation is needed.

[2] This describes a system of interacting electrons since the $\frac{1}{|r_i - r_j|}$ can not be broken into a sum of terms containing only r_i and only r_j.

[3] The constant just establishes the arbitrary origin for energies.

Thus, we can rewrite the Hamiltonian (2.2) like this:

$$\hat{H}_{tot} = \underbrace{\hat{T}_e + \hat{V}_{ee} + \hat{V}_{eN}}_{\hat{H}_e} + \underbrace{\cancel{\hat{T}_N} + \hat{V}_{NN}}_{\hat{H}_N}. \tag{2.9}$$

So, the time-independent Schrödinger equation we have to solve for the electronic ground-state is:

$$\hat{H}_e\Psi(\vec{r}_i, \{\vec{R}\}) = (\hat{T}_e + \hat{V}_{ee} + \hat{V}_{eN})\Psi(\vec{r}_i, \{\vec{R}\}) = E(\{\vec{R}\})\Psi(\vec{r}_i, \{\vec{R}\}) \tag{2.10}$$

where $\vec{r}_i = \vec{r}_1, ..., \vec{r}_n$ are the coordinates of the n electrons. $\Psi(\vec{r}_i, \{\vec{R}\})$ is the many-electron wave function which describes the motion of the electrons at fixed nuclei positions $\{\vec{R}\}$ and $E\{\vec{R}\}$ is the electronic energy for fixed positions of the nuclei. The nuclear coordinates $\vec{R}$ are parameters not variables. Eq.(2.10) should be solved for each group of nuclear fixed positions $\vec{R}$. Since the movement of nuclei and electrons are split, we can write the total wave function Ψ as product of the electronic part $\Psi_e(\vec{r}_i, \{\vec{R}\})$ and the nuclear part $\Psi_N\{\vec{R}\}$:

$$\Psi(\vec{r}_i, \{\vec{R}\}) = \Psi_e(\vec{r}_i, \{\vec{R}\})\Psi_N(\{\vec{R}\}). \tag{2.11}$$

The solution to Eq. (2.10) is too complex to be found exactly except for hydrogen molecule-ion (H_2^+) [117]. For larger systems, further approximations have to be introduced. Two are the fundamental electronic structure methods to study the total energy ground-state (see Fig.2.1):

1. Wave function based methods: the many-body problem is translated into a single particle problem and the Slater determinant is needed to incorporate the antisymmetry of the wave function $\Psi(\vec{r}_i, \{\vec{R}\})$. There are semi-empirical methods and *ab initio*[4] methods. Within the latter one, the Hartree-Fock method is one of the most popular methods, but it becomes computationally expensive as the number if electrons increases.

2. Electronic density based methods: These methods use the density of electrons as a fundamental property instead of dealing directly with wave functions to describe the quantum state. Density Functional Theory (DFT) is the most widely used method in condensed matter physics. We are going to provide a brief introduction to DFT method in the next sections.

[4]The term *ab initio* comes from the Latin words "from the beginning". This means that there are not experimental parameters, only the fundamental constants are used.

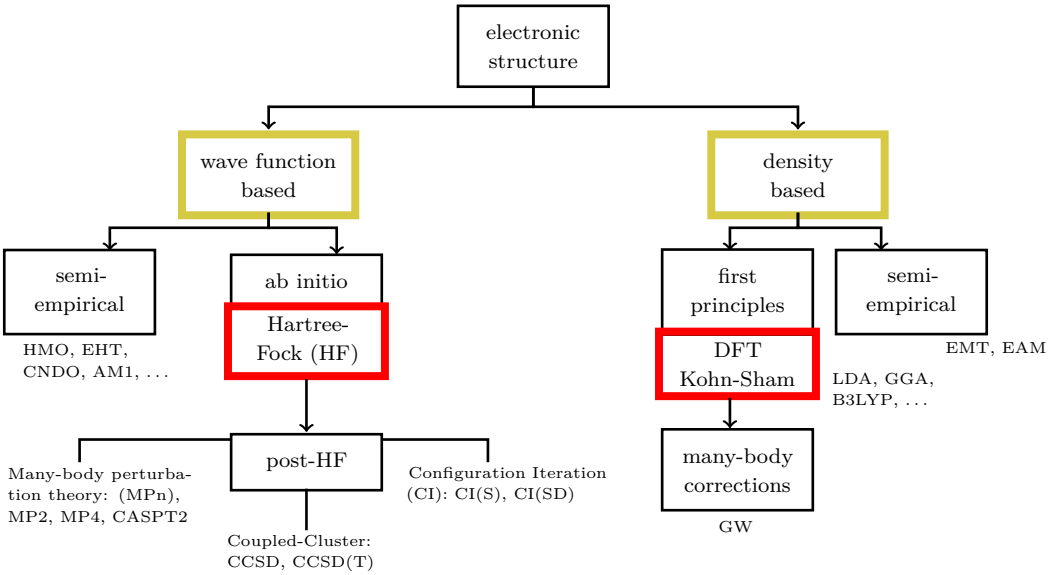

Figure 2.1: Electronic Structure Methods.

2.3 Density Functional Theory (DFT)

The principal problem is to find and calculate the electronic wave function and the electronic energy. Once of those quantities are known, a wide range of chemically and physically important properties can be determined. This is only exactly solvable for the hydrogen atom. Thus, to solve for larger systems other approximations have to be applied.

DFT is based on the concept of *electron probability density*. The growing popularity of DFT method is due to its lower computational cost with a moderately high accuracy [117–123].

The main idea behind DFT is that the ground-state energy and other properties of a given system can be obtained by the electron density instead of using a wave function, in others words, there exists a one-to-one correspondence between the electron density and the energy [124]. The wave function of an n-electron system depends on 4n variables, three spatial and one spin coordinates per electron, while the electron density only depends on 3 variables, namely, DFT transforms the 4n variational problem into a 3-dimensional variational problem. The disadvantage is that, except for the simplest systems, the relation (functional) between the density and the energy of the system remains unknown, so we use approximations.

The history of DFT started a century ago. The first attempt was when Llewellyn Thomas [125] and Enrico Fermi [126] developed the initial ideas of DFT in the late 1920s. They tried to calculate the energy and the electronic structure of an atom by introducing an approximation method based on the electronic density. This model was improved by Paul Dirac [127] who added an exchange energy functional

in 1928. Though wonderfully simple, this theory fails qualitatively because it is unable to reproduce atomic shell structure[5]. The theoretical basis for the DFT was established in 1964, when Pierre Hohenberg and Walter Kohn demonstrated that the total electron density completely and exactly determines all the (ground-state) properties of an n-electron system. Moreover, the next year (1965), Walter Kohn and Lu Sham provided a practical scheme for solving the quantum-mechanical problem based on the Hohenberg-Kohn (HK) theorem. Thus, Hohenberg, Kohn and Sham established the rigorous theory that finally legitimized the intuitive ideas of Thomas, Fermi and Dirac.

The Density Functional Theory began to be very popular in the 1970s for the study of solid-state physics. However, it was not considered accurate enough for quantum chemistry until some approximations were improved. Nowadays, DFT is a fundamental method to calculate the electronic structure. For example, for systems including d-block metals, DFT yields results that very frequently agree more closely with experiments than Hartree-Fock [117].

In the following sections, we will discuss the basic ideas about the standard time-independent Density Functional Theory. Firstly, the Thomas-Fermi model is presented as is the initial attempt to use electronic density. The next point will be the Hohenberg-Kohn theorems. Finally, we will introduce the Kohn-Sham formalism.

2.3.1 Thomas-Fermi Model: the Origin of DFT

The statistical view for the atomic electrons was established by Thomas [125] and Fermi [126] in 1927. The Thomas-Fermi Model is also known as *the inhomogeneous electron-gas model*. The original purpose was to study the energy and charge density for atoms with a large number n of electrons. The idea is to replace the 3n-dimensional wave functions $\Psi(\vec{r}, \vec{r}_2, ..., \vec{r}_n)$ and the Schrödinger[6] equation associated to the system by an equation involving the density $\rho(\vec{r})$[7] which only depends on the three spatial coordinates [128]. The electron density is a physical observable, thus, it can be calculated and experimentally measured (the wave function can not be measured). For a system with n electrons, the definition of the density is:

$$\begin{aligned}\rho(\vec{r}) &= n \int \Psi^*(\vec{r}, \vec{r}_2, ..., \vec{r}_n)\Psi(\vec{r}, \vec{r}_2, ..., \vec{r}_n)\mathrm{d}\vec{r}_2...\mathrm{d}\vec{r}_n \\ &= n \int |\Psi(\vec{r}, \vec{r}_2, ..., \vec{r}_n)|^2 \mathrm{d}\vec{r}_2...\mathrm{d}\vec{r}_n.\end{aligned} \tag{2.12}$$

The TF approach is semi-classical. Some ideas come from quantum mechanics and others operate with normal functions instead of quantum mechanics operators; the

[5]Shell structure is a consequence of the Pauli exclusion principle.

[6]Schrödinger equation, which would give the exact density and energy, can not be easily handled when n is large.

[7]For a system of n electrons, $\rho(\vec{r})$ denotes the total electron density at a particular point $\vec{r}$.

kinetic energy is derived from quantum-statistical theory and the electron-electron and the electron-nucleus interactions are treated classically.

The total electronic energy which is a *functional* of the ground-state electronic charge $\rho(\vec{r})$ can be written as (see [129] for a complete derivation):

$$\begin{aligned} E[\rho(\vec{r})] =& \frac{3h^2}{10m}\left(\frac{3}{8\pi}\right)^{\frac{2}{3}}\int[\rho(\vec{r})]^{\frac{5}{3}}\mathrm{d}\vec{r}+\int\rho(\vec{r})V_{eN}(\vec{r})\mathrm{d}\vec{r} \\ &+\frac{1}{2}\frac{1}{4\pi\epsilon}\int\int\frac{\rho(\vec{r}_1)\rho(\vec{r}_2)}{|\vec{r}_1-\vec{r}_2|}\mathrm{d}\vec{r}_1\mathrm{d}\vec{r}_2=\frac{3h^2}{10m}\left(\frac{3}{8\pi}\right)^{\frac{2}{3}}\int[\rho(\vec{r})]^{\frac{5}{3}}\mathrm{d}\vec{r} \\ &-Z\int\frac{\rho(\vec{r})}{r}\mathrm{d}\vec{r}+\frac{1}{2}\frac{1}{4\pi\epsilon}\int\int\frac{\rho(\vec{r}_1)\rho(\vec{r}_2)}{|\vec{r}_1-\vec{r}_2|}\mathrm{d}\vec{r}_1\mathrm{d}\vec{r}_2. \end{aligned} \tag{2.13}$$

The first term of the sum is the kinetic energy of n non-interacting electrons needed to produce a density $\rho(\vec{r})$, the second and third terms of the sum represent the electron-nucleus and electron-electron interactions, respectively. The factor $\frac{1}{2}$ in the last term of the sum is introduced to avoid counting interactions twice. The electron-nucleus interactions are introduced as an external potential. The energy only depends on the electron density.

As we have said, an important correction was made by Dirac [127] when he introduced the *exchange* into the TF theory. It is a quantum-mechanical effect that only occurs between identical particles. He added a term in Eq.(2.13) and the model is called then Thomas-Fermi-Dirac (TFD). In spite of this correction, the model is still imprecise. The biggest errors are found in the kinetic energy and in the fact of ignoring completely the *correlation*. Other issues that the TF model does not explain are that atoms do not bind to give molecules or solids and there is not shell structure (no periodic table). The connection between the electronic density and the wave function is still missing. Hohenberg, Kohn and Sham theoretical frameworks provided this connection.

2.3.2 Hohenberg-Kohn Theorems

As aforementioned, the basic idea behind DFT is that the energy of an electronic system can be written in terms of the electron density $\rho(\vec{r})$. The electronic energy is a *functional* of the electron density $E[\rho(\vec{r})]$, in the sense that for given function $\rho(\vec{r})$, there is a single corresponding energy [117, 123, 130]. In 1964, Hohenberg and Kohn showed that the ground-state energy and all the other ground-state electronic properties are completely determined by the electron density; also they showed that the energy is a functional of the density and that the ground-state density minimizes this functional.

Hohenberg and Kohn published two important theorems that year [131]. The first one states: *"$V_{ext}(\vec{r})$ (the external potential) is (to within a constant) a unique functional of $\rho(\vec{r})$; since, in turn, $V_{ext}(\vec{r})$ fixes $\hat{H}$ we see that the full many-particle*

ground-state is a unique functional of $\rho(\vec{r})$*"* [129, 131]. Namely, for any system of interacting particles under the influence of an external potential $V_{ext}(\vec{r})$, the external potential is uniquely determined (plus an arbitrary constant) by the non-degenerate ground-state density $\rho_0(\vec{r})$ which has all the information of a given electronic system, see Fig.2.2. This functional is also universal, this is, it is independent of the external potential V_{ext}. This first theorem introduces the density as the basic variable.

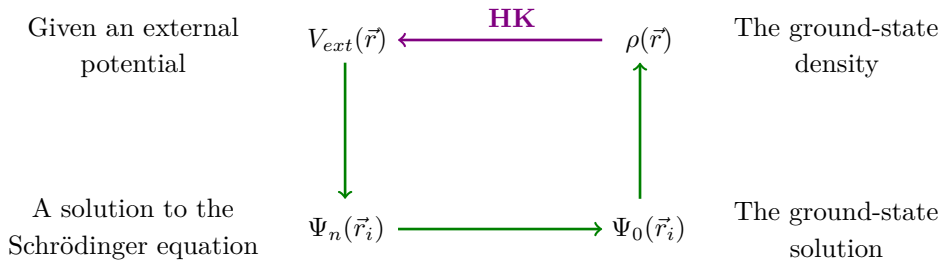

Figure 2.2: Scheme of the first Hohenberg-Kohn theorem. The ground-state density $\rho_0(\vec{r})$ can be known from the external potential V_{ext}, but HK demonstrated that this relation can be inverted closing the cycle (purple arrow). Namely, the external potential can be known from the ground-state density.

The proof to this theorem proceeds by *reductio ad absurdum*. First we need to prove that two different external potentials do not produce the same ground density. Suppose that two different potentials give the same electron ground-state density $\rho_0(\vec{r})$, and these two potentials, $V_{ext1}(\vec{r})$ and $V_{ext2}(\vec{r})$, differ in more than a constant (i.e., $V_{ext1}(\vec{r}) \neq V_{ext2}(\vec{r}) + constant$). As the two external potentials are different, we have two different Hamiltonians H_1 and H_2[8], thus the ground-state wave functions Ψ_1 and Ψ_2 are different since they are eigenstates of different Hamiltonians. Then, applying the Ritz method[9] and assuming that the two densities are the same, we will obtain[10]:

$$\begin{aligned} E_1 &= \langle\Psi_1|\hat{H}_1|\Psi_1\rangle < \langle\Psi_2|\hat{H}_1|\Psi_2\rangle = \langle\Psi_2|\hat{H}_2 + V_{ext1} - V_{ext2}|\Psi_2\rangle \\ &= E_2 + \int \rho_0(\vec{r})[V_{ext1}(\vec{r}) - V_{ext2}(\vec{r})]\mathrm{d}\vec{r}. \end{aligned} \tag{2.14}$$

[8]We need to remember that the Hamiltonian is the sum of the external potential, the Coulomb potential and the kinetic energy: H=T+V+V_{ext}.

[9]Ritz method is an approximative technique to find the solution of a variational problem. The Ritz function Ψ is a linear combination of N known basis functions Ψ_i, parametrized by unknown coefficients $\Psi = \sum_{i=1}^{N} c_i\Psi_i$. These coefficients are adjustable, they are varied to find the lowest energy configuration and they must satisfy predetermined periodic boundary conditions. It can be shown that the ground-state energy, E_0, satisfies an inequality: $E_0 \leq \frac{\langle\Psi|\hat{H}|\Psi\rangle}{\langle\Psi|\Psi\rangle}$. That is, the ground-state energy is less than this value. The trial wave function will always give an expectation value larger than or equal to the ground energy.

[10]In general, H=T+V+V_{ext}; then H_1=T+V+V_{ext1} and H_2=T+V+V_{ext2}, this implies $H_1 = H_2 - V_{ext2} + V_{ext1}$.

Doing the same for the non-degenerate ground-state Ψ_2:

$$\begin{aligned} E_2 = \langle\Psi_2|\hat{H}_2|\Psi_2\rangle &< \langle\Psi_1|\hat{H}_2|\Psi_1\rangle = \langle\Psi_1|\hat{H}_1 + V_{ext2} - V_{ext1}|\Psi_1\rangle \\ &= E_1 + \int \rho_0(\vec{r})[V_{ext2}(\vec{r}) - V_{ext1}(\vec{r})]\mathrm{d}\vec{r}. \end{aligned} \tag{2.15}$$

If we add Equations (2.14) and (2.15) we obtain:

$$E_1 + E_2 < E_1 + E_2. \tag{2.16}$$

Obviously this equation is a contradiction. We conclude that the density distribution $\rho(\vec{r})$ can not be reproduced by two different ground-states given by two different potentials.

The second HK theorem states that the energy is a functional of the density, and the density that minimizes the total energy functional is the exact ground-state density [132]. The energy can be written as:

$$E[\rho(\vec{r})] = T[\rho(\vec{r})] + V_{ee}[\rho(\vec{r})] + V_{ext}[\rho(\vec{r})]. \tag{2.17}$$

For convenience we can separate the energy functional into a universal part (independent of the number of electrons (n), charge of nuclei, etc.) and a system dependent part, (i.e. dependent on $\mathrm{V_{ext}}$):

$$\begin{aligned} E[\rho(\vec{r})] &= \underbrace{F_{HK}[\rho(\vec{r})]}_{\text{universal}} + \underbrace{\int V_{ext}(\vec{r})\rho(\vec{r})\mathrm{d}\vec{r}}_{\text{system dependent}}; \\ F_{HK}[\rho(\vec{r})] &= T[\rho(\vec{r})] + V_{ee}[\rho(\vec{r})]. \end{aligned} \tag{2.18}$$

F_{HK} is the HK functional which only depends on $\rho(\vec{r})$. The proof of the second theorem is also straightforward. Let us consider a system of n interacting electrons in a given external potential. We will prove that $E[\rho(\vec{r})]$ takes a lower value for the correct $[\rho(\vec{r})]$ than for any other density distribution $[\rho'(\vec{r})]$ with the same total number of electrons n. Assuming the non-degeneracy of Ψ, we define the following energy functional of the density $\rho'(\vec{r})$:

$$E[\rho'(\vec{r})] = F_{HK}[\rho'(\vec{r})] + \int V_{ext}(\vec{r})\rho'(\vec{r})\mathrm{d}\vec{r}. \tag{2.19}$$

This energy has a lower value for the correct Ψ than for any other Ψ'. Applying the variational principle:

$$\begin{aligned} \langle\Psi'|\hat{F}_{HK}|\Psi'\rangle + \langle\Psi'|\hat{V}_{ext}|\Psi'\rangle &> \langle\Psi|\hat{F}_{HK}|\Psi\rangle + \langle\Psi|\hat{V}_{ext}|\Psi\rangle \\ \int \rho'(\vec{r})V_{ext}(\vec{r})\mathrm{d}\vec{r} + F_{HK}[\rho'(\vec{r})] &> \int V_{ext}(\vec{r})\rho(\vec{r})\mathrm{d}\vec{r} + F_{HK}[\rho(\vec{r})]. \end{aligned} \tag{2.20}$$

Finally the second Hohenberg-Kohn theorem is obtained:

$$E[\rho'(\vec{r})] > E[\rho(\vec{r})]. \tag{2.21}$$

Unfortunately, the HK theorems do not tell us the *form* of the functional which relates the energy to density. This is, there is not direct link from the density to, for example, the kinetic energy. It only confirms that such a functional exists [117]. In this point, DFT is in principle exact (there are not approximations) but impractical or hard to compute it. Kohn and Sham created a simple method for carrying out DFT calculations that retains the exact nature of DFT. This practical scheme is described in the next section.

2.3.3 Kohn-Sham Model

In 1965, Kohn and Sham published an article [133] that transformed DFT into a practical way to perform electronic structure calculations. The principal idea of KS model is the construction of a fictitious auxiliary system of n non-interacting particles which generates the same density as a given system of n interacting particles. The challenge is then shifted from finding the universal HK functional to find the fictitious system of non-interacting electrons which has the same density as the "real" one with the interacting electrons (see Fig.2.3). In order to see how it works, we first need to examine the Hamiltonian equation for n non-interacting electrons.

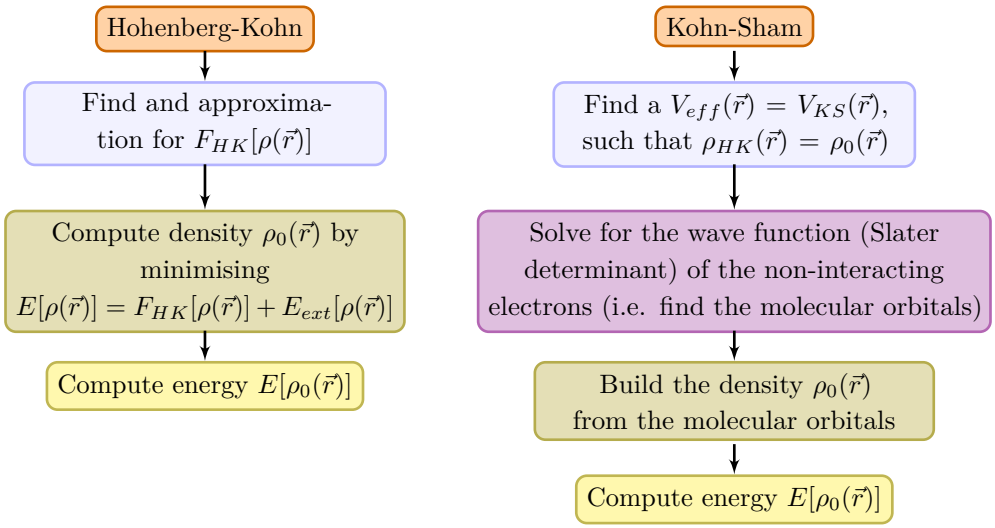

Figure 2.3: Hohengberg-Kohn vs. Kohn-Sham approaches.

The exact Hamiltonian for interacting electrons is given in Eq.(2.10). The first term of the sum is given by Eq.(2.4), the second term is given by (2.6) and the last term of the sum is given by Eq.(2.5). For an n non-interacting electron system the

Hamiltonian is:

$$\hat{H}_{eff} = -\frac{\hbar^2}{2m_e}\sum_{i=1}^{n}\vec{\nabla}_i^2 + \sum_{i=1}^{n}V_{ext}(\vec{r}_i) + \sum_{i=1}^{n}V_{average}(\vec{r}_i) \tag{2.22}$$

$$= -\frac{\hbar^2}{2m_e}\sum_{i=1}^{n}\vec{\nabla}_i^2 + \sum_{i=1}^{n}(V_{ext}(\vec{r}_i) + V_{average}(\vec{r}_i)) \tag{2.23}$$

$$= -\frac{\hbar^2}{2m_e}\sum_{i=1}^{n}\vec{\nabla}_i^2 + \sum_{i=1}^{n}V_{eff}(\vec{r}_i) \tag{2.24}$$

$$= \sum_{i=1}^{n}\left\{-\frac{\hbar^2}{2m_e}\vec{\nabla}_i^2 + V_{eff}(\vec{r}_i)\right\} \tag{2.25}$$

$$= \sum_{i=1}^{n}\hat{h}_i(\vec{r}_i). \tag{2.26}$$

So the entire Hamiltonian can be written as just a sum of one-electron Hamiltonians: one for each electron.

The ground-state electron density is obtained by summing over the n_{occ} lowest occupied electron states:

$$\rho(\vec{r}) = \sum_{i=1}^{n_{occ}}\psi_i^*(\vec{r})\psi_i(\vec{r}) = \sum_{i=1}^{n_{occ}}|\psi_i(\vec{r})|^2 \tag{2.27}$$

where $\psi_i(\vec{r})$ are the one-electron wave functions or Kohn-Sham orbitals determined by the Kohn-Sham equations, which are [129, 133]:

$$\left(-\frac{\hbar^2}{2m_e}\vec{\nabla}_i^2 + V_{eff}(\vec{r}_i)\right)\psi_i(\vec{r}) = \epsilon_i\psi_i(\vec{r}) \tag{2.28}$$

$$\hat{H}_{KS}\psi_i(\vec{r}) = \epsilon_i\psi_i(\vec{r}). \tag{2.29}$$

ϵ_i is the energy for each orbital. The first term of the sum in Eq.(2.28) describes the kinetic energy of the i-electron in an n non-interacting electrons system and the second term of the sum, $V_{eff}(\vec{r}_i)$, is the effective Kohn-Sham potential which is the sum of the $V_{ext}(\vec{r}_i)$ and the $V_{average}(\vec{r}_i)$. $V_{average}(\vec{r}_i)$ substitutes the electron-electron interactions by an "average" effect of these interactions. The electron-electron interactions are composed by two terms:

$$V_{average}(\vec{r}_i) = V_{Coulomb}(\vec{r}_i) + V_{XC}(\vec{r}_i), \tag{2.30}$$

the first term of the sum is the Coulomb interaction and the second term is the *exchange-correlation*, which takes in account all the quantum-mechanical interactions that are not included in the first term of the sum. Thus, $V_{eff}(\vec{r}_i)$ is written as:

$$\begin{aligned} V_{eff}(\vec{r}_i) &= V_{ext}(\vec{r}_i) + \overbrace{V_{Coulomb}(\vec{r}_i) + V_{XC}(\vec{r}_i)}^{V_{average}} \\ &= V_{ext}(\vec{r}_i) + \frac{1}{2}\frac{q_e^2}{4\pi\epsilon_0}\int\frac{\rho(\vec{r}_1)\rho(\vec{r}_2)}{|\vec{r}_1 - \vec{r}_2|}\mathrm{d}\vec{r}_1\mathrm{d}\vec{r}_2 + V_{XC}(\vec{r}_i). \end{aligned} \tag{2.31}$$

We can also write the exact ground-state electronic energy as (see [117, 124] for further information):

$$E_{KS}[\rho] = T[\rho(\vec{r})] + E_{ext}[\rho(\vec{r})] + E_{Coulomb}[\rho(\vec{r})] + E_{XC}[\rho(\vec{r})], \tag{2.32}$$

where $T[\rho(\vec{r})]$ is the kinetic energy, $E_{Coulomb}[\rho(\vec{r})]$ is the Coulomb potential energy and $E_{ext}[\rho(\vec{r})]$ is the external potential energy, which usually represents the interaction between one electron and the atomic nuclei, this is, the electron-nucleus attraction over all N nuclei. $E_{XC}[\rho(\vec{r})]$ is the *exchange-correlation*[11] potential energy of the system and takes into account all non-classical electron-electron interactions (exchange-correlation interactions). $E_{XC}[\rho(\vec{r})]$ is related to V_{XC} as:

$$V_{XC} = \frac{\delta E_{XC}[\rho(\vec{r})]}{\delta \rho(\vec{r})}. \tag{2.33}$$

The exchange-correlation potential is the functional derivative of the exchange-correlation energy functional $E_{XC}[\rho(\vec{r})]$. The exchange-correlation functional is generally divided in two separated terms: exchange $E_X[\rho]$ and correlation $E_C[\rho]$, $E_{XC} = E_X[\rho] + E_C[\rho]$. The *exchange* term is associated to two electrons which can not have the same quantum state as they are indistinguishable particles. The *correlation* term refers to all the effects that are missed when the electrons are treated as independent and it is a measure of how much the movement of one electron is influenced by the presence of all other electrons. These two terms are also functionals of the electron density.

The KS equations are solved in a self-consistent way. We start with an initial electron density $\rho(\vec{r})$. Then V_{eff} can be calculated from Eq.(2.31) and then, KS equations can be solved (Eq.(2.28)). From KS equations solutions, $\psi_i(\vec{r})$, we can obtain a new electron density, $\rho_{KS}(\vec{r})$, from Eq.(2.27). If the new density, $\rho_{KS}(\vec{r})$, is equal to the initial one, $\rho(\vec{r})$, then $\rho_{KS}(\vec{r})$ should be the ground-state density and it is used to calculate the minimum energy of the system. If the two densities are different, then the initial energy has to be updated and the process is started again by using the new electron density $\rho_{KS}(\vec{r})$ as the initial one. This process is repeated iteratively until convergence, see Fig.2.4.

The results of KS method will lead to the exact ground-state energy and density, but unfortunately, the exact form of the exchange-correlation functional is unknown and we need to look for good approximations of this term $E_{XC}[\rho(\vec{r})]$. In the next section, we present some approximations for the exchange and correlation functionals.

[11] For an electron with spin, let's say, "up", the charge density of spin "up" is reduced in its neighbourhood. This additional interaction due to the Pauli principle is the exchange interaction; it lowers the total energy (since it increases the inter-electron separation).

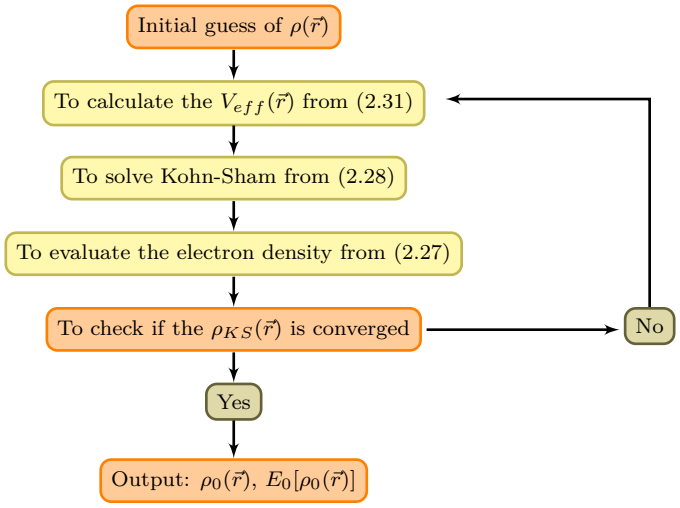

Figure 2.4: Flow-chart diagram of self-consistent scheme to solve the one-electron Khon-Sham equations.

2.4 Approximations for the Exchange-Correlation Energy

As we have seen, the Hohenberg, Kohn and Sham methods are in principle, an exact alternative to the Shrödinger equation to find the exact ground-state energy. Despite the progress that DFT produced in this field, the main source of error in DFT method usually arises from the approximate nature of the exchange-correlation functional E_{XC}.

This functional can be derived exactly in one case, which is the uniform electron gas, as the electron density is constant at all points in space $\rho(\vec{r}) = C$. But real materials do not behave like this. The variations in the electron density define many properties, such as chemical bonds. The search for functionals is one of the most interesting and important areas of condensed matter physics. There are four main generations of exchange and correlation approximations. From the lowest accuracy to the highest they are: (i) Local Density Approximation (LDA), depending on the electron density at a given point $\rho(\vec{r})$, (ii) gradient corrected or generalized gradient approximation (GGA), which depends on both the electron density $\rho(\vec{r})$ and its gradient $\vec{\nabla}\rho$, (iii) meta-GGA, which uses the electron density $\rho(\vec{r})$, its gradient $\vec{\nabla}\rho$ and some terms related to the kinetic energy $\nabla^2\rho$ and (iv) hybrid functionals, which add a portion of exact exchange from Hartree-Fock theory to the DFT exchange-correlation term.

2.4.1 Local Density Approximation

The Local Density Approximation (LDA) is the simplest approximation for the exchange-correlation functional. It is also the basis of all exchange-correlation approximations.

In the original paper by Kohn-Sham [133], they provided a solution for the KS equations. In a spin-unpolarized system with slowly varying density, a local-density approximation for the total exchange-correlation energy can be written as:

$$E_{XC}^{LDA}[\rho(\vec{r})] = \int \rho(\vec{r})\epsilon_{XC}^{hom}[\rho(\vec{r})]\mathrm{d}\vec{r} \tag{2.34}$$

where $\epsilon_{XC}^{hom}[\rho(\vec{r})]$ is the exchange-correlation energy per particle of a homogeneous electron gas[12] for a given density $\rho(\vec{r})$ [113, 124, 129]. The energy per particle is weighted with the density $\rho(\vec{r})$. This expression for the exchange-correlation energy is obviously an approximation because neither the positive charges nor the electronic charges are uniformly distributed in real systems.

A customary expression for the exchange term, let's say the *first* LDA approximation, was proposed by Dirac [134] in the late 1920's. The equation for the proposed $E_{XLDA}^{hom}[\rho(\vec{r})]$ is [129]:

$$E_{XLDA}^{hom}[\rho(\vec{r})] = -\frac{3}{4}\left(\frac{3}{\pi}\right)^{\frac{1}{3}} \int \rho^{\frac{4}{3}}(\vec{r})\mathrm{d}\vec{r}. \tag{2.35}$$

In LDA, the exact expression for the correlation energy $E_C[\rho(\vec{r})]$ is difficult to obtain separately from the exchange energy. However, several approximations have been proposed, for example Vosko-Wilk-Nusair functional [135] or Perdew and Zunger functional [136]. The LDA is exact in the limit of slowly-varying densities, but for systems of interest, the density is generally rapidly varying, and LDA would appear to be a crude approximation in these cases. Its use is justified *a posteriori* by its surprising success at predicting physical properties in real systems [137] such as metallic solids with delocalized electrons, which are similar to the uniform electron gas. However, LDA in general, ignores the inhomogeneities in electron density leading to systematic shortcomings, underestimation of bond distances, overestimation of binding energies or small band-gaps.

LDA assumes that the exchange-correlation effects are local and only depend on the value of the electron density at each point. Sometimes, we need to take into account not only the local value of the electron density, but also its gradient. This leads to the generalized gradient approximation which we will explain in the next section.

[12] In a hypothetical homogeneous electron gas, an infinite number of electrons travel throughout a space of infinite volume in which there is an uniform and continuous distribution of positive charge to retain electroneutrality [117, 128].

2.4.2 Generalized Gradient Approximation

LDA fails in situations where the density undergoes rapid changes such as in molecules. An improvement to this can be made by considering the gradient of the electron density, $\vec{\nabla}\rho(\vec{r})$, as well as the electronic density, $\rho(\vec{r})$. This is the so-called Generalized Gradient Approximation (GGA) or gradient corrected functional. GGA takes into account the value of the density $\rho(\vec{r})$ at each point and how the density varies at each point $\vec{\nabla}\rho(\vec{r})$[13]. The GGA exchange-correlation energy functional can be written as:

$$E_{XC}^{\mathrm{GGA}}[\rho(\vec{r}), \vec{\nabla}\rho(\vec{r})] = \int f^{\mathrm{GGA}}(\rho(\vec{r}), \vec{\nabla}\rho(\vec{r}))\mathrm{d}\vec{r}. \tag{2.36}$$

The functional form of f^{GGA} is taken as a correction to the LDA exchange-correlation functional. The GGA exchange energy is written as:

$$E_{X}^{\mathrm{GGA}}[\rho(\vec{r}), \vec{\nabla}\rho(\vec{r})] = \int \rho(\vec{r})\epsilon_{X}^{\mathrm{hom}}[\rho(\vec{r})]F_{X}^{\mathrm{GGA}}(s), \tag{2.37}$$

F_X^{GGA} is the exchange enhancement factor and describes how much the LDA exchange energy is enhanced. The choice of F_X^{GGA} defines the type of the GGA approximation. When the density gradient is zero, $F_X^{\mathrm{GGA}} = 1$ and we obtain again LDA. s depends on the density $\rho(\vec{r})$ and on the density gradient $\vec{\nabla}\rho(\vec{r})$ as:

$$s = \frac{|\vec{\nabla}\rho(\vec{r})|}{2(3\pi^2)^{\frac{1}{3}}\rho(\vec{r})^{\frac{4}{3}}}. \tag{2.38}$$

To illustrate what F_X^{GGA} is like, two very popular GGA exchange functionals applied in this thesis are now briefly discussed. These functionals are Perdew-Wang 1991 (PW91) [138, 139] and Perdew-Burke-Ernzerhof (PBE) [140], which have the following forms:

$$F_{X}^{\mathrm{PW91}}(s) = \frac{1 + 0.19645s \cdot sinh^{-1}(7.7956s) + (0.2743 - 0.1508e^{-100s^2})s^2}{1 + 0.19645s \cdot sinh^{-1}(7.7956s) + 0.004s^4} \tag{2.39}$$

$$F_{X}^{\mathrm{PBE}}(s) = 1 + \kappa - \frac{\kappa}{(1 + \frac{\mu s^2}{\kappa})}. \tag{2.40}$$

In PW91, s has the same form as in Eq.(2.38). In PBE, κ and μ are obtained from physical constraints (non-empirical). The functional form of the GGA correlation energy (E_C^{GGA}) is expressed as complex function of s for both, PW91 and PBE. A detailed description of the PW91 and PBE correlation energy terms can be found in [138, 139] and in [124, 140], respectively. PBE is a simplification of the PW91 exchange-correlation functional, yielding almost identical numerical results with simpler formulas. A few of the most common gradient corrected correlation

[13] The way to measure how a magnitude changes in a given direction, is applying or using the gradient. More precisely, the gradient points in the direction of the greatest rate of change of the function.

functionals are PBE [140], PW91 [138,139] or Lee-Yang-Parr (LYP) [141]. Generally, LYP is applied with Becke 1988 (B88) exchange [142].

GGA approximations have reduced the LDA errors. For the geometries, ground-state energies and electronic densities of molecules and solids, GGA provides better results than LDA, including systems with hydrogen bonds. However, GGA still fails to describe dispersion interactions.

2.4.3 Meta-Generalized Gradient Approximation

Meta Generalized Gradient Approximation (Meta-GGA) are higher in accuracy than the methods described until now [143,144]. They include the local density $\rho(\vec{r})$, the gradient of the density $\vec{\nabla}\rho(\vec{r})$ and the second derivative of the density $\nabla^2\rho(\vec{r})$, i.e. kinetic energy terms $\tau(\vec{r})$.

One of the most important Meta-GGA functionals was developed by Tao's group in 2003 and is known as Tao-Perdew-Staroverov-Scuseria (TPSS) functional [144].

2.4.4 Hybrid Funtionals

The hybrid approach was introduced by Becke in 1993 [145]. The hybrid density functional methods include in DFT the exchange-correlation term an exchange portion from Hartree-Fock theory. Hybridization with Hartree-Fock exchange provides a simple improvement for the calculation of many properties in molecular systems, such as atomization energies, bond lengths and vibration frequencies, which tend to be poorly described with simple DFT functionals [146]. Some of the hybrid exchange and correlation functionals can be written as:

$$E_{XC}^{\text{hybrid}} = E_C^{\text{DFT1}} + \alpha E_X^{\text{HF}} + (1-\alpha) E_X^{\text{DFT2}} \tag{2.41}$$

where DFT1 and DFT2 can be functionals from the GGA or LDA scheme. The contribution of DFT and Hartree-Fock (HF) is weighted with α. The most common functional which belong to this scheme is Becke's 3 parameter exchange-correlation functional (B3LYP) [145, 147]. B3LYP uses 3 parameters to mix a Hartree-Fock exchange part, a LDA exchange-correlation part and a GGA (LYP) exchange-correlation part [141]. Other popular empirical parameter-free hybrid functionals are PBE0 [148] and Heyd-Scuseria-Ernzerhof (HSE) [149]. In general, hybrid functionals differ on the choice of the value of mixing parameter "α" and on the exchange-correlation DFT functional term. A diagram which collects the majority of exchange-correlation functionals is shown in Figure 2.5.

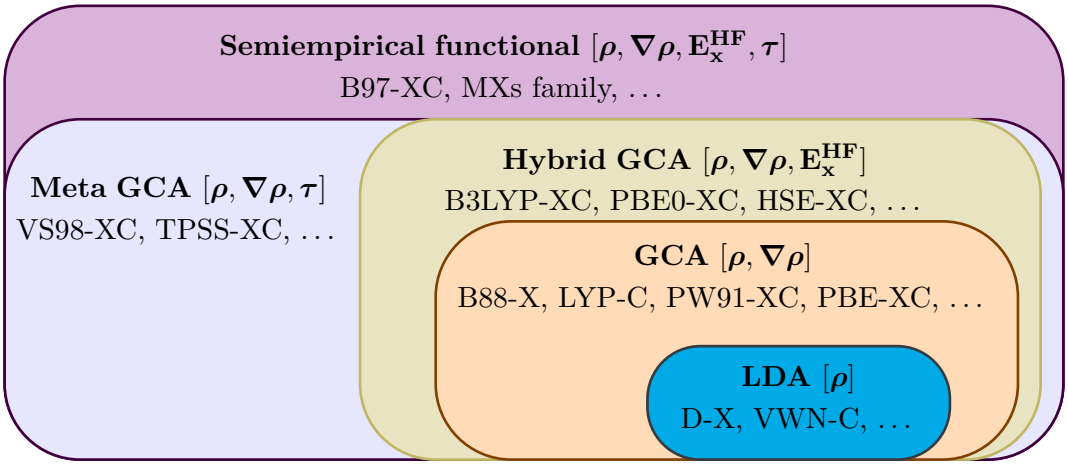

Figure 2.5: Classification of major exchange-correlation functionals. The suffix X and C indicate exchange and correlation functionals, respectively.

2.5 Dispersion Interactions and DFT

In general, DFT methods are quite good at providing geometries, dipole moments or reaction barriers with not very high computational costs. Nevertheless, there are some cases or properties which DFT can not explain very well. For example, DFT underestimates the band gaps in semiconductors and insulators and DFT calculations give inaccurate results for the *long range or dispersion interactions* between atoms and molecules. To overcome DFT inaccuracy to describe dispersion interactions, a very popular approach has been developed: *Grimme dispersion correction or DFT-D3 correction* [150–153]. DFT-D3 correction is added to a standard Kohn-Sham DFT result. Thus, the total energy is given by:

$$E_{total} = E_{KS-DFT} + E_{disp}^{DFT-D3}. \tag{2.42}$$

E_{KS-DFT} is the Kohn-Sham (KS) energy as obtained from the chosen DFT and E_{disp}^{DFT-D3} is the dispersion correction. The general form for the dispersion energy is written as:

$$E_{disp}^{DFT-D3} = -\frac{1}{2}\sum_{A\neq B}^{Natm}\sum_{n=6,8,10,...} s_n \frac{C_n^{AB}}{R_{AB}^n}. \tag{2.43}$$

The sum is over all atom pairs in the system ($Natm$). C_n^{AB} denotes the averaged (isotropic) nth dispersion coefficient (orders $n = 6, 8, 10,...$) for atom pair AB. R_{AB} is their internuclear distance and s_n are the global functional-dependent scaling factors. These factors are used to adjust the correction to the repulsive behaviour of the chosen exchange-correlation density functional. To take into account the short range behaviour of the dispersion correction a damping function $f_{damp}(R_{AB})$ must be defined. There are two principal damping functions, the Becke-Johnson damping function BJ and the zero or Chai-Head-Gordon or zero (CHG) damping function.

The zero damping function term and the energy dispersion contribution are [151]:

$$E_{disp}^{zero} = -\frac{1}{2}\sum_{A\neq B}^{Natm}\sum_{n=6,8} s_n \frac{C_n^{AB}}{R_{AB}^n} f_{damp,n}^{zero}(R_{AB}) \tag{2.44}$$

with

$$f_{damp,n}^{zero}(R_{AB}) = \frac{1}{1+6\left(\frac{R_{AB}}{s_{r,n}R_{AB}^0}\right)^{-\alpha_n}}, \tag{2.45}$$

where R_{AB}^0 is a cut-off radius for atom pair AB. $s_{r,8}$ and s_6 are held constant at 1. s_8 and $s_{r,6}$ are parameters for each DFT functional. α_6 and α_8 are set to 14 and 16, respectively. The dispersion correction energy for the BJ f_{damp} is given by [152]:

$$E_{disp}^{BJ} = -\frac{1}{2}\sum_{A\neq B}^{Natm}\sum_{n=6,8} s_n \frac{C_n^{AB}}{R_{AB}^n + f_{damp}^{BJ}(R_{AB}^0)^n} \tag{2.46}$$

with

$$f_{damp}^{BJ}(R_{AB}^0) = a_1 R_{AB}^0 + a_2 \tag{2.47}$$

and

$$R_{AB}^0 = \sqrt{\frac{C_8^{AB}}{C_6^{AB}}}. \tag{2.48}$$

$s_6 = 1$ and a_1, a_2 and s_8 are free fit parameters for each GGA functional. Some improvements of the BJ and zero damping functions have lead to the modified Becke-Johnson (BJM or D3M(BJ)) and the zero modified (zero-m or D3M) schemes [120,153]. In zerom, the zero-damping function is modified to:

$$f_{damp,n}^{zero-m}(R_{AB}) = \frac{1}{1+6\left(\frac{R_{AB}}{s_{r,n}R_{AB}^0} + \beta R_{AB}^0\right)^{-\alpha_n}}. \tag{2.49}$$

where $s_{r,8}$, s_6, α_6 and α_8 are kept fixed at the same values as before and s_8, $s_{r,6}$ and β are refitted. In BJM, the damping function is retained and solely the parameters a_1, a_2 and s_8 are refitted for several DFT functionals such as PBE, BLYP and Becke's 3 parameter exchange-correlation functional (B3LYP).

Chapter 3

Implementation of DFT

A head full of fears has no space for dreams.

In previous sections we have discussed how the total energy of a system can be calculated from first-principles, using the Density Functional Theory (DFT). We have analysed DFT in detail because this is the basis of the computational framework used in all the calculations in this work.

In this Chapter, we are going to introduce definitions, ideas and technical aspects that we need for describing the systems investigated in this thesis. We are interested in simulations of finite systems. For efficient computational implementation of DFT, the Kohn-Sham wave functions should be expanded in terms of a basis set. Basis sets can be classified in two main groups: (i) localized basis set or (ii) plane waves (PW) basis set. To describe the structures of this thesis, we have chosen the second option and then we need to transform our finite system to a periodic solid problem. This transformation allows us, by using plane waves, to characterize our structures with high accuracy and low computational cost. We have chosen Dacapo code which is a suitable computational code for describing these kind of systems. Dacapo is a plane waves based code. Its suitability is due to the efficiency of using plane waves as the basis set for the expansion of wave functions. Figure 3.1 shows a scheme with the different options to implement the computational codes which integrate numerically the Kohn-Sham equations.

3.1 Periodic Systems

A crystal is a solid formed by adding *identical* building blocks in the three dimensions of the space [154]. These blocks (one block is called *basis*) formed by one or more atoms have the same composition and arrangement. In order to describe the system we need a coordinate system, the basis and a *lattice*[1]. A lattice in three dimensions is

[1] A lattice is a set of mathematical points to which the basis is attached to.

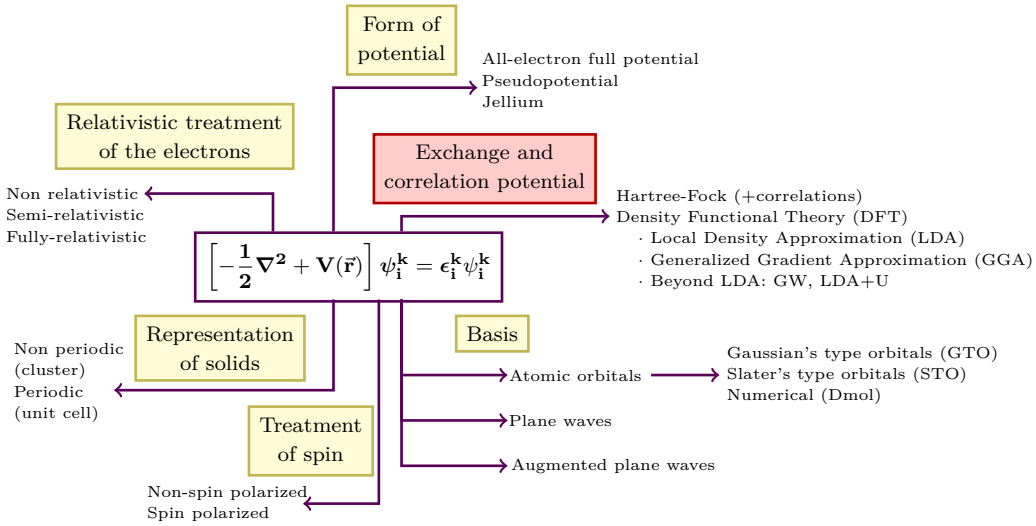

Figure 3.1: Different implementations for Kohn-Sham equation.

defined by three translation vectors $\vec{a}_1$, $\vec{a}_2$ and $\vec{a}_3$. This means that the arrangement of atoms in the crystal looks the same when is viewed from the point $\vec{r}$ as when is viewed from the point $\vec{r}'$ translated by an integer multiple of the vectors $\vec{a}_i$:

$$\vec{r}' = \vec{r} + u_1\vec{a}_1 + u_2\vec{a}_2 + u_3\vec{a}_3 = \vec{r} + \vec{T} \tag{3.1}$$

where u_1, u_2 and u_3 are arbitrary integers and the set of points $\vec{r}$, obtained from all u_i, defines the lattice. These vectors $\vec{a}_i$ are known as *unit translation vectors*. The parallelepiped (in a three-dimensional solid) defined by these translational vectors is called the *unit cell*. The unit cell with the minimum value of the volume described by the vectors $\vec{a}_i$ is called the *primitive cell*. The advantage of periodic solids is that by studying the behaviour of most properties in the primitive cell, this behaviour can be extended to the entire solid.

However, when a perturbative element is introduced in the system, for instance a punctual defect, we need to enlarge the size of the primitive cell so that the perturbative defects are isolated and they do not interact with the other perturbative elements from the repeated cells. This is the so-called **supercell method**.

3.2 Reciprocal Space

The reciprocal lattice plays a fundamental role in most analytic studies of periodic structures. The *reciprocal space* is the Fourier transform of the *real space* and it simplifies considerably the description of many material properties. The reciprocal space is defined by its reciprocal-cell vectors which are related to the real-cell vectors as:

$$\vec{b}_i = 2\pi \frac{\vec{a}_j \times \vec{a}_k}{\vec{a}_i \cdot (\vec{a}_j \times \vec{a}_k)} = 2\pi \frac{\vec{a}_j \times \vec{a}_k}{\Omega} \qquad \forall i, j, k \ \in \{1, 2, 3\}. \tag{3.2}$$

Each of these vectors is orthogonal to two axis vectors of the real lattice (see Fig.3.2), namely, they satisfy [154, 155]:

$$\vec{a}_i \cdot \vec{b}_j = 2\pi\delta_{ij}. \tag{3.3}$$

A vector of this form $\vec{G} = v_1\vec{b}_1 + v_2\vec{b}_2 + v_3\vec{b}_3$ is a *reciprocal lattice vector*. The v_i are arbitrary integers. Points in the reciprocal lattice are mapped by the set of vectors obtained from all v_i. If $\vec{T}$ is any real lattice vector, then:

$$\vec{T} = u_1\vec{a}_1 + u_2\vec{a}_2 + u_3\vec{a}_3 \tag{3.4}$$

thus from (3.3):

$$\vec{G} \cdot \vec{T} = 2\pi(u_1v_1 + u_2v_2 + u_3v_3) = 2\pi m \tag{3.5}$$

where m is any integer number. Every crystalline/solid structure has two lattices associated: real lattice and reciprocal lattice. Vectors in the real lattice have dimensions of length and vectors in reciprocal lattice of 1/length, thus, they are wave vectors and they are always drawn in Fourier space. A consequence of this is that if we make the cell longer in one direction, the allowed wave vectors in that direction become shorter, namely, the volume in the reciprocal space becomes smaller when the volume in the real space increases.

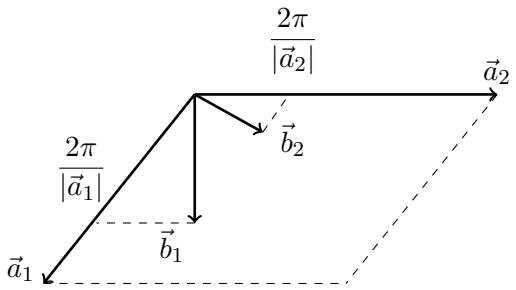

Figure 3.2: 2-dimensional relation between real-cell vectors and reciprocal-cell vectors.

The description of the primitive real cell can be done studying the correspondent primitive reciprocal cell. The primitive reciprocal cell is called *First Brillouin Zone* (FBZ).

3.3 Bloch's Theorem

As we have seen before, the electrons in a solid form a many-body problem in which the Hamiltonian includes electron-nuclei interactions Eq.(2.6) and the electron-electron interactions Eq.(2.5). We can represent all these interactions by an effective potential V_{eff}. Independently of the form of this potential, if the crystal is perfectly periodic it must to satisfy the condition $V(\vec{r} + \vec{T}) = V(\vec{r})$ for all translation vectors

$\vec{T}$ of the real lattice. The Bloch's theorem states that the wave function of the one electron Hamiltonian $H = -\frac{\hbar^2}{2m_e}\vec{\nabla}^2 + V(\vec{r})$ where $V(\vec{r}) = V(\vec{r}+\vec{T})$, can be chosen as the product of a plane wave part $e^{i\vec{k}\cdot\vec{r}}$ and a lattice periodic part or Bloch function $u_{n,\vec{k}}(\vec{r})$ [155, 156]:

$$\Psi_{n,\vec{k}}(\vec{r}) = e^{i\vec{k}\cdot\vec{r}} u_{n,\vec{k}}(\vec{r}) \tag{3.6}$$

where

$$u_{n,\vec{k}}(\vec{r}) = u_{n,\vec{k}}(\vec{r}+\vec{T}). \tag{3.7}$$

n is a discrete index called the *band* index. $\vec{k}$ is a wave vector confined to the First Brillouin Zone (FBZ). A demonstration of this theorem can be found in [154,155,157]. $u_{n,\vec{k}}$ can be expanded in Fourier series [154]:

$$u_{n,\vec{k}}(\vec{r}) = \frac{1}{\sqrt{\Omega}} \sum_{\vec{G}} C_{n,\vec{k}+\vec{G}} e^{i\vec{G}\cdot\vec{r}} \tag{3.8}$$

where Ω is the volume of the unit cell, $C_{n,\vec{k}+\vec{G}}$ are complex Fourier coefficients and the sum is over all wave vectors $\vec{G}$ [158, 159]. Each of the Fourier basis functions, $e^{i\vec{G}\cdot\vec{r}}$, represent a plane wave travelling in space (reciprocal lattice). The direction of the wave propagation is the direction of the vector $\vec{G}$, thus, the wavefront is perpendicular to the vector $\vec{G}$. The electronic wave function can be written as a sum of plane waves:

$$\Psi_{n,\vec{k}}(\vec{r}) = \frac{1}{\sqrt{\Omega}} \sum_{G} C_{n,\vec{k}+\vec{G}} e^{i(\vec{k}+\vec{G})\cdot\vec{r}}. \tag{3.9}$$

The electronic wave function is represented in terms of reciprocal space vectors within the First Brillouin Zone (FBZ).

3.4 Plane-wave (PW) Basis Set Representation

In calculations of periodic solids or surfaces, which are the principal types of systems that DFT is applied to in this thesis, plane-wave basis set is a very common choice. We have seen that the electronic wave functions (at each k-point) are expressed in terms of a discrete plane-wave basis set. This offers a complete basis set that is independent of the type of crystal (composition and atom's positions) and treats all areas of space equally. This feature is very important since the solid is considered as an infinite periodic system and thus, we need a basis set which describes the whole space. Namely, plane waves are not based around the nucleus but are spread across space. Then Kohn-Sham wave functions can be expanded with plane-wave basis sets as:

$$\Psi_{n,\vec{k}}(\vec{r}) = e^{i\vec{k}\cdot\vec{r}} \sum_{\vec{G}} C_{n,\vec{k}} e^{i\vec{G}\cdot\vec{r}} = \sum_{\vec{G}} C_{n,\vec{k}} e^{i(\vec{G}+\vec{k})\cdot\vec{r}} \tag{3.10}$$

and then, Kohn-Sham equations can be written as:

$$\sum_{G}\left[\frac{1}{2m}|\vec{k}+\vec{G}|^2\delta_{\vec{G}\vec{G}'}+V_{eff}(\vec{G}-\vec{G}')\right]C_{n,\vec{k}+\vec{G}}=\epsilon_{n,\vec{k}}C_{n,\vec{k}+\vec{G}}. \tag{3.11}$$

$\delta_{\vec{G}\vec{G}'}$ is the Kronecker δ which indicates that the kinetic energy is diagonal, $V_{eff}(\vec{G}-\vec{G}')$ is the Fourier transform of the effective potential in the real space and have the same periodicity as $u_{n,\vec{k}}(\vec{r})$ and the $C_{n,\vec{k}+\vec{G}}$ are the coefficients for the plane waves after Fourier transformation. There is an infinite number of allowed $\vec{G}$. For finding the exact solution to Eq.(3.11) an infinite number of plane waves is needed. However, the coefficients, $C_{n,\vec{k}+\vec{G}}$, for the plane waves with small kinetic energies, $|\vec{k}+\vec{G}|^2$, are more important than those with large kinetic energies. Then, the basis set can be truncated to a finite number of plane waves that have kinetic energies less than a particular value, ***energy cut-off*** (E_{cutoff}), see Fig.3.3:

$$\frac{1}{2m}|\vec{k}+\vec{G}|^2\leqslant E_{cutoff}. \tag{3.12}$$

We always have to ensure the cut-off energy is high enough to give accurate results. Using a finite basis set we are introducing approximations which may lead to less accurate results, but increasing the number of plane waves used in the expansion, namely, increasing the energy cut-off, we can avoid this problem.

On the other hand, since the *electronic density* is the square of the wave function, it can vary twice as rapidly. The density is also expanded in plane waves:

$$\rho(\vec{r})=\sum_{n}u_n^*(\vec{r})u_n(\vec{r})=\sum_{\vec{G}}\tilde{\rho}(\vec{G})e^{i\vec{G}\cdot\vec{r}}. \tag{3.13}$$

The density usually contains more plane waves than the corresponding wave function:

$$\rho_{cutoff}(\vec{r})\leqslant\frac{1}{2m}|\vec{k}+\vec{G}|^2\leqslant 4E_{cutoff}. \tag{3.14}$$

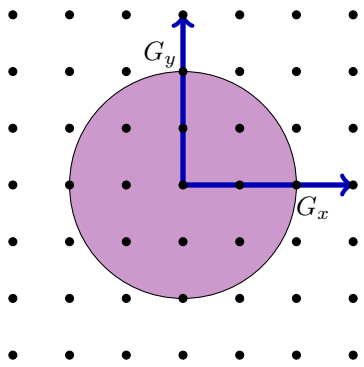

Figure 3.3: Schematic representation of the cut-off energy concept.

In practice, plane-wave basis sets are often used in combination with an "effective core potential" or *pseudopotential*, so that the plane waves are only used to describe

the valence electronic density. This is because core electrons interact strongly with nuclei, resulting in large wave function and density gradients near the nuclei which are not easily described by a plane-wave basis set unless a very high energy cut-off is used, namely, one can improve the accuracy of PWs increasing the cut-off energy.

3.4.1 K-points

Bloch's theorem allows us to only consider the electrons within the unit cell at an infinite number of k-points within the First Brillouin Zone (FBZ).In addition, wave functions at k-points which are close to each other, are quite similar, namely, the wave functions vary smoothly with respect to $\vec{k}$. This allows us to represent the First Brillouin Zone (FBZ) with a *finite* set of k-points. Thus, choosing a sufficiently dense mesh of integration points is crucial for the convergence of the results. If we increase the number of k-points, an increase in the calculation accuracy is expected. However, this leads in an increase in the computational cost. There are several efficient methods to choose special finite sets of k-points, for obtaining an accurate electronic potential, electron density, and total energy without increasing the computational cost. Some these methods are: Monkhorst-Pack method (MP) [160], Tetrahedron method [161], Evarestov-Smirnov method [162], which is a Modified Monkhorst-Pack (MMP) version for cubic systems and the Chadi-Cohen method [163] which is used for hexagonal symmetry systems. We are going to explain the first method as is the one used in our calculations.

MP method uses a homogeneous distribution of k-points over the FBZ. It generates a regular mesh of equally spaced k-points along the three reciprocal space vectors. As a consequence, the entire Brillouin zone is tiled by small polyhedra of the same shape as the Brillouin zone itself and dimensions $M_x \times M_y \times M_z$. It is necessary for well converged energy calculation that the energy does not depend on the number of k-points, namely, if for smaller number of k-points, the energy varies considerably the number of k-points is not sufficient to give good results, and should be increased. In general, a thin grid is needed, or many k-points, to describe small real cells and only one k-point, Γ point, for big real cells.

3.5 Pseudopotentials Approach

Most properties of condensed matter are given by only few electrons, the most external ones (valence electrons). The core electrons have less effect on these properties. Near the nucleus, the valence-electron wave functions show very fast oscillations due to the orthogonality between the valence-electron and core-electron wave functions. Because fast oscillations correspond to high kinetic energies, all-electron (AE) plane wave calculations demand huge computational costs. However, by realising that the

electronic structure of the core electrons remains unchanged in different chemical and physical problems, and in general is of low interest, huge computational costs can be overcome by the use of *pseudopotential approximations* [164, 165]. Pseudopotentials smooth out this region to be able to use plane waves.

This approach was proposed independently by Fermi [166] and Hellman [167] in the 1930s. Then, in the late 1950s Phillips and Kleinman [164, 168] developed a new pseudopotential method. Finally, the norm-conserving and **ultrasoft potentials** were developed in the 1980s and in the 1990s, respectively.

There are many pseudopotential methods, but all of them must accomplish some criteria, such as: (i) should be soft enough that the expansion of the valence pseudo-functions can be performed using a low number of plane waves, (ii) pseudo-wave functions must be continuous at the *core radius* or *cut-off radius* (r_{cut}) and (iii) should be transferable among different configurations. Figure 3.4 shows a typical pseudopotential, which is much weaker than the all-electron potential (Coulomb potential), and the pseudo-wave function, which has not radial nodes inside the core region ($r < r_{cut}$). The pseudo-wave functions and the pseudopotential have to be identical to the original wave functions and potentials outside the core radius. This condition has to be carefully checked to prevent the introduction of new non-physical states (the so-called *ghost states*) into the calculation.

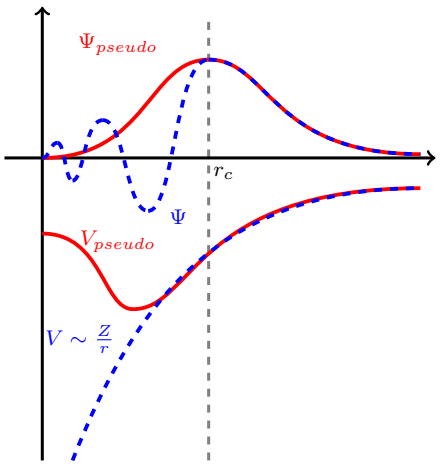

Figure 3.4: The pseudopotential approximation replaces the strong ionic potential $V \sim \dfrac{Z}{r}$ (blue) in the core region by a weaker pseudopotential V_{pseudo} (red). The corresponding set of pseudo-wave functions Ψ_{pseudo} and the all-electron wave functions Ψ are identical outside of a chosen cut-off radius $r_c = r_{cut}$. Ψ_{pseudo} does not possess the nodal structure that causes the oscillations inside r_c.

There are two principal pseudopotential methods: norm-conserving (NC) pseudopotentials (PP) and Ultrasoft Pseudopotentials (USPP), also known as Vanderbilt pseudopotentials [169]. The Ultrasoft Pseudopotentials scheme is the procedure used in this thesis for performing the calculations. Ultrasoft Pseudopotentials were

introduced in order to fill the gaps that the norm-conserving methods left. The principal idea is to break the *norm conservation rule*[2] in order to reduce the basis set size. This leads to a deficit in the charge inside the core region which is compensated with additional charges in that region. These additional charges are defined as:

$$Q_{ij} = \langle \Psi_i^{AE} | \Psi_j^{AE} \rangle_R - \langle \Psi_i^{USPP} | \Psi_j^{USPP} \rangle_R \tag{3.15}$$

where R is a radius which is chosen large enough that pseudo and AE potential and wave functions agree at R. In order to recover the full electronic charge, the electron density given by the square moduli of the wave functions is augmented in the core region. The electron density can be subdivided into a hard part localized in the core regions and a soft part localized outside the core regions. Thus pseudo-wave functions are allowed to be as soft as possible within the core, yielding an important reduction in the cut-off energy. The combination of DFT, plane-wave basis set and pseudopotentials has become a well-established methodology of the present day DFT calculations.

3.6 Simulation Techniques

All the methods and procedures explained previously in this Chapter have served to introduce DFT as a practical technique to calculate electronic structures. Nowadays, there are several DFT codes in the market to study the properties of the materials. We can divide the different codes in many ways: if they are periodic or not, if they incorporate all the electrons or a pseudopotential, the basis set used to expand the wave functions, etc. We have chosen the second way, (i) the all-electron codes, which include all the electrons surrounding the atoms, and (ii) the pseudopotential-based codes. In the first category we can find very popular codes such as WIEN2k [170] or Gaussian [171, 172]. In the second category we can find: *Dacapo* code [173], VASP [174–177], ABINIT [178] and QUANTUM ESPRESSO [179] which all use plane-waves basis sets and SIESTA [180] which uses atomic orbitals basis sets. In this thesis the principal code used has been **Dacapo** code.

As we have said, the common procedure to calculate the electronic structure of a system through DFT starts with an initial electronic density from which the corresponding effective potential V_{eff} is calculated. Finally KS equations (Eq.(2.28)) are solved. The process is repeated until it converges, see Figure 2.4. Different convergence criteria are used to achieve the final electronic density. If the requirements to accomplish the convergence criteria are not reached in the loop between two iterations, a new cycle is started with the new electronic density[3].

[2]The norm conservation states: $\int_0^{r_c} |\Psi_{PS}(\vec{r})|^2 r^2 \mathrm{d}\vec{r} = \int_0^{r_c} |\Psi_{AE}(\vec{r})|^2 r^2 \mathrm{d}\vec{r}$. AE is All-Electron and PS is Pseudopotential.

[3]Unfortunately, when we use the electronic density obtained from the previous iteration, it

3.6.1 Structural Relaxation

We need to find the structure with the lowest energy. To do this, there are many algorithms which calculate the energy and forces among atoms. Structural relaxation uses the forces on the atoms to find the equilibrium structure of the system. Namely, for a given configuration, a self-consistent single-point calculation is carried out, and from this, the forces are obtained. Then each atom is moved along the direction of the force acting on that atom. The process is continued while these forces are greater than some minimum tolerance and when the tolerance limit is reached, the process is stopped.

We start from different structures to ensure that we find the structure with the lowest energy under our specific conditions. Obtaining the equilibrium structure is of capital importance for studying the geometry, the associated energy and the electronic density. We also need to establish some criteria for controlling the convergence of the forces that we present in the next section.

3.6.2 Dacapo Code

Dacapo is a DFT based code to calculate structures, total energies, electron density and related properties of a system of many atoms. It uses a plane-wave basis set for the valence electronic states and describes the interactions between core and valence electrons with Vanderbilt ultrasoft pseudopotentials. The program performs self-consistent calculations for both Local Density Approximation (LDA) and various Generalized Gradient Approximation (GGA) exchange-correlations potentials, using iterative algorithms. The code may perform molecular dynamics and structural relaxations. Calculations using Dacapo are done using the Atomic Simulation Environment (ASE)[4] [181].

For starting, we need a file where all the configurations for the system under study have to be given to the Dacapo *calculator*[5]. To run a calculation in Dacapo, we need to set:

- The “plane wave cut-off" (explained in section 3.3). In this thesis, unless explicitly indicated, we use **350 eV**.
- The density cut-off: **1000 eV**.

usually leads to important instabilities. To avoid this, it is common to mix the three last electronic densities.

[4]The Atomic Simulation Environment (ASE) is a set of tools and Python modules for setting up, manipulating, running, visualizing and analysing atomistic simulations.

[5]In ASE, a calculator is a black box that can take atomic numbers and atomic positions from an “atoms object file” and calculate the energy and forces and sometimes also stresses.

- The number of occupied bands: we set, in general, a number of occupied bands $n = \sum_i^N n_i \frac{n_{ei}}{2}$ where the index $i = 1, ..., N$ indicates the different types of atoms, n_i is the number of atoms of i-type and n_{ei}[6] is the number of valence electrons of atoms of i-type. We always set a few more bands that those strictly needed. For example, if we had three carbon and two palladium atoms, with four and ten valence electrons, respectively, then the minimum number of bands would be $n = 3\frac{4}{2} + 2\frac{10}{2} = 16$.

- The cell size: for all our calculations the supercell chosen is: $\vec{\boldsymbol{a}}_{\mathbf{1}} = (12.33, 0, 0)$Å, $\vec{\boldsymbol{a}}_{\mathbf{2}} = (6.1661, 10.68, 0)$Å and $\vec{\boldsymbol{a}}_{\mathbf{3}} = (0, 0, 14)$Å. This size is big enough to fit all the orbitals of the atoms, but allowing that the calculations do not become much expensive. It is also big enough to avoid interactions between images in different supercells.

- The XC functional: **PW91** for both, exchange and correlation functionals. When dispersion-interaction correction is calculated (Grimme model) the PBE exchange-correlation functional is applied.

- The number of k-points: we use the Monkhorst-Pack scheme explained above and set $\mathbf{k_x = 2}$, $\mathbf{k_y = 2}$ **and** $\mathbf{k_z = 1}$. The FBZ is small enough to be represented with this number of k-points.

- Spin polarized: all our calculations allow for spin polarization, namely, the spin is not fixed nor neglected.

- Two output files: out.nc and out.txt, for each calculation.

Table 3.1: Computational approximations and parameters.

XC-Functional	GGA-PW91
Pseudopotential	Vanderbilt ultrasoft
Fermi Temperature	0.005 K
Spin polarization	yes
k-points	[2,2,1] Monkhorst-Pack
Basis set	Plane waves
Density cut-off	1000 eV
Energy cut-off	350 eV

When setting the number of bands we need to specify the occupation statistics and the **Fermi-Dirac (FD) statics**[7] is chosen for this thesis, Fig.3.5. As FD statistics

[6] n_{ei} is divided by two as each band can accommodate two electrons (spin up and down).
[7] Fermi-Dirac (FD) statistics is applied to identical particles with half integer spin.

depends on the electronic temperature, we have chosen a small value, **0.005 K**, to avoid fractional occupancies as much as possible. All these parameters can not be changed if we are going to compare properties between systems. Table 3.1 summarizes the parameters described above.

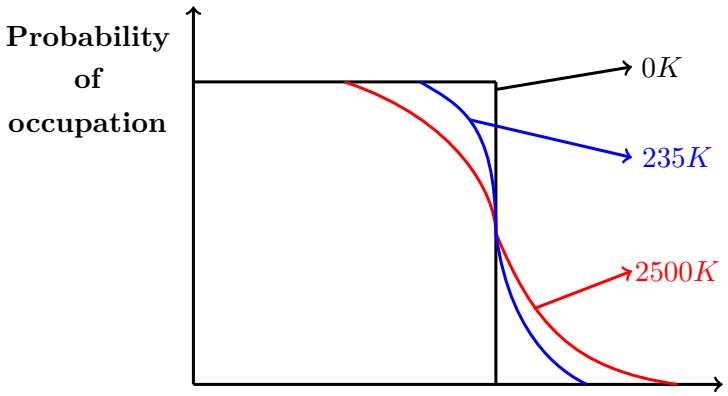

Figure 3.5: Fermi-Dirac statistics as a function of the temperature.

Other parameters that do not change in our calculations are the parameters defined to accomplish the convergence criteria[8]. These parameters, called *control of the convergence of the electronic cycles*, are used to stop the calculations when the iterations and repetitions reach the chosen tolerance values. In our case, energy convergence **0.0005 eV**, density convergence **0.01 eV**, maximum number of iterations **8000**[9] and occupation states convergence **0.01**. For the control of the convergence of the relaxation of the geometry (see 3.6.1), this is the forces, we have set the absolute force change at **0.05 eV/Å** and for the relative force change **0.05%**. All these parameters are introduced with the positions of the atoms, magnetic moments and the cell size in a input file with extension **.py**.

Finally, since Dacapo code does not include dispersion interactions we have calculate them using Grimme's DFT-D3 program combined with the PBE functional for exchange-correlation. The reason for using PBE is that the PW91 functional has not been implemented in the DFT-D3 program.

Nudged Elastic Bands (NEBs)

A common and important problem in condensed matter is the identification of a lowest energy pathway for a rearrangement of a group of atoms from one stable configuration to another. The nudged elastic band (NEB) method is a technique for finding transition paths (and corresponding energy barriers) between given initial and

[8]Convergence parameters are parameters defined to stop the calculation when some good criteria, which depends on the system of study, are satisfied or reached.

[9]This parameter is used when the system does not converge and we need the calculation to be stopped.

final states. Also, the possible intermediates and transition states are identified. The method involves constructing and optimizing a number of intermediate images which should be considered snap shots of the system during an event with an energetic barrier. These images are coupled and relaxed together, to form a time like evolution of the system during the event. Dacapo code is able to perform NEBs calculations. The basic parts in a NEB step is as follows: The set of images (N) between the initial and final states, in our case around **eight** images, is obtained by linear interpolation. The N images are optimised with respect to all degrees of freedom except that of the reaction pathway. A spring constant is added to ensure the continuity of the path and maintaining equal spacing to its neighbouring images. The total force acting on an atom is the sum of the spring force (parallel to the pathway) and the physical and chemical forces (perpendicular to the pathway). These forces are calculated by Dacapo. After forces of all images are obtained, the coupling between images are calculated by the NEB module and finally the atoms are moved in each image. This cycle is repeated until the reaction path is converged.

Chapter 4

H_2 Adsorption on Pd Clusters Supported on a Graphene Vacancy

Compassion without curiosity is ineffective.
Curiosity without compassion is inhuman.

Victor Weisskopf.

Several experimental works [33, 44, 47, 50, 76, 77, 93] indicate that the hydrogen storage capacity of nanoporous carbon materials is enhanced by doping them with Pd atoms and clusters. The walls of the pores of nanoporous carbons can be mimicked by graphene layers [40, 182] and previous studies have investigated the adsorption of hydrogen on pristine graphene doped with Pd clusters [80, 183, 184]. However, the bonding of the Pd clusters with the pristine graphene is quite weak, and desorption of Pd_6-H_2 complexes competes with the desorption of hydrogen [80]. Pd_6-H_2 might inhibit the beneficial effect of Pd doping. To overcome this problem, it has been proposed [81] to attach the Pd atoms and clusters to defects of the graphene layer, for instance graphene vacancies. In this Chapter we have investigated the effect that anchoring Pd_6 clusters on graphene mono-vacancies has on the adsorption channels of hydrogen (molecular adsorption and dissociative chemisorption) and on hydrogen desorption. We have studied the competition between those two adsorption channels as a function of the number of adsorbed molecules. Moreover, we have analysed the competition between desorption of hydrogen and the desorption of Pd-H complexes. This Chapter is organized as follows: In Section 4.1 we provide a brief description of the theoretical model. The references and a detailed discussion of the results can be found in the accompanying article (Section 4.2). Section 4.3 reports some updates to the results of the paper included in Section 4.2 and additional results that complete the results presented in that paper. A discussion on activation energy barriers for several partial processes of interest is included. Finally, in Section 4.4 some conclusions are provided.

4.1 Theoretical Model

Computational simulations investigating the preferred channels for hydrogen adsorption were performed. The computational details are identical to the ones which have been already described in Section 3.6.2 and have been summarized in Table 3.1.

A defective graphene mono-layer has been considered as appropriate model for the walls of nanoporous carbon materials. Three dimensional palladium aggregates are grown and strongly adhered to graphene vacancies. Then, an extensive search for the preferred sites for the adsorption of hydrogen atoms and molecules has been performed and the structures have been fully optimized until the energies were converged within 10 meV. A more complete description of the theoretical model can be found in the accompanying article.

4.2 Publication: Competition Between Molecular and Dissociative Adsorption of Hydrogen on Palladium Clusters Deposited on Defective Graphene

RSC Advances

PAPER

View Article Online
View Journal | View Issue

Cite this: *RSC Adv.*, 2015, **5**, 47945

Competition between molecular and dissociative adsorption of hydrogen on palladium clusters deposited on defective graphene

Alejandra Granja,[a] Julio A. Alonso,[ab] Iván Cabria[a] and María J. López*[a]

Received 27th February 2015
Accepted 8th May 2015

DOI: 10.1039/c5ra08091f

www.rsc.org/advances

The contribution of Pd doping to enhance the hydrogen storage capacity of porous carbon materials is investigated. Using the Density Functional Formalism, we studied the competition between the molecular adsorption and the dissociative chemisorption of H_2 on Pd clusters anchored on graphene vacancies. The molecular adsorption of H_2 takes place with energies in the range of 0.7–0.3 eV for adsorption of one to six hydrogen molecules. Six molecules saturate the cluster, and additional hydrogen could only be adsorbed, with much smaller adsorption energies, at farther distances from the cluster. Dissociative chemisorption is the preferred adsorption channel from one to three hydrogen molecules, with adsorption energies in the range of 1.2–0.6 eV. After the first three molecules are dissociatively chemisorbed, three additional hydrogen molecules can be adsorbed non-dissociatively onto the Pd cluster with adsorption energies of 0.5 eV. The desorption of Pd–H complexes is prevented in all cases because the Pd clusters are firmly anchored to graphene vacancies. Our results are very promising and show that Pd clusters anchored on graphene vacancies retain their capacity to adsorb hydrogen and completely prevent the desorption of Pd–H complexes that would spoil the hydrogen releasing step of the cycle.

1 Introduction

The successful storage of hydrogen is a technological requirement to boost its use in electric cars powered by hydrogen fuel cells. However, the technological problem of storing 5.5 wt% hydrogen[1] at room temperature and moderate pressures remains elusive and efforts are being invested in different directions.[2] The most promising technologies focus on the storage of hydrogen adsorbed in light solid materials, such as porous carbons. These materials exhibit a reasonably high storage capacity[3,4] of about 6 wt% hydrogen at low temperatures (77 K) but their capacity drops dramatically to about 1 wt% hydrogen at room temperatures and moderate pressures, which is far from the technological requirement. Optimization of the size and shape of the pores yields some improvement[5,6] but the hydrogen storage capacity of these materials remains too low for practical application. The main difficulty arises from the small adsorption energy,[7–10] below 100 meV, of hydrogen to the pore walls.

A recent experimental work by Contescu *et al.*[11] indicated an enhancement in the hydrogen storage capacity of porous carbon materials doped with palladium. It is, therefore, of great interest to understand and explain the mechanisms through which the Pd dopant contributes to the enhancement of the storage capacity of these materials. Recent computer simulations of the structure of nanoporous carbons performed by some of the authors[12] indicate that the walls of the pores are one atom thick planar or curved graphene-like layers containing defects. These results suggest that the pore walls of these materials can be modeled through a combination of pristine and defective graphene layers. Previous work has focused on the study of hydrogen adsorption on palladium atoms[13,14] and clusters[15] deposited on pristine graphene. We have shown[15] that hydrogen adsorption takes place with enhanced adsorption energies, which seems to indicate a beneficial effect of palladium doping on the hydrogen storage capacity of porous carbons. However, since the bonding of the palladium clusters with the pristine graphene layer is relatively weak, about 1 eV, desorption of Pd–H complexes competes with the desorption of hydrogen. Evidently, the desorption of hydrogen is a key step in the storage cycle and, therefore, the desorption of Pd–H complexes may inhibit the beneficial effect of Pd doping.

We have proposed,[16] as a way to overcome this difficulty, to attach the Pd atoms and clusters to defects of the graphene layer, for instance to graphene vacancies. Pd atoms and clusters attach strongly to the vacancies, where they get firmly anchored to the graphene layer. Preliminary results on the adsorption of molecular hydrogen on a single Pd atom saturating a graphene vacancy[16] or a vacant site in the wall of a carbon nanotube,[17] CNT, were quite promising. In this paper we have investigated

[a]*Departamento de Física Teórica, Atómica y Óptica, Universidad de Valladolid, 47011, Valladolid, Spain. E-mail: maria.lopez@fta.uva.es; Fax: +34-983-423013*
[b]*Donostia International Physics Center, 20080 San Sebastián, Spain*

the effect that anchoring small Pd clusters on graphene vacancies has on the adsorption/desorption of molecular hydrogen. This effect cannot be inferred from previous studies on pristine graphene. We have performed simulations, using the Density Functional Formalism, investigating the different adsorption channels, molecular and dissociative, of hydrogen on Pd clusters anchored on graphene vacancies, and the competition between those channels as a function of the number of adsorbed molecules. We have also studied the desorption step and the competition between desorption of hydrogen and desorption of Pd–H complexes. In Section 2 we present the key features of the Density Functional Formalism used in our computer simulations. Section 3 presents the results and we finish with some Conclusions in Section 4.

2 Theoretical model

We investigated the adsorption of hydrogen on a Pd_6 cluster anchored on a graphene vacancy using the Density Functional Formalism (DFT). The graphene layer is considered here as a model of the graphitic walls of nanoporous carbon materials, and the vacancies simulate defects of the walls. As we have shown in previous works,[15,18] palladium exhibits a strong tendency to aggregate and form three dimensional clusters on the surface of graphene. The clusters grow preferentially in the neighborhood of vacancies of the graphene layer, where they attach strongly. The DFT calculations were performed with the DACAPO code.[19] The code implements the supercell methodology. The graphene layer is represented by a supercell containing 5×5 hexagonal unit cells, each of which contains two C atoms (see Fig. 1). Thus the supercell size in the X direction is 12.33 Å. In the Z direction the supercell is taken to be large enough (14 Å) to avoid interactions between the images of the graphene layer in different supercells. The interactions of the valence electrons with the nuclear cores are described through Vanderbilt ultrasoft pseudopotentials.[20] A basis set of plane waves is used to expand the wave functions and the electronic density, with cutoff values of 350 eV and 1000 eV, respectively, for good convergence. We considered four k points in the first Brillouin zone, following the Monkhorst–Pack scheme.[21] Since the supercells used in the calculations are quite large, this selection is sufficient to guarantee convergence in the cohesive energies better than 10 meV. The generalized gradient approximation of Perdew and Wang (GGA-PW91)[22] for the exchange–correlation functional is employed. An extensive search on the possible adsorption sites of the hydrogen molecules and of the hydrogen atoms of the dissociated molecule on the Pd_6 cluster has been performed. The search included the adsorption of hydrogen molecules and of hydrogen atoms on the vertices, edges and faces of the Pd_6 cluster. Then, all the structures, the graphene layer with the vacant site, the Pd_6 on the graphene monovacancy and the molecular and dissociated hydrogen adsorbed on the supported palladium clusters, were fully optimized until the forces acting on all the atoms were smaller than 0.05 eV $Å^{-1}$.

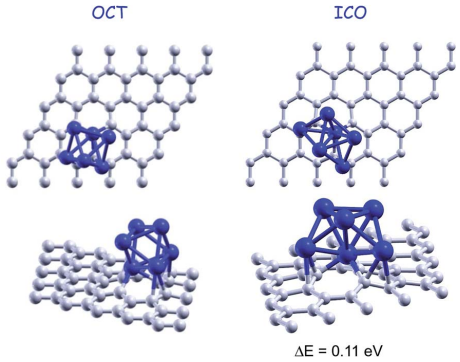

Fig. 1 Top and side views of the octahedral structure, OCT, and the icosahedral-type structure, ICO, of Pd_6 adsorbed on a graphene vacancy. The OCT structure binds to the graphene vacancy with an energy of 5.62 eV. The adsorbed ICO structure is 0.11 eV higher in energy than the OCT structure.

3 Results

We investigated the mechanisms of adsorption of hydrogen on Pd_6 clusters bound to a graphene vacancy. Pd_6 clusters are taken as representatives for clusters in the small size range. The lowest energy octahedral, OCT, structure of free Pd_6 clusters experiences only a minor distortion upon deposition on a graphene layer with a vacancy, although it adsorbs with a substantial energy of 5.62 eV (see Fig. 1). Pd_6 rests supported on one of its triangular faces. One of the Pd atoms of this face is sitting above the center of the vacancy, saturating the dangling bonds of the three C atoms around the vacant site. The other two Pd atoms are above two C–C bonds around the vacancy. The graphene layer distorts about the vacancy and the adsorbed Pd cluster. The C atoms in direct contact with the Pd-saturated vacancy get out of plane (in the direction of the Pd cluster) about 0.5–0.7 Å and the next shell of C atoms (counted from the vacancy) about 0.3–0.4 Å. The magnetic moment $\mu = 2\mu_B$ of the free Pd_6 cluster is quenched down to zero upon adsorption on the vacancy. This is in contrast with Pd_6 deposited on pristine graphene, which retains the magnetic moment of the free cluster. Molecular hydrogen may adsorb on the Pd_6 clusters anchored on graphene vacancies following two adsorption modes: (i) molecular adsorption, in which the molecule is slightly activated but the hydrogen atoms remain bound to each other and (ii) dissociative adsorption, in which the molecule is broken and each hydrogen atom chemisorbs independently to the Pd cluster. These two adsorption modes were also found for hydrogen adsorption on palladium clusters supported on pristine graphene. We have studied in detail the competition between the two adsorption channels for palladium clusters anchored to a graphene vacancy as a function of the hydrogen content, that is, as additional hydrogen molecules adsorb into the clusters. The adsorption energies of the successively attached hydrogen molecules to the Pd clusters are defined as

$$E_{ad}^{nth}(H_2) = E[(n-1)H_2 + Pd_6 \text{ on } G_{vac}] + E(H_2) - E[nH_2 + Pd_6 \text{ on } G_{vac}], \quad (1)$$

where $E[nH_2 + Pd_6 \text{ on } G_{vac}]$ is the energy of the system with n adsorbed hydrogen molecules, $E[(n-1)H_2 + Pd_6 \text{ on } G_{vac}]$ is the energy of the system with $n-1$ adsorbed molecules, and $E(H_2)$ is the energy of a free hydrogen molecule. Clearly, $E_{ad}^{nth}(H_2)$ gives the adsorption energy for the n^{th} hydrogen molecule adsorbing on a palladium cluster with $n-1$ adsorbed hydrogen molecules. This definition is valid for molecular adsorption and dissociative chemisorption, and, in each case, the configuration of the system with $n-1$ adsorbed molecules and the adsorption channel of the n^{th} hydrogen molecule will be indicated.

3.1 Molecular adsorption of hydrogen

The preferred site for the molecular adsorption of H_2 is on top of one of the Pd atoms which is not in direct contact with the graphene surface. The same behaviour was found for hydrogen adsorption on Pd_6 deposited on pristine graphene. The adsorption energy is 0.74 eV, somewhat higher than the adsorption energy, 0.56 eV, on Pd_6 supported on pristine graphene. The hydrogen molecule is slightly activated and the H–H distance becomes 0.86 Å. A slightly smaller activation, with H–H distances of 0.79–0.80 Å, is found for hydrogen molecules adsorbed on single Pd atoms saturating graphene or CNT vacancies.[16,17] The H–H distance of the free H_2 molecule is 0.75 Å. The H–H bond is weakened but not broken. One hydrogen molecule can adsorb on top of any of the Pd atoms of the cluster, except on top the Pd atom which is saturating the vacancy. The adsorption energies are quite similar, about 0.7 eV, for the three Pd atoms which are not in direct contact with the graphene layer, and are substantially reduced to 0.3–0.4 eV for the two Pd atoms directly in contact with the graphene surface.

Fig. 2 shows the structures of the successive adsorption of molecular hydrogen on the OCT structure of Pd_6 anchored on a graphene vacancy. With the first molecule adsorbed, a second hydrogen molecule adsorbs preferentially on top of a different Pd atom, with a practically identical adsorption energy, 0.73 eV. Adsorption of a second molecule on top of the same Pd atom as the first one leads to a smaller adsorption energy of 0.44 eV. A somewhat lower adsorption energy, 0.53 eV, than the first two molecules is found for adsorption of the third hydrogen molecule on top of the remaining Pd atom which is not in direct contact with the graphene surface. On the other hand, adsorption on one of the occupied vertices leads to a smaller adsorption energy, 0.40 eV. The fourth and fifth hydrogen molecules can still be adsorbed on the two Pd atoms which are not occupied by previous hydrogen molecules, the two Pd atoms supported on the graphene layer, with adsorption energies of 0.47 and 0.34 eV, respectively. However the fourth molecule has a slightly higher adsorption energy, 0.50 eV, for adsorption on one of the vertices which is not in direct contact with the graphene surface, although it is already occupied by another H_2 molecule. Then the fifth molecule adsorbs on one of the Pd atoms in contact with the graphene surface with an energy of 0.36 eV, and a sixth molecule may adsorb on the remaining Pd atom in contact with graphene with an energy of 0.34 eV. All these results are summarized in Table 1. The distance between the hydrogen molecules and the corresponding Pd atoms where they are attached is quite constant, about 1.7–1.8 Å, for the first 6 hydrogen molecules adsorbing onto the Pd_6 cluster supported on the graphene vacancy. This distance is about 10% smaller than the distance of 2.0 Å between the hydrogen molecule and a single Pd atom saturating a graphene[16] or a CNT[17] vacancy. This indicates a stronger interaction of the hydrogen molecules with the Pd clusters than with the Pd atoms saturating carbon vacancies.

Direct adsorption of six hydrogen molecules seems to be the saturation limit on Pd_6 anchored on a vacancy. Because of the steric effects produced by the presence of the supporting graphene layer and by the previously bound hydrogen molecules, the seventh molecule cannot attach directly to the Pd cluster. This molecule will begin forming a second hydrogen shell around the Pd cluster, at a substantially longer distance, 3.2 Å, than the hydrogen molecules of the first layer, and with quite a small adsorption energy of the order of a few tens of meV. This adsorption strength is similar to that found for the second hydrogen layer covering pure carbon nanotubes.[23] We are not investigating this second layer because molecules having such small adsorption energies are not relevant for hydrogen storage at normal temperatures.

3.2 Dissociative chemisorption of hydrogen

The dissociative chemisorption channel is preferred over the molecular adsorption of hydrogen. The hydrogen molecule dissociates and the two hydrogen atoms adsorb on a face and an edge of the octahedron, respectively. The chemisorption energy of 1.03 eV is substantially larger than the molecular adsorption energy. The adsorption of the hydrogen atoms on two faces of the octahedron is slightly less stable, by only 0.05 eV (see Fig. 3). Those structures, however, do not correspond to the lowest energy configuration. The dissociative chemisorption of hydrogen induces a structural transition in the palladium cluster from the octahedral structure to the structure of an incomplete pentagonal bipyramid in which one of the atoms of the pentagonal base is missing. One of the apex atoms of the bipyramid saturates the vacant site of graphene and the two base Pd atoms next to the empty base position attach to two C–C bonds, respectively, around the vacancy. We will refer to this Pd_6 structure as the ICO structure, because it can be viewed as part of an icosahedron (see Fig. 1). We find a distortion of the graphene layer around the ICO structure of Pd_6 similar to that about the OCT structure. The ICO structure of the free Pd_6 cluster has a cohesive energy 0.29 eV lower (less stable) than the octahedral structure. Upon adsorption on a graphene vacancy the ICO structure gains some stability but it is still 0.11 eV less stable than the supported octahedron. It is the dissociative adsorption of hydrogen that prompts the structural change. The two hydrogen atoms attach to the two non-adjacent triangular faces at the side of the bipyramid whose apex atom is not the one saturating the vacancy (upper side of the bipyramid, for

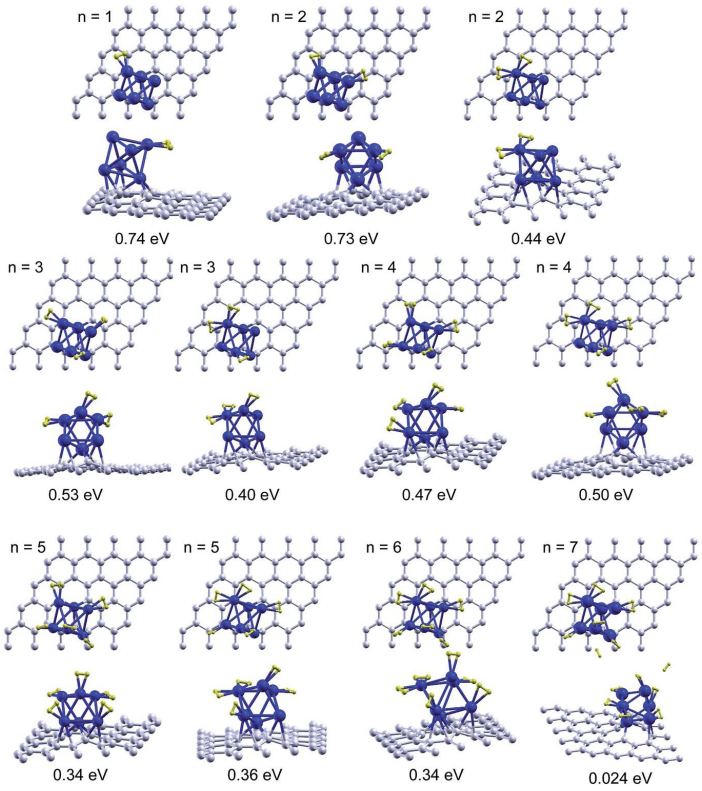

Fig. 2 Top and side views of successive molecular adsorption of hydrogen on the OCT structure of Pd_6 anchored on a graphene vacancy. The reported energies are the adsorption energies of the last hydrogen molecule calculated using eqn (1).

Table 1 Successive adsorption of hydrogen, in the molecular channel, on Pd_6 with octahedral structure anchored on a graphene vacancy. The star (*) indicates the most stable configuration of the molecular channel with a fixed number n of molecules adsorbed on the Pd_6 cluster. The adsorption energies are calculated from eqn (1) where $E[(n-1)H_2 + Pd_6 \text{ on } G_{vac}]$ is the energy of the most stable configuration of the molecular channel with $n-1$ adsorbed molecules. The energies are given in eV

n	Different vertices E_{ad}^{nth}	Two in same vertex E_{ad}^{nth}
1	0.74*	
2	0.73*	0.44
3	0.53*	0.40
4	0.47	0.50*
5	0.34	0.36*
6		0.34*

further reference). The hydrogen chemisorption energy, 1.25 eV per molecule, is 0.22 eV higher than the adsorption energy of the dissociated molecule on the octahedral structure. The chemisorbed structures are shown in Fig. 3. The dissociative chemisorption of hydrogen is also the preferred adsorption channel on Pd_6 supported on pristine graphene, with an energy of 1.30 eV. However, in this case the chemisorption of hydrogen does not induce a structural change in the Pd cluster.

3.3 Competition between dissociative chemisorption and molecular adsorption of hydrogen

We investigated the adsorption of several hydrogen molecules, and the competition between dissociative chemisorption and molecular adsorption. We started with the lowest energy ICO structure of Pd_6 supported on a graphene vacancy with one dissociatively chemisorbed hydrogen molecule, and investigated the adsorption of additional molecules. The structures are shown in Fig. 4. A second hydrogen molecule adsorbs preferentially on the upper side of the bipyramid following the dissociative chemisorption channel, with an adsorption energy of 0.90 eV. This energy is reduced slightly with respect to the chemisorption of the first molecule. One of the hydrogen atoms becomes attached to the remaining face of the upper side of the bipyramid, and the second atom to one Pd–Pd bond of the

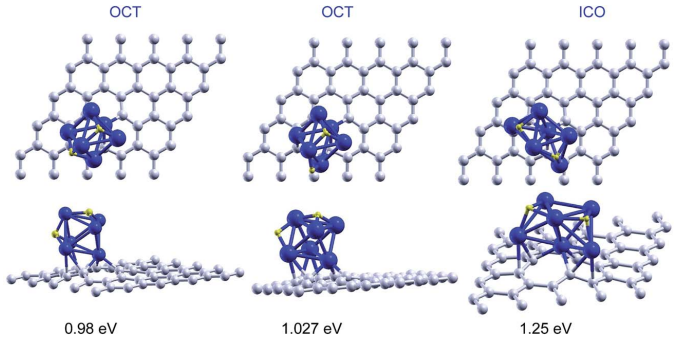

Fig. 3 Top and side views of the dissociative chemisorption of one hydrogen molecule on the OCT and ICO structures of Pd_6 anchored on a graphene vacancy. The reported energies are the adsorption energies calculated using eqn (1) for $n = 1$.

bipyramid base, and one of the previously attached H atoms moves a little from a face position to above a Pd–Pd bond. This molecule may also attach as a nondissociated molecule on top of one of the Pd atoms of the base not in direct contact with the graphene layer, with almost the same energy of 0.87 eV. For adsorption of a third molecule, the two adsorption channels are almost degenerate in energy. The adsorption energies of a third molecule on Pd_6 with two dissociated hydrogen molecules are 0.61 eV (molecular adsorption) and 0.58 eV (chemisorption). The dissociative channel is only 30 meV less stable than the molecular channel, which is within the limits of accuracy of our calculations. The dissociative chemisorption of the third molecule changes the adsorption site of one H atom, pushing it out of face. Then, finally, one H atom is attached to a face and the remaining H atoms attach to different Pd–Pd bonds. A fourth molecule cannot dissociate on Pd_6 with three dissociated hydrogen molecules. The adsorption energy is negative, −0.27 eV, which means that this is not a bound state with respect to a desorbed hydrogen molecule. Instead, the fourth molecule attaches as a molecule to one of the Pd atoms of the cluster with an adsorption energy of 0.51 eV. Almost degenerate in energy, although slightly more stable, 0.52 eV, is the configuration with two dissociated molecules and two non-dissociated adsorbed molecules. The successive molecular adsorption of the fifth and sixth hydrogen molecules on the Pd_6 with three dissociated and one non-dissociated adsorbed hydrogen molecules takes place with adsorption energies of 0.52 eV and 0.42 eV, respectively. The adsorption energies drop dramatically down to 0.16 eV, 0.10 eV, and 0.09 eV, respectively, for the successive adsorption of three more hydrogen molecules. Adsorption energies below 0.2 eV are of little interest for the storage of hydrogen at room temperature. In summary, Pd_6 is able to chemisorb dissociatively up to three hydrogen molecules, and to adsorb, with reasonably high energies, three non-dissociated additional molecules. These results are summarized in the columns labelled as ICO of Table 2. The transition from stable dissociative chemisorption to molecular adsorption takes place when all the favorable sites of the upper side of the bipyramid (faces and Pd–Pd bonds not in direct contact with the graphene surface and not involving the Pd atom saturating the vacancy) have been filled. Note that due to steric effects it is not possible to fill out all the favorable faces and edges. For instance, the adsorption of H atoms on two edges of a triangle prevents the adsorption of a H atom on the face.

For completeness, we also studied the competition between dissociative and molecular adsorption on the octahedral structure, OCT, of the anchored Pd_6 cluster with one dissociatively chemisorbed hydrogen molecule. The dissociative channel is preferred for the adsorption of the second hydrogen molecule, with an adsorption energy of 0.81 eV, whereas the molecular adsorption energy is 0.78 eV. The third hydrogen molecule adsorbs on Pd_6 with similar energies of 0.65 eV and 0.62 eV for the dissociative and the molecular channels, respectively. In contrast to the ICO case, the fourth molecule can dissociate on the octahedral Pd_6 cluster with three dissociated hydrogen molecules, but the adsorption energy is very small, 0.03 eV, with respect to the desorbed molecule. However the fourth molecule can attach as a non-dissociated molecule with an energy of 0.56 eV. The fifth and sixth hydrogen molecules can also attach as non-dissociated molecules with adsorption energies of 0.48 eV and 0.50 eV, respectively. A seventh molecule cannot attach directly to the Pd cluster and begins to form a second layer at a larger distance and with a much lower adsorption energy. Those structures are shown in Fig. 5 and the results are summarized in the columns labelled as OCT of Table 2.

From our results we conclude that the successive adsorption of hydrogen on Pd clusters anchored on graphene vacancies does not depend much on the structure of the Pd clusters, since a similar behaviour has been found for Pd_6 in the ICO and the OCT structures. Once the Pd cluster is saturated with dissociated hydrogen molecules, it is still able to adsorb more hydrogen following the molecular channel. Therefore, the Pd clusters anchored on graphene vacancies retain their capacity to adsorb hydrogen. Clearly, the number of adsorbed hydrogen molecules in the supported clusters is smaller than that for free gas phase clusters[24] due to the steric effects of the graphene layer. However, gas phase clusters are not appropriate models

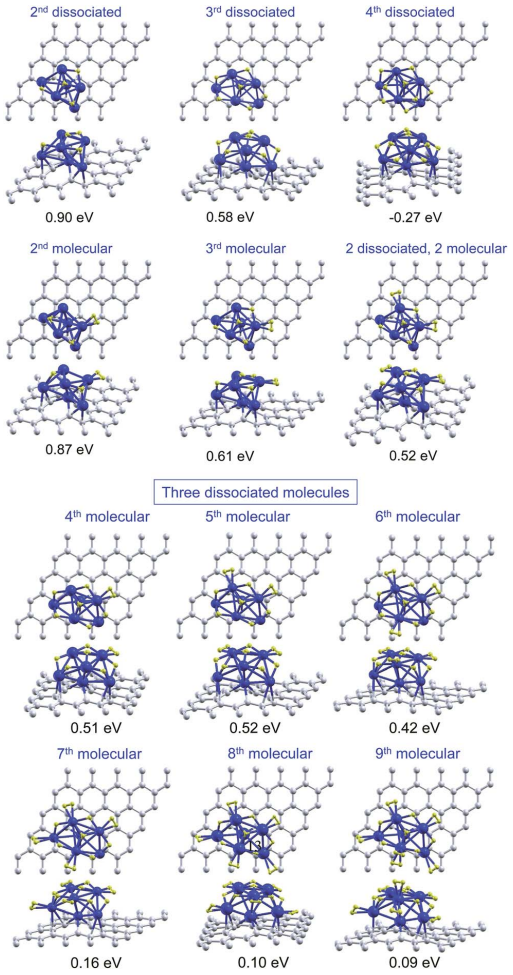

Fig. 4 Top and side views of successive adsorption of hydrogen on the ICO structure of anchored Pd_6 with one dissociatively chemisorbed hydrogen molecule. Both the molecular and the dissociative channels are shown from $n = 2$ to $n = 4$, and only the molecular channel is shown for $n = 5$–9. The adsorption energies of the last hydrogen molecule are calculated using eqn (1).

for hydrogen storage or other material applications. Pd doping contributes to an enhancement of the amount of hydrogen stored in a Pd-doped porous carbon material.

Further, the so-called spillover mechanism[25] has been proposed as responsible for the enhancement. According to this mechanism, molecules adsorbed on a first surface are transported to a second surface that does not adsorb the molecules under the same conditions. Our results on the adsorption and saturation with hydrogen of supported Pd clusters correspond to the first step of the spillover mechanism. The transfer mechanism of hydrogen attached to Pd towards the graphene layer, where the adsorption energies of hydrogen are less than 100 meV, remains to be elucidated. It is also interesting to notice that in order to use the stored hydrogen as a fuel, molecular hydrogen has to be catalytically dissociated in the anode of the hydrogen fuel cell. Palladium and other transition metals are usually employed as catalysts in this dissociation step. Our results on the dissociation of H_2 on supported palladium clusters provide a first hint of the role played by Pd clusters in the anode of hydrogen fuel cells.

3.4 Bonding between hydrogen and the Pd cluster

To investigate the nature of the bonding between hydrogen and the Pd cluster, both in the molecular and the dissociative channels, we calculated the electronic density difference between the system with adsorbed hydrogen and the two separated subsystems, formed by the Pd cluster anchored to the graphene vacancy on one hand and the free hydrogen molecule or free hydrogen atoms, in the proper positions, on the other. Fig. 6 shows the electronic density difference for the molecular adsorption of one, two and three hydrogen molecules on the OCT Pd_6. There is an increase (yellow surface in the figure) of electronic density in the region between the hydrogen molecule and the Pd atom to which the molecule is attached, which indicates a covalent-type of bonding between the hydrogen molecule and the Pd atom. Moreover, some polarization of the electronic density is also apparent. It is interesting to notice that the same type of bonding is observed for an increasing number of hydrogen molecules attached to different Pd atoms and also in the case of two hydrogen molecules attached to the same Pd atom. This indicates that the hydrogen molecules bind independently to the Pd cluster. The top panels of Fig. 7 show the electronic density difference for the dissociative chemisorption of hydrogen on the ICO and the OCT structures of Pd_6. Here, each hydrogen atom is embedded in a region of positive electronic density difference, that is, each hydrogen builds up an excess of electronic density around it. This type of bonding is typical of metal hydrides and could be interpreted as an ionic type of bonding. A similar behaviour is found in the case of two dissociatively chemisorbed hydrogen molecules on ICO Pd_6 (see lower left panel of Fig. 7). Both bonding types can be observed simultaneously in the case of two adsorbed hydrogen molecules, one dissociatively chemisorbed and the second adsorbed as a non-dissociated molecule (see lower right panel of Fig. 7). This indicates that the two adsorption channels take place independently of each other, and do not involve the complete Pd cluster but only locally involve the nearby Pd atoms . It is also notable that the graphene layer does not participate actively in the adsorption of hydrogen on the anchored Pd clusters.

Since the adsorption and dissociation of hydrogen is mainly due to local interactions with the palladium clusters, we expect similar adsorption and dissociation mechanisms on Pd clusters anchored on graphene vacancies and on Pd clusters deposited on pristine graphene. The hydrogen dissociation barriers in the latter are about 0.3 eV (ref. 15) and, therefore, similar values are expected for the dissociation of hydrogen on Pd clusters anchored on graphene vacancies.

Table 2 Adsorption energies of the successive adsorption of hydrogen on Pd_6 with ICO (OCT) structure anchored on a graphene vacancy. The n^{th} molecule is adsorbed on previous ICO (OCT) configurations (structures with $n-1$ hydrogen molecules). For $n=1$ the adsorption energy is calculated with respect to the most stable OCT structure of Pd_6 anchored on a graphene vacancy. The star (*) indicates the preferred adsorption channel for the nth molecule adsorbed on the icosahedral (octahedral) structure. Energies are given in eV

n	ICO dissociative channel E_{ad}^{nth} n dissociated	ICO molecular channel E_{ad}^{nth} 1 molecular	OCT dissociative channel E_{ad}^{nth} n dissociated	OCT molecular channel E_{ad}^{nth} 1 molecular
1	1.25*		1.03*	0.74
2	0.90*	0.87	0.81*	0.78
3	0.58	0.61*	0.65*	0.62
4	−0.27	0.51	0.03	0.56*
		($n-2$) molecular		
5		0.52*		
		($n-3$) molecular		($n-3$) molecular
6		0.52*		0.48*
7		0.42*		0.50*
8		0.16*		
9		0.10*		
10		0.09*		

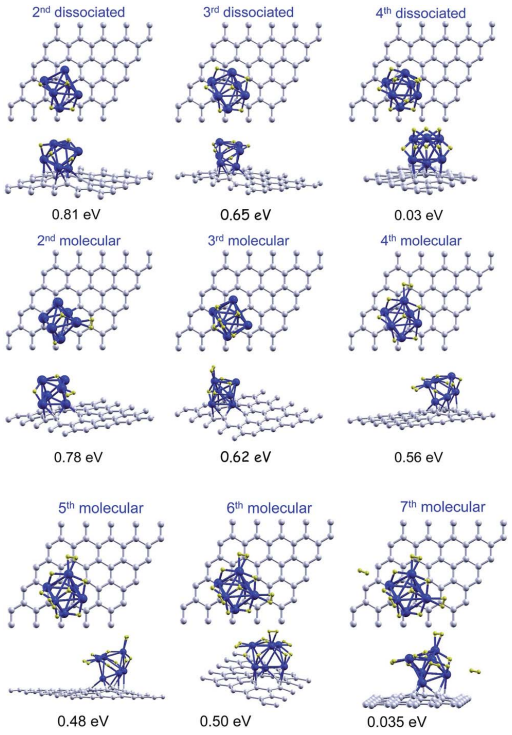

Fig. 5 Top and side views of successive adsorption of hydrogen on the OCT structure of anchored Pd_6 with one dissociatively chemisorbed hydrogen molecule. Both the molecular and the dissociative channels are shown from $n=2$ to $n=4$, and only the molecular channel is shown for $n=5$–7. The adsorption energies of the last hydrogen molecule are calculated using eqn (1).

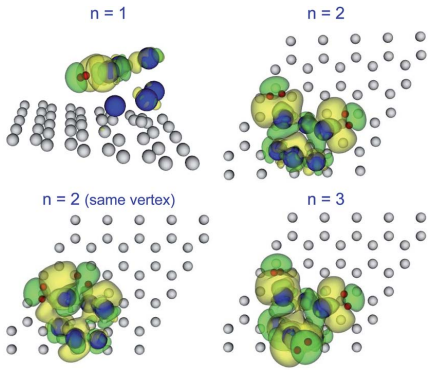

Fig. 6 Electronic density difference between the system with adsorbed hydrogen and the separated subsystems, formed by the Pd cluster anchored to the graphene vacancy on one hand and the free hydrogen molecule (in the proper position) on the other, for the molecular adsorption of $n=1$–3 hydrogen molecules on the OCT structure of Pd_6. The yellow isosurfaces correspond to positive values of the electronic density difference and the green isosurfaces to negative values. Red, blue and grey balls represent H, Pd and C atoms, respectively.

3.5 Desorption of hydrogen

Let us now focus on the desorption step of the hydrogen storage cycle. The desorption energy of hydrogen is equal to the adsorption energy. This energy was compared with the energy required to desorb the Pd_6–H_2 complexes for both the molecular adsorption and the dissociative chemisorption channels. The desorption energy of the Pd_6–H_2 complex from the graphene layer with a vacancy in the case of molecular adsorption on the OCT structure of Pd_6 is 5.66 eV. Similar energies, 5.62 and 5.89

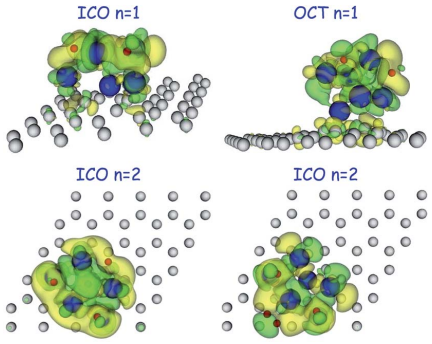

Fig. 7 Electronic density difference between the system with adsorbed hydrogen and the separated subsystems formed by the Pd cluster anchored to the graphene vacancy on one hand and the free hydrogen atoms or the free molecule (in the proper position) on the other. Top panels are the dissociative chemisorption of one hydrogen molecule on the ICO (left) and the OCT (right) structure of Pd_6. The lower panels are the adsorption of two hydrogen molecules: on the left, the two molecules are chemisorbed; on the right, one molecule is chemisorbed and the other adsorbed as a non-dissociated molecule. Yellow isosurfaces correspond to positive values of the electronic density difference and green isosurfaces to negative values. Red, blue and grey balls represent H, Pd and C atoms, respectively.

eV, are found for desorption of the Pd_6–H_2 complex when hydrogen is dissociatively chemisorbed on the OCT and ICO structures of Pd_6, respectively. All those energies are much higher than the desorption energies of the H_2 molecule: 0.74 eV in the case of molecular adsorption on OCT Pd_6, and 1.03 and 1.25 eV for the cases of dissociative chemisorption on the OCT and ICO structures of Pd_6, respectively. Therefore in the desorption step of the storage cycle, only hydrogen will be released because the energies required to release the Pd–H complexes are too high. This is in contrast with the desorption behaviour found for Pd clusters deposited on pristine graphene. There, the desorption energies of the Pd–H complexes are similar to the desorption energies of hydrogen molecules (roughly between 0.5 and 1 eV) and, therefore, desorption of the complexes competes with the desorption of hydrogen, thus spoiling the beneficial effect of the Pd dopant on the storage capacity of the nanoporous carbon materials. Here, the Pd clusters are firmly anchored to a graphene vacancy (5.62 eV), which prevents the desorption of the Pd–H complexes. As a conclusion we find that anchoring Pd_6 to a graphene vacancy retains the capabilities of the cluster to adsorb hydrogen but completely inhibits the possibility of desorption of the Pd–H complexes. A similar behaviour was found for Pd atoms anchored on graphene vacancies. This solves the problem of desorption of Pd–H complexes that was present in the case of Pd atoms and clusters supported on pristine graphene.

4 Conclusions

Hydrogen adsorption on nanoporous carbon materials is one of the most promising technologies for hydrogen storage. In this paper we have investigated the adsorption, dissociation and desorption of hydrogen from Pd_6 clusters anchored on graphene vacancies, on the basis of the Density Functional Formalism. A graphene layer with a vacancy was used as a model of the defective pore walls of nanoporous carbons and the Pd_6 cluster was considered as representative of small-size Pd clusters. The effect of vacancies on hydrogen adsorption cannot be assessed from studies of Pd clusters supported on pristine graphene. Pd_6 anchored on a vacancy may attach directly up to six hydrogen molecules with adsorption energies in the range of 0.3–0.7 eV. Six adsorbed molecules saturate the cluster and, due to steric effects, additional hydrogen molecules cannot attach directly to the Pd cluster and will begin to form a second hydrogen shell at a larger distance from the cluster and very weakly bound to it. The dissociative chemisorption of hydrogen is preferred over the molecular adsorption for adsorption from one to three hydrogen molecules. The dissociative adsorption energies are in the range of 0.6–1.2 eV. The six atoms of three hydrogen molecules saturate all the favorable sites of the Pd cluster for chemisorption: the faces and Pd–Pd bonds not in direct contact with the graphene layer and not involving the Pd atom which saturates the graphene vacancy. However, not all those faces and edges can be simultaneously filled due to steric effects. Three additional hydrogen molecules can be adsorbed as non-dissociated molecules onto the Pd cluster with three chemisorbed molecules, with adsorption energies of 0.5 eV. The desorption of hydrogen takes place with desorption energies in the range of 0.3–1.2 eV. Furthermore, since the Pd cluster is firmly anchored to the graphene vacancy, desorption of the Pd–H complexes requires much higher energies, by a factor of 5, than the desorption of hydrogen. Then, the desorption step of the storage cycle involves only desorption of hydrogen. Therefore, anchoring the Pd clusters to vacancies is very promising because (i) the anchored Pd clusters retain their capacity for adsorbing hydrogen, and (ii) it completely prevents the desorption of Pd–H complexes, which was a problem in the case of Pd clusters supported on pristine graphene. Our results on the dissociative adsorption channel are also of interest for the catalytic dissociation process in the anode of the hydrogen fuel cells.

Acknowledgements

This work was supported by MICINN of Spain (Grant MAT2011-22781) and Junta de Castilla y León (Grant VA050U14).

References

1 DOE, Multi-Year Research, Development and Demonstration Plan: Planned Program Activities for 2005-2015. Technical Plan–Storage. Updated April 2009, http://www1.eere.energy.gov/hydrogenandfuelcells/mypp/pdfs/storage.pdf, 2009.
2 P. Jena, *J. Phys. Chem. Lett.*, 2011, **2**, 206–211.
3 Y. Gogotsi, R. K. Dash, G. Yushin, T. Yildirim, G. Laudisio and J. E. Fischer, *J. Am. Chem. Soc.*, 2005, **127**, 16006–16007.
4 A. Linares-Solano, M. Jordá-Beneyto, D. L.-C. M. Kunowsky, F. Suárez-García and D. Cazorla-Amorós, in *Carbon*

Materials: Theory and Practice, ed. P. G. A. P. Terzyk and P. Kowalczyk, Research Signpost, Kerala, India, 2008, pp. 245–281.
5 I. Cabria, M. J. López and J. A. Alonso, *Carbon*, 2007, **45**, 2649–2658.
6 I. Cabria, M. J. López and J. A. Alonso, *Int. J. Hydrogen Energy*, 2011, **36**, 10748–10759.
7 J. S. Arellano, L. M. Molina, A. Rubio and J. A. Alonso, *J. Chem. Phys.*, 2000, **112**, 8114–8119.
8 J. A. Alonso, J. S. Arellano, L. M. Molina, A. Rubio and M. J. López, *IEEE Trans. Nanotechnol.*, 2004, **3**, 304–310.
9 B. K. Pradhan, G. U. Sumanasekera, K. W. Adu, H. E. Romero, K. A. Williams and P. C. Eklund, *Phys. B*, 2002, **323**, 115–121.
10 G. E. Froudakis, *J. Phys.: Condens. Matter*, 2002, **14**, R453.
11 C. I. Contescu, K. van Benthem, S. Li, C. S. Bonifacio, S. J. Pennycook, P. Jena and N. C. Gallego, *Carbon*, 2011, **49**, 4050–4058.
12 M. J. López, I. Cabria and J. A. Alonso, *J. Chem. Phys.*, 2011, **135**, 104706.
13 I. López-Corral, E. Germán, M. A. Volpe, G. P. Brizuela and A. Juan, *Int. J. Hydrogen Energy*, 2010, **35**, 2377–2384.
14 I. López-Corral, E. Germán, A. Juan, M. A. Volpe and G. P. Brizuela, *J. Phys. Chem. C*, 2011, **115**, 4315–4323.
15 I. Cabria, M. J. López, S. Fraile and J. A. Alonso, *J. Phys. Chem. C*, 2012, **116**, 21179–21189.
16 M. J. López, I. Cabria and J. A. Alonso, *J. Phys. Chem. C*, 2014, **118**, 5081–5090.
17 I. López-Corral, J. D. Celis, A. Juan and B. Irigoyen, *Int. J. Hydrogen Energy*, 2012, **37**, 10156–10164.
18 I. Cabria, M. J. López and J. A. Alonso, *Phys. Rev. B*, 2010, **81**, 035403.
19 Dacapo, see http://wiki.fysik.dtu.dk/dacapo for a description of the total energy code, based on the density functional theory, 2009.
20 D. Vanderbilt, *Phys. Rev. B*, 1990, **41**, R7892.
21 H. Monkhorst and J. Pack, *Phys. Rev. B*, 1976, **13**, 5188–5192.
22 J. P. Perdew and Y. Wang, *Phys. Rev. B*, 1992, **45**, 13244.
23 I. Cabria, M. J. López and J. A. Alonso, *Comput. Mater. Sci.*, 2006, **35**, 238–242.
24 C. Zhou, S. Yao, J. Wu, R. C. Forrey, L. Chen, A. Tachibana and H. Cheng, *Phys. Chem. Chem. Phys.*, 2008, **10**, 5445–5451.
25 W. Conner and J. Falconer, *Chem. Rev.*, 1995, **95**, 759–788.

4.3 Updated and Additional Results

Additional new results were obtained after publishing the accompanying article. Updates were found for both molecular and dissociative hydrogen adsorption pathways. The new results do not change the final conclusions about the competition between dissociative chemisorption and molecular physisorption of hydrogen. Energetic barriers for these processes have been also explored and included in this section.

4.3.1 Molecular Hydrogen Adsorption

Our first results (contained in the paper of the previous section) indicated that Pd_6 anchored on a graphene vacancy is saturated with six hydrogen molecules adsorbed in the molecular form. However, a subsequent extensive search on the possible adsorption sites for additional hydrogen molecules led to an increase of the saturation limit from six to eight H_2 molecules directly attached to Pd_6 in the OCT structure. Starting from the structure of the supported Pd_6 with six adsorbed H_2 molecules, the seventh hydrogen molecule is adsorbed on one of the palladium atoms which is not directly in contact with the graphene layer and that had only one H_2 molecule previously attached to it. The adsorption energy is 0.26 eV. The two palladium atoms in direct contact with the graphene layer (not the one saturating the vacancy) already had one adsorbed hydrogen molecule each of them and due to the proximity to the graphene surface, there is insufficient space to adsorb further molecules. The eighth molecule is adsorbed on the remaining Pd atom which is not in contact with the graphene layer and that had only one H_2 molecule previously attached to it. Its adsorption energy is 0.07 eV. Direct adsorption of the eighth molecule seems to be the saturation limit on Pd_6 anchored on a vacancy. Because of the steric effects produced by the graphene surface and by the previously bound hydrogen molecules, the ninth molecule can not be adsorbed directly to the Pd cluster. This ninth molecule will begin forming a second hydrogen shell with a small adsorption energy on the order of 10 meV. Figure 4.1 shows the geometries for the supported Pd_6 with seven to nine adsorbed hydrogen molecules. The successive adsorption energies of hydrogen in the molecular channel are summarized in Table 4.1. The adsorption energies for n=1 and 2 have been updated.

Table 4.1: Successive adsorption energies of hydrogen molecules on Pd_6 anchored on a graphene vacancy. Only the most stable configurations are shown. n represents the total number of molecules adsorbed on Pd nanoparticle. (*) New optimizations gave slightly different energies than the ones reported in the accompanying article for these structures. First column shows the adsorption energies of the last hydrogen molecule while having all of them attached in diferent vertices of the Pd_6 cluster. The second column exhibits the adsorption energies for the last hydrogen molecule while having at least two hydrogen molecules on the same vertex.

n	E_{ad}^{nth} Different vertices	E_{ad}^{nth} Two in same vertex
1	0.76*	
2	0.68*	
3	0.53	
4		0.50
5		0.36
6		0.34
7		0.26
8		0.07

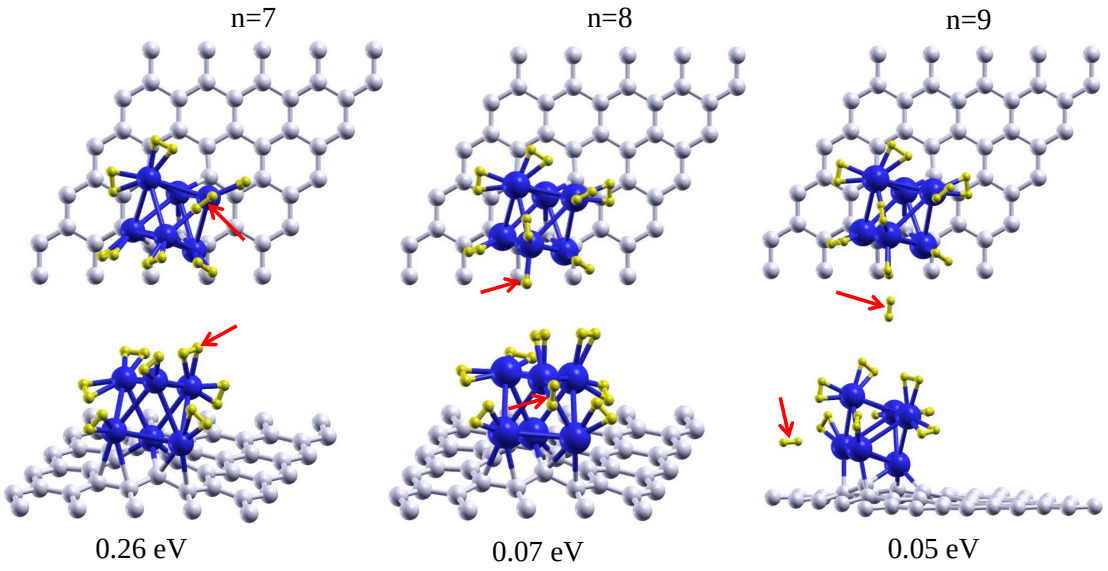

Figure 4.1: Top and side views of the seven, eight and nine hydrogen molecules adsorbed on the Pd cluster. The ninth H_2 molecule is not directly attached to the Pd_6 cluster. Red arrows point out the successively adsorbed seventh, eighth and ninth hydrogen molecules. Adsorption energies are calculated using Equation (1) from the accompanying article.

4.3.2 Competition Between Molecular Adsorption and Dissociative Chemisorption

As it is shown in the published paper of this chapter, the dissociative chemisorption Channel is preferred over the molecular adsorption of hydrogen (see Fig. 4.2) and the dissociative chemisorption induces a structural transition in the Pd_6 cluster from the OCT to the ICO structure[1]. Pd_6 is able to dissociate a maximum of three hydrogen molecules. Three additional hydrogen molecules can be adsorbed in the molecular form with moderate adsorption energies of 0.51, 0.52 and 0.42 eV for the fourth, fifth and sixth hydrogen molecules, respectively. An extensive search of adsorption sites for more additional hydrogen molecules (from seven to nine) lead to new structures (not reported in the paper) with higher adsorption energies than the corresponding ones given in the paper. The new adsorption energies of the seventh, eighth and ninth molecule on Pd_6 with three dissociated and three molecular adsorbed H_2 are 0.21, 0.14, and 0.23 eV, respectively.

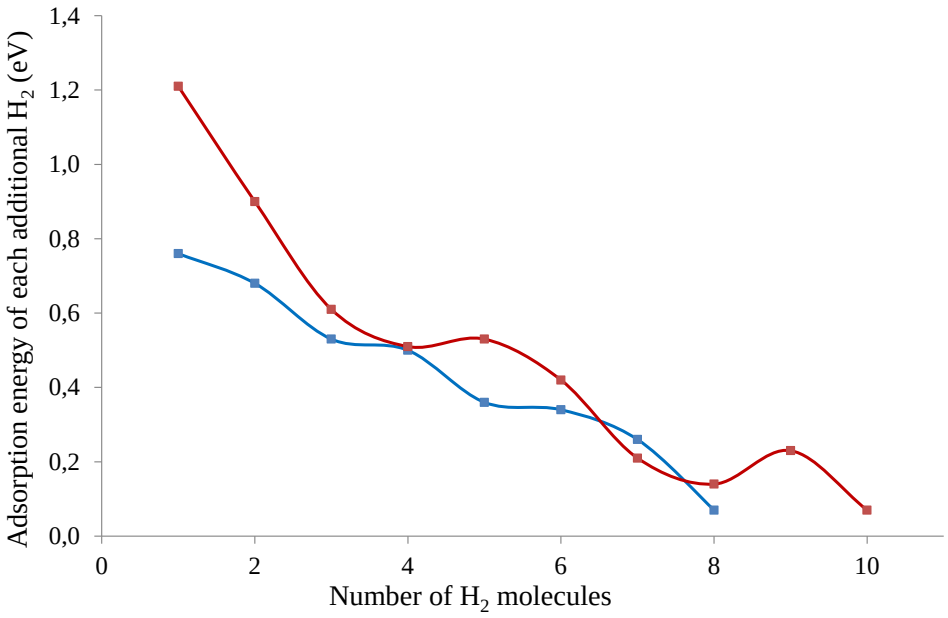

Figure 4.2: The adsorption energy of the last adsorbed hydrogen molecule against the total number of hydrogen molecules is represented. The blue curve is for molecular channel on OCT structure and the red one is for adsorption on ICO structure (dissociative channel up to $n = 3$, and then molecular channel).

In these new configurations, the palladium cluster is lifted up from the graphene layer and the five Pd atoms which are not saturating the vacancy, are not attached

[1]ICO structure is the way we refer to an **incomplete pentagonal bipyramid** in which one of the atoms of the pentagonal base is missing.

to any carbon of the graphene layer. As a result, more space is provided to rearrange the adsorbed hydrogen in systems with $n = 7 - 9$ adsorbed hydrogen molecules. Due to these more opened structures, one more hydrogen molecule can be adsorbed on the Pd cluster. Thus, the tenth molecule is attached with an adsorption energy of 0.07 eV. Table 4.2 collates all the updated results and Figures 4.3 and 4.4 show the new geometries for the seventh, eighth and ninth adsorbed molecules and for the new additional tenth molecule.

Table 4.2: Successive hydrogen adsorption energies on Pd_6 anchored on a graphene vacancy. Only the most stable configurations are shown. (*) New optimizations gave a slightly different energies than the ones reported in the accompanying article for this structure. (Notice that there is a missprint in Table 2 of the published paper. The n values for $n = 5 - 10$ should be one less unit each, that is $n = 4 - 9$, respectively).

n	dissociative channel E_{ad}^{nth} dissociated	molecular channel E_{ad}^{nth} molecular
1	1.21*	
2	0.90	
3	0.58	0.61
4		0.51
5		0.52
6		0.42
7		0.21
8		0.14
9		0.23
10		0.07

4.3.3 Hydrogen Desorption

The desorption of hydrogen is an important step of the hydrogen storage cycle. Clearly, the hydrogen desorption energy is equal in magnitude to the adsorption energy. A comparison between the desorption of hydrogen and the desorption of Pd_6-H_2 complexes for both molecular and dissociative adsorption channels for ICO and octahedral structure (OCT) structures can be found in the accompanying article.

Our results show that desorption of the Pd_6-H_2 complexes does not compete with desorption of hydrogen. The reason is that the Pd_6 cluster is firmly anchored on the

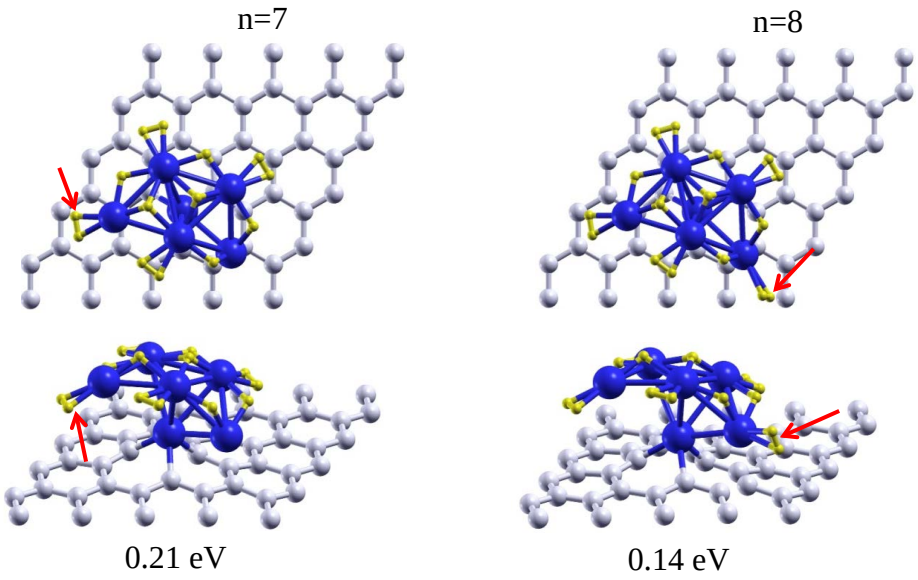

Figure 4.3: Top and side views of the seventh and eighth hydrogen molecules adsorbed on Pd_6 anchored on a graphene vacancy. Adsorption energies are calculated using equation (1) from the accompanying article to this Chapter. Red arrows point out the seventh and eighth molecules.

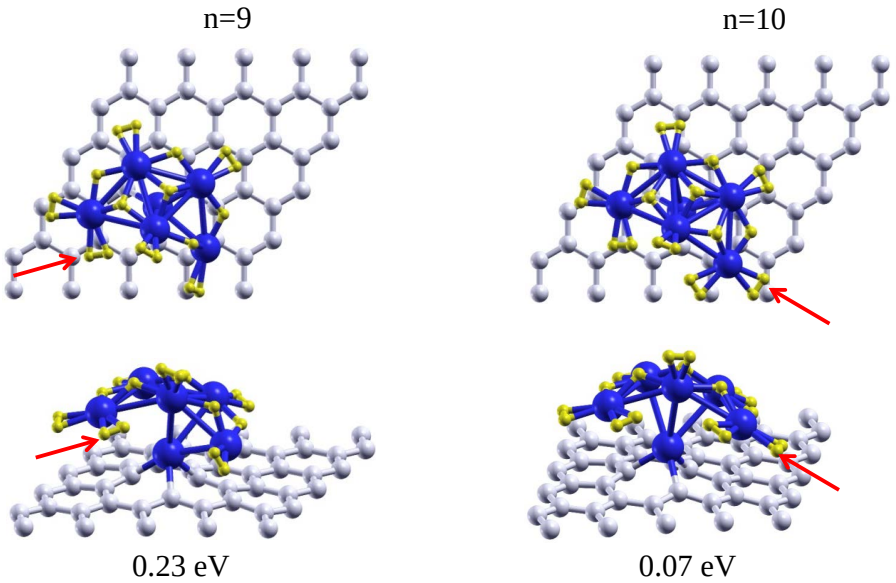

Figure 4.4: Top and side views of the ninth and tenth hydrogen molecules adsorbed on Pd_6 anchored on a graphene vacancy. Adsorption energies are calculated using Equation (1) from the accompanying article to this Chapter. Red arrows point out the ninth and tenth molecules.

graphene vacancy and therefore desorption of the complexes costs about five times more energy than desorption of hydrogen.

However, as it has been shown in the previous Section, the saturation of Pd_6 with seven to ten hydrogen molecules tends to lift up the Pd cluster from the graphene layer and only the Pd atom saturating the vacancy remains directly bonded to the graphene layer (see Figure 4.4, side view). Therefore, it is of interest to investigate the competition between desorption of the Pd_5-H_2 complexes (these are the Pd_6-H_2 complexes minus the Pd atom that saturates the graphene vacancy) and desorption of hydrogen, for the hydrogen saturated system. The energy required to desorb the Pd_5-$10H_2$ complex leaving behind the graphene layer with a Pd atom anchored to the vacancy is 1.27 eV. This value is much higher than the desorption energy of the tenth H_2 molecule from the saturated cluster, 0.07 eV. Therefore, in the desorption step, only hydrogen will be released as the energies required to desorb the Pd_5-$10H_2$ complexes are comparatively high. As hydrogen is desorbed molecule by molecule from the saturated cluster, the cluster anchorage to the graphene surface becomes stronger until reaching the 5.89 eV needed for desorbing the Pd_6-2H complex.

4.3.4 Energy Barriers

In the previous Sections we have investigated the thermodynamical aspects of the adsorption and dissociation of molecular hydrogen on Pd_6 anchored on a graphene vacancy, that is, the energies of the final adsorbed or dissociated states. However, the kinetics of the adsorption and dissociation processes is mainly determined by the activation energy barriers that have to be surmounted to reach the corresponding final states. Therefore in this section we investigate the energy barriers for several partial processes which are relevant for the adsorption and storage of hydrogen: (i) the adsorption of one hydrogen molecule, (ii) transition from OCT to ICO structure of Pd_6 anchored on a graphene vacancy induced by the dissociative adsorption of H_2 (notice that OCT is the lowest energy structure of clean Pd_6 anchored on a graphene vacancy whereas ICO is the minimum energy structure when one or more hydrogen molecules are dissociatively adsorbed on the cluster) and (iii) the diffusion of one hydrogen atom on Pd_6 anchored on a vacancy. Nudged elastic band method (NEB) and Density Functional Theory calculations were used for finding local minimum pathways. For the initial and final state structures we have chosen the lowest energy configurations calculated from static relaxations.

Adsorption of H_2 on Pd_6 anchored on a graphene vacancy takes place without activation barrier. In the initial configuration the H_2 molecule is placed at a far (4.8 Å) distance from the Pd cluster. The molecule approaches the cluster until the distance is 1.75 Å in the adsorbed configuration. The adsorption energy is 0.70 eV. Figure 4.5 shows the minimum energy path for the first molecular hydrogen adsorption process.

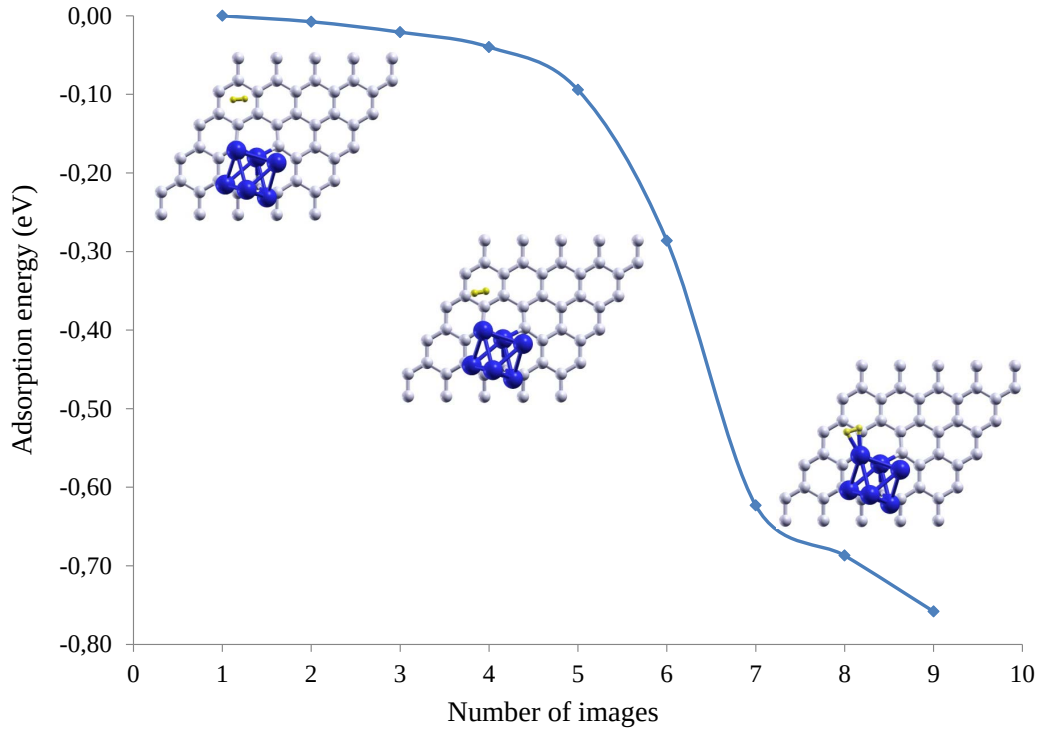

Figure 4.5: Minimum Energy Path for the molecular adsorption of H_2 on Pd_6 anchored on a graphene vacancy. Pd_6 is in the lowest on OCT structure. Snapshots of the structures for images 1, 5 and 9 have been included in the chart.

The energy barrier for the interconversion between the OCT and ICO structures induced by the dissociative adsorption of H_2 was calculated. In order to take into account only the structural transformation from OCT and ICO structures, we have place the hydrogen atoms in the same configuration on the OCT and on the ICO structures. This is, in the initial configuration, the hydrogen atoms are adsorbed on an edge and a face of the OCT structure which share a vertex. In the final state, hydrogen atoms are found in the same sites but on the ICO structure, that is, at the same edge and at the same face as on the OCT structure. Both configurations are not the lowest configuration for OCT structure nor for ICO structure. The energy barrier for this process is 0.25 eV (Fig. 4.6). This energy is required to break the Pd-Pd bond in the OCT structure between the two Pd atoms supported on the graphene layer (not the one saturating the vacancy) and to move and re-accommodate the Pd cluster on graphene surface. To achieve this structural transformation, the Pd_6 has to break some Pd-C bonds and make new ones. The Pd-Pd distance of the broken edge is 4.48 Å.

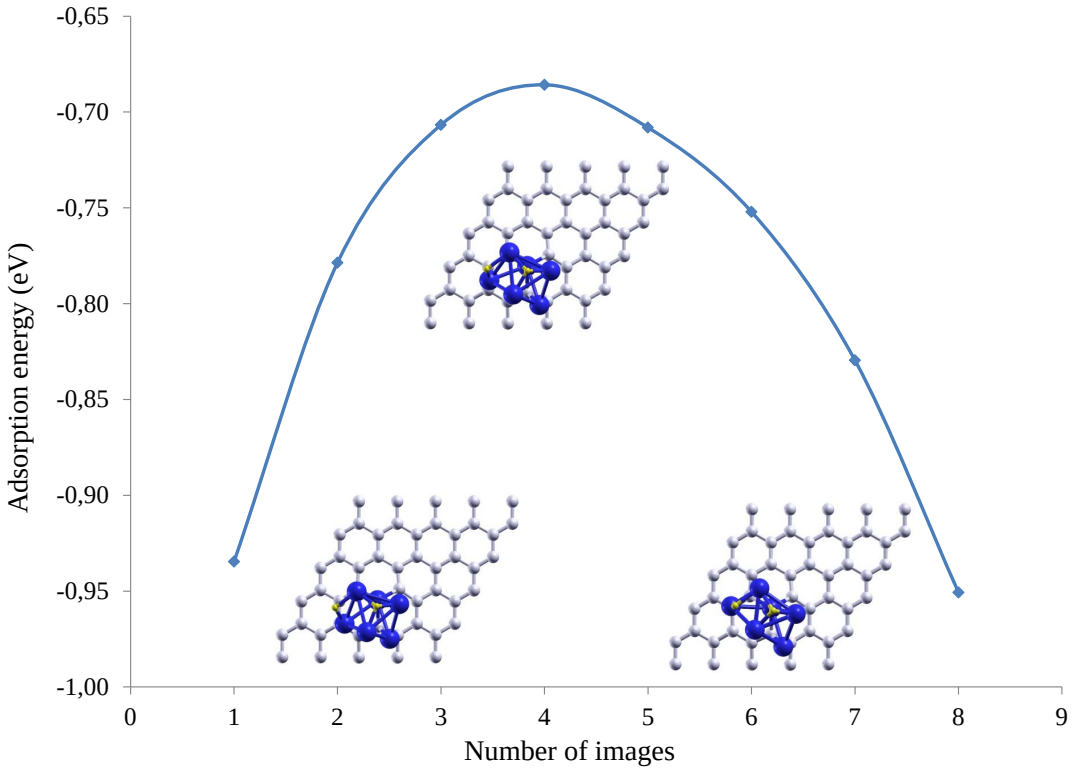

Figure 4.6: Minimum energy path for the structural transition from OCT to ICO structures. The energy barrier for the transformation is of 0.25 eV. Pictures for images 1, 4 and 9 have been added to the chart.

Once the structural interconversion have taken place, hydrogen atoms have to diffuse on the Pd_6 in order to reach the lowest energy structure. Therefore, the energy barrier for the diffusion of one hydrogen atom on the Pd_6 cluster was also calculated. The initial configuration has the two hydrogen atoms on two faces of the Pd ICO structure which share an edge. In the final state, the two hydrogen atoms are attached to the two non-adjacent triangular faces at the upper side of the bipyramid. This is the side of the bipyramid whose apex atom is not the one saturating the vacancy. The single-atom hydrogen diffusion, on the Pd cluster, is found to have a barrier of 40 meV (Fig. 4.7).

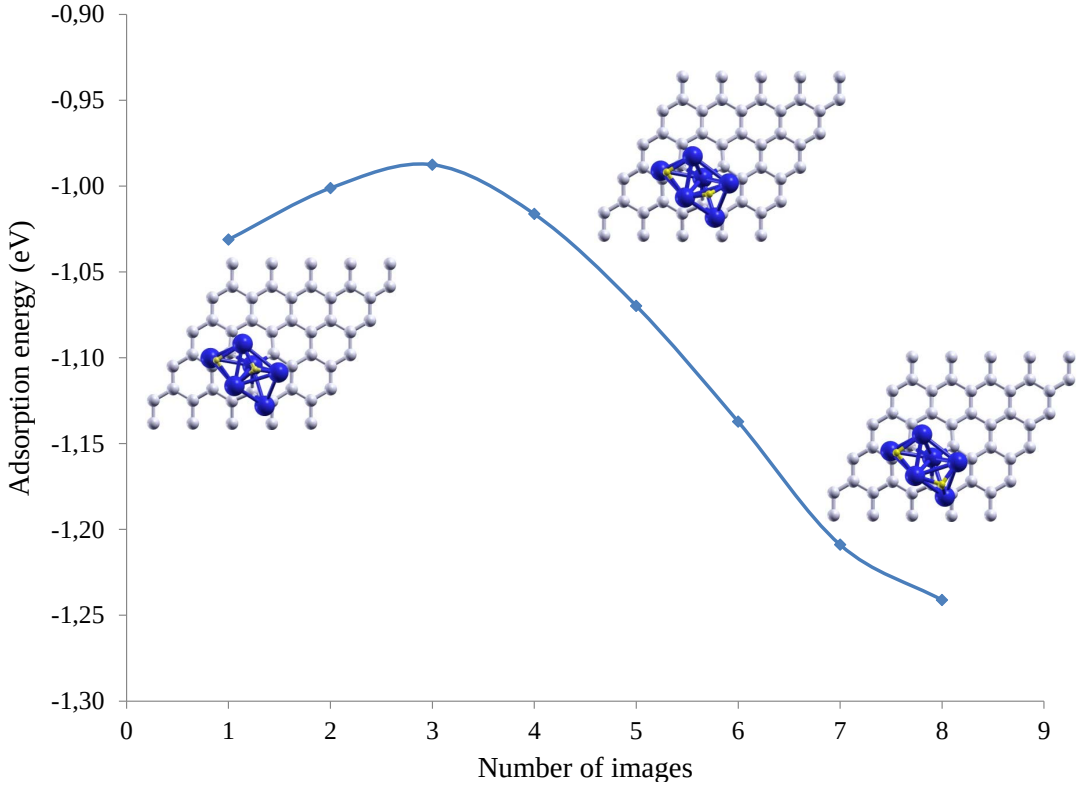

Figure 4.7: Minimum energy path for the diffusion of one hydrogen atom through Pd_6 cluster anchored on a graphene vacancy. Pictures for images 1, 4 and 8 have been added to the chart.

4.4 Conclusions

Hydrogen adsorption, dissociation, desorption and saturation limit of Pd_6 clusters anchored on a graphene mono-vacancy have been investigated. The graphene layer with a vacancy was considered as model of the defective pore walls of nanoporous carbons and Pd_6 was considered as being representative of small palladium clusters.

Up to a maximum of eight hydrogen molecules can be adsorbed on the Pd_6 cluster with energies in the range of 0.07-0.7 eV. Additional hydrogen molecules can not be attached directly to the Pd cluster. They start forming a second hydrogen shell. The first hydrogen molecule adsorption is carried out without any energy barrier.

The dissociative H_2 adsorption channel is preferred to the molecular channel for hydrogen adsorption and Pd_6 is able to dissociate up to three hydrogen molecules. The dissociative adsorption energies range from 0.58-1.21 eV. The dissociative chemisorption induces a structural transition in the Pd_6 cluster from the OCT to the ICO structure. The energy barrier of the structural transition is 0.25 eV. Seven non-dissociated additional molecules can be adsorbed on the ICO Pd cluster with three chemisorbed molecules, with adsorption energies in the range of 0.07-0.51 eV.

The Pd cluster is strongly anchored to the graphene vacancy, and thus, the desorption of the Pd_6-H_2 complexes requires much higher energies than the desorption of hydrogen. As a consequence, the desorption step of the storage cycle would only involve the desorption of hydrogen. Hence, we can conclude that anchoring the Pd clusters on graphene vacancies is necessary since it prevents the desorption of the Pd_6-H_2 complexes.

Chapter 5

Steric and Chemical Effects on the Hydrogen Adsorption

If at first you do not succeed, try, try again.

William Edward Hickson.

There is of fundamental interest to understand the role played by the Pd dopant on the enhancement of the storage capacity of nanoporous carbons. In the previous chapter it has been shown that several hydrogen molecules can be adsorbed (either as molecules or dissociated) on palladium clusters supported on graphene vacancies. This chapter is devoted to understand the effects of the graphitic substrate and of the defects in the substrate on the adsorption of hydrogen on Pd clusters. Effects on the hydrogen adsorption mechanisms and on the hydrogen saturation limit of Pd clusters are considered. To this aim, this chapter presents a comparative study of the adsorption of hydrogen on free Pd_6 clusters, Pd_6 supported on a perfect graphene surface and Pd_6 supported on a graphene vacancy. It is important to study all the systems, free and supported clusters, on the same footing for a fair comparison among them.

In Section 5.1, we present a brief description of the theoretical model. The references and a more detailed description of the results can be found in the attached article (Section 5.2). Section 5.3 reports additional results to the accompanying article, such as, the energy barriers for several processes on free Pd_6 clusters. Finally, in Section 5.4 some conclusions are provided.

Note about nomenclature: The structure of Pd_6 consisting in an incomplete pentagonal bipyramid. Sometimes, also referred as ICO structure (iPB), that is, a pentagonal bipyramid in which one of the atoms of the pentagon has been removed, has been named as ICO structure in the previous Chapter. However, in this and

subsequent chapters that structure is referred to as iPB structure.

5.1 Theoretical Model

In this work, we performed computational simulations for investigating the role of Pd_6 nanoparticle on the hydrogen adsorption and dissociation. As mentioned in former sections and in order to compare among systems, the computational details are identical to the ones which have been already described in Section 3.6.2 and have been summarized in Table 3.1.

Free, supported on pristine graphene and anchored on graphene vacancy Pd_6 were considered as suitable models to unravel the effect of the support on the hydrogen adsorption and dissociation mechanisms and on the hydrogen saturation limit of both systems, free and anchored Pd aggregates on the graphene defect. Several combinations for searching the lowest energy configurations of adsorbed and dissociated hydrogen molecules and saturation limits on free and supported Pd_6 aggregates were performed and fully optimized. A more complete description of the theoretical model can be found in the accompanying article.

5.2 Publication: Steric and Chemical Effects on the Hydrogen Adsorption and Dissociation on Free and Graphene-supported Palladium Clusters

Computational and Theoretical Chemistry 1107 (2017) 23–29

Contents lists available at ScienceDirect

Computational and Theoretical Chemistry

journal homepage: www.elsevier.com/locate/comptc

Steric and chemical effects on the hydrogen adsorption and dissociation on free and graphene–supported palladium clusters

Alejandra Granja-DelRío, Julio A. Alonso, María J. López *

Departamento de Física Teórica, Atómica y Óptica, Universidad de Valladolid, 47011 Valladolid, Spain

ARTICLE INFO

Article history:
Received 25 October 2016
Received in revised form 22 November 2016
Accepted 23 November 2016
Available online 24 November 2016

Keywords:
Hydrogen adsorption
Palladium clusters
Nanoporous carbons
Graphene

ABSTRACT

Palladium doping enhances the hydrogen storage capacity of nanoporous carbons. The purpose of this work is to asses the effect of the carbonaceous support on the adsorption of hydrogen on Pd clusters. Hydrogen adsorbs on Pd clusters following two channels: molecular adsorption and dissociative chemisorption. These two adsorption channels are investigated on free Pd clusters and Pd clusters supported on pristine and defective (with vacancies) graphene using the Density Functional Formalism. Pd_6 is taken as case study. Free Pd_6 can adsorb twelve hydrogen molecules in the molecular form, a number higher than the nine and eight molecules that can be adsorbed on the cluster supported on pristine graphene and on a graphene vacancy, respectively. However the most stable adsorption channel is, in all cases, the dissociative chemisorption of hydrogen. As the cluster is being loaded with hydrogen, there is a competition between the two adsorption channels. Pd_6 supported on a graphene vacancy is able to dissociate three hydrogen molecules, whereas the free cluster can dissociate up to seven molecules. In both cases, six additional molecules can be adsorbed in the molecular form. The higher saturation limit obtained for the free clusters is explained in terms of the steric and chemical effects of the supporting layer. These effects are of primarily importance to asses the role of the Pd dopant on the adsorption and storage of hydrogen on nanoporous carbons.

1. Introduction

Hydrogen adsorption on porous carbons is a promising technology for hydrogen storage [1–3]. However, the technological requirement [4] of storing 5.5 weight per cent of hydrogen at room temperature and moderate pressures is very demanding, and pure carbon materials do not reach that technological target. Some experiments [5–7] indicate that doping the porous materials with palladium clusters enhances the storage capacity of those materials. Thus, there is a great interest to understand the role played by the Pd dopant on the adsorption and storage mechanism. In previous work we have investigated the adsorption of hydrogen on supported Pd clusters [8–10] using the Density Functional Formalism. Pristine graphene and graphene with vacancies were considered as suitable models for the walls of porous carbons [11]. The adsorption of hydrogen on free Pd clusters [12,13] has been also studied. All previous studies focused either on supported [14–16] or on free clusters; however, to fully understand the role played by the Pd dopant in the adsorption and storage of hydrogen on porous carbons one has to understand also the role of the graphitic support. Thus the aim of this work is to unravel the effect of the graphene support and of the graphene defects on the hydrogen adsorption mechanisms and the hydrogen saturation limit of Pd clusters. With this purpose in mind we have investigated and compared the adsorption and dissociation of hydrogen on free Pd clusters and on Pd clusters supported on pristine and defective (with vacancies) graphene. Pd_6 is taken as a representative cluster. Steric and chemical effects of the supporting layer are investigated. It is important to study all the systems, free and supported clusters, on the same footing for a fair comparison among them. In Section 2 we present the key technical features of the Density Functional Formalism used in our computer simulations. Section 3 presents the results and we close with some conclusions in Section 4.

2. Theoretical model

Hydrogen adsorption and dissociation on free Pd clusters and on Pd clusters supported on pristine and defective (with vacancies) graphene is investigated using the Density Functional Formalism (DFT). Pristine and defective graphene are considered as appropriate models for the walls of nanoporous carbon materials.

* Corresponding author.
E-mail address: maria.lopez@fta.uva.es (M.J. López).

http://dx.doi.org/10.1016/j.comptc.2016.11.029
2210-271X/

The supercell methodology is used for the DFT calculations, as implemented in the Dacapo code [17]. The graphene layer is represented by a hexagonal supercell in the *XY* plane with a lattice parameter of 12.33 Å, containing 50 carbon atoms. In the *Z* direction the supercell is large enough (14 Å) to avoid interactions between the images of the graphene layer in different supercells. The same supercell is used for the free Pd clusters. The calculations are performed using (i) Vanderbilt ultrasoft pseudopotentials [18], (ii) the generalized gradient approximation of Perdew and Wang (GGA-PW91) [19] for the exchange-correlation functional, (iii) a plane waves basis set with cutoffs of 350 eV and 1000 eV for the expansion of the wave functions and the electronic density, respectively, and (iv) four *k* points distributed in the Brillouin zone following the Monkhorst-Pack scheme [20]. All the calculations allowed for spin polarization.

An extensive search for the lowest energy configurations of free and supported Pd clusters has been performed. For the supported clusters, several orientations (lying on one atom, an edge, or one face) and positions of the cluster with respect to the graphitic substrate have been considered. The preferred configurations of the two lowest energy structures of Pd_6 (OCT and iPB, see below) on graphene are supported on one face of the cluster. In the case of a graphene vacancy, one Pd atom sits at the center of the vacancy and the other two Pd atoms bind to C–C bonds adjacent to the vacancy. Configurations in which two neighbor Pd atoms of the cluster saturated the vacancy were either unstable or too high in energy. In addition, an extensive search for the lowest energy configurations of adsorbed and dissociated hydrogen on free and supported Pd clusters has also been performed. Initial structures included several Pd_6 geometries and hydrogen molecules and hydrogen atoms adsorbed on different vertices, edges and faces of the Pd cluster. All the structures have been fully optimized until the forces acting on all the atoms were smaller than 0.05 eV/Å and the cohesive energies were converged within 10 meV.

3. Results

Palladium exhibits a strong tendency to aggregate and form three dimensional clusters on the surface of graphene [21] or attached to graphene vacancies [9]. Small Pd_n clusters with $2 \leqslant n \leqslant 6$ supported on pristine graphene and anchored to graphene vacancies retain, with minor distortions, the main structural features of the free clusters. The energy ordering of the low lying isomeric structures of the free clusters is also preserved upon deposition of the clusters, but the energy difference between isomers may change. For instance, the lowest energy octahedral (OCT) structure of the free Pd_6 cluster is 0.29 eV more stable than the first isomer, which has a structure of an incomplete pentagonal bipyramid (iPB). When supported on pristine graphene the energy difference between the two structures is 0.60 eV, but this difference drops to 0.11 eV when the clusters are anchored on a graphene vacancy. The magnetic moments of the free Pd_n clusters [22] with $n = 2$–6 are $\mu = 2\mu_B$. These magnetic moments, however, are quenched down to zero upon deposition of the clusters on graphene vacancies due to the strong cluster-defect interaction, with binding energies of about 5 eV [9]. The interaction of the palladium clusters with pristine graphene is milder, with adsorption energies around 1 eV. Thus, the deposition of the clusters on pristine graphene preserves the magnetic moment for Pd_3, Pd_4, and Pd_6 but leads to zero moments for Pd_2 and Pd_5 [21]. In this paper we investigate the effect of the graphitic substrate and of graphene vacancies on the hydrogen adsorption properties of palladium clusters. We focuss on Pd_6 as a case study.

Hydrogen adsorbs on Pd clusters supported on pristine graphene following two different adsorption modes: molecular adsorption and dissociative chemisorption [8]. In the molecular adsorption mode, the hydrogen molecule becomes activated and the H–H bond is stretched by about 15% from the free molecular bond distance of 0.754 Å but it does not break. In the dissociative adsorption mode, however, the H–H bond is broken and the two H atoms chemisorb independently on the cluster surface. Interestingly, these two adsorption modes are also found on Pd clusters anchored on graphene vacancies [10] and on free Pd clusters [13]. There is a competition between the two adsorption modes as successive hydrogen molecules are adsorbed on the cluster. Here we investigate how the details of this competition, as well as the hydrogen saturation limit (maximum number of hydrogen molecules that can be adsorbed), depend on whether the Pd cluster is free or supported on pristine or on defective graphene. Steric and chemical effects of the supporting layer are discussed.

Starting with the molecular adsorption of H_2 on Pd_6, the same preferred adsorption sites (on top the Pd atoms) are found for free and supported clusters. In the case of the lowest energy, OCT structure of free Pd_6, successive H_2 molecules adsorb on top of different Pd atoms. After each one of all the six Pd atoms is decorated with one H_2 molecule, a second H_2 molecule can be accomodated on each vertex of the OCT structure, that is, on each Pd atom, up to a maximum of twelve adsorbed H_2 molecules that completely saturate the free cluster. Notice, however, that for the highest hydrogen coverages (from 7 to 12 molecules) some molecules lean towards a Pd–Pd bond becoming highly activated with H–H distances close to 0.97 Å and the structure of Pd_6 deforms a little from the perfect octahedron. The thirteenth molecule does not bind directly to the cluster and begins to form a second hydrogen layer at a larger distance of about 3.22 Å from the closest Pd atom of the cluster. It has a very small binding energy, 35 meV, one order of magnitude smaller than the binding energies for hydrogen molecules directly bound to the Pd cluster. In contrast with the OCT structure, hydrogen molecules adsorbed on the iPB structure of free Pd_6 begin to share Pd vertices before decorating all the Pd atoms. In fact, the fifth H_2 molecule adsorbs on one of the Pd vertices already occupied by another molecule. Finally, additional hydrogen molecules decorate all the Pd atoms. Fig. 1 shows some structures of molecular hydrogen adsorbed on free Pd_6 in the lowest OCT structure and in the first isomeric iPB structure. The iPB structure is slightly more active than the OCT structure: the hydrogen adsorption energies on this structure are 50–100 meV higher than the adsorption energies on the OCT structure. However the OCT structures with adsorbed hydrogen are more stable than the corresponding iPB structures for all hydrogen compositions.

Hydrogen molecules adsorb on the OCT structure of Pd_6 anchored on a graphene vacancy decorating, first, the three Pd atoms which are not in direct contact with the graphene surface (see the structure of the anchored Pd_6 in Fig. 2). The forth molecule shares one of the occupied Pd vertices and the fifth and sixth H_2 molecules attach, respectively, to the two Pd atoms lying on the graphene surface. Finally, eight molecules saturate the palladium cluster: two attached to each of the three Pd atoms not in contact with graphene and one to each of the two atoms lying on the surface. No molecule adorbs on the Pd atom that saturates the graphene vacancy. Pd_6 supported on pristine graphene can adsorb up to nine H_2 molecules: two attached to each Pd atom not in contact with graphene, and one to each of the three Pd atoms lying on the surface. The successive molecular adsorption of hydrogen does not change the lowest OCT structure of the free and supported Pd clusters. Fig. 2 shows the hydrogen saturated structures of Pd_6 supported on pristine graphene and anchored on a graphene vacancy.

The adsorption energies of hydrogen molecules successively attached on the free Pd_6 cluster and on the cluster anchored on a graphene vacancy are shown in Fig. 3a. In both cases, the adsorption energy of each newly attached molecule decreases with the

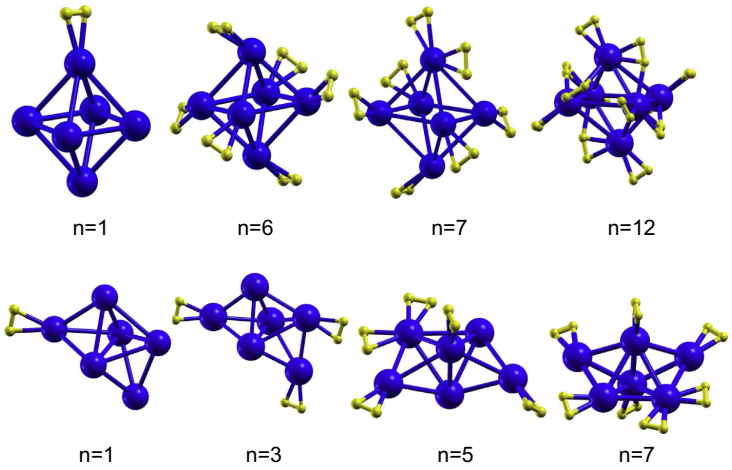

Fig. 1. Optimized structures of molecular hydrogen adsorbed on free Pd_6 clusters. Configurations for Pd_6 in the lowest energy OCT structure (first row) and in the isomeric iPB structure (second row) are shown. *n* indicates the number of adsorbed molecules. The Cartesian coordinates of all the structures are available in the Supplementary Material.

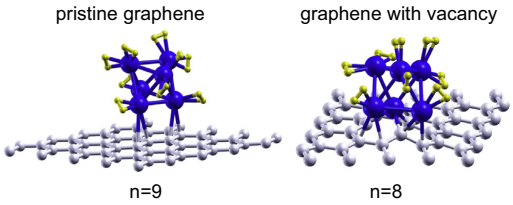

Fig. 2. Optimized structures of Pd_6 supported on pristine graphene and anchored on a graphene vacancy fully saturated with nine and eight adsorbed hydrogen molecules, respectively. The Cartesian coordinates of all the structures are available in the Supplementary Material.

number of adsorbed molecules. It is remarkable that the adsorption energies on free and on supported clusters are not too different, except for the sixth molecule. The peak in the adsorption energy for the sixth hydrogen molecule adsorbed on free Pd_6 is due to a change in the magnetic moment of this cluster that quenches down from 2 μ_B to zero. This reduction in the magnetic moment is accompanied by the opening of a gap at the Fermi level that stabilizes the cluster. In our opinion, those peculiar magnetic and electronic effects are driven by the very symmetric structure of the $Pd_6(H_2)_6$ cluster as compared to the others.

In summary, the free Pd_6 cluster is saturated with twelve molecularly adsorbed hydrogen molecules. The hydrogen saturation limit is reduced to nine for Pd clusters supported on pristine graphene and it is reduced further down to eight hydrogen molecules for Pd clusters anchored on a graphene vacancy. This reduction in the saturation limit is due, on one hand, to the steric effect of the graphene layer, similar for pristine and defective graphene, that prevents the hydrogen molecules to surround completely the palladium cluster. On the other hand, the strong chemical effect of the defect prevents the hydrogen molecules to adsorb on the Pd atom that saturates the vacancy. The supporting layer, however, seems not to have a major effect on the adsorption energies since the H_2–Pd interaction is quite local (see below the electron density redistribution) and the support does not modify substantially the electronic structure around the Pd atoms, except for the one that saturates the graphene vacancy.

The most stable channel for hydrogen adsorption on free and supported palladium clusters is the dissociative chemisorption of the molecule. In the case of free Pd_6 in its lowest energy OCT structure, the two hydrogen atoms of the dissociated molecule chemisorb on the center of two opposed triangular faces (see Fig. 4). The H atoms tend to be as separated as possible on the cluster surface. In the case of Pd_6 supported on pristine graphene, the two H atoms chemisorb, respectively, on two lateral faces that have only one Pd atom in direct contact with the surface. This optimal structure arises from the compromise between separating the H atoms as much as possible and binding them to Pd faces that have the least number of Pd atoms in direct contact with the graphene layer. When Pd_6 is anchored to a graphene vacancy, one H atom chemisorbs on the triangular face of the Pd cluster not in contact with graphene and the other one on a lateral Pd–Pd bond. This last configuration, however, is not the most stable structure. Instead, the dissociative chemisorption of hydrogen induces a structural change on the anchored Pd cluster from OCT to iPB. The two H atoms chemisorb on two non-adjacent triangular faces of the incomplete bipyramid which are not in direct contact with the supporting layer. The driving force for this structural change is that the iPB structure is more reactive towards hydrogen than the OCT structure. The adsorption energy of hydrogen, in the dissociated state, on the iPB cluster anchored on a vacancy is 0.37 eV higher than on the OCT structure anchored on a vacancy. This energy is sufficient to compensate the lower stability (by 0.15 eV) of the supported iPB structure. On the other hand, the OCT structure of free Pd_6 does not change upon dissociative chemisorption of a single hydrogen molecule. The reason is that, for the free clusters, the difference between the adsorption energy of the molecule, in the dissociated state, on iPB and OCT is reduced to 0.14 eV and does not compensate for the larger energy difference of 0.29 eV between the OCT and the iPB structures.

Dissociative chemisorption of additional hydrogen molecules on Pd_6 anchored on a graphene vacancy does not change the iPB structure of the Pd cluster. This structure is able to dissociate a maximum of three hydrogen molecules. Dissociation of a forth molecule leads to an unstable configuration with respect to des-

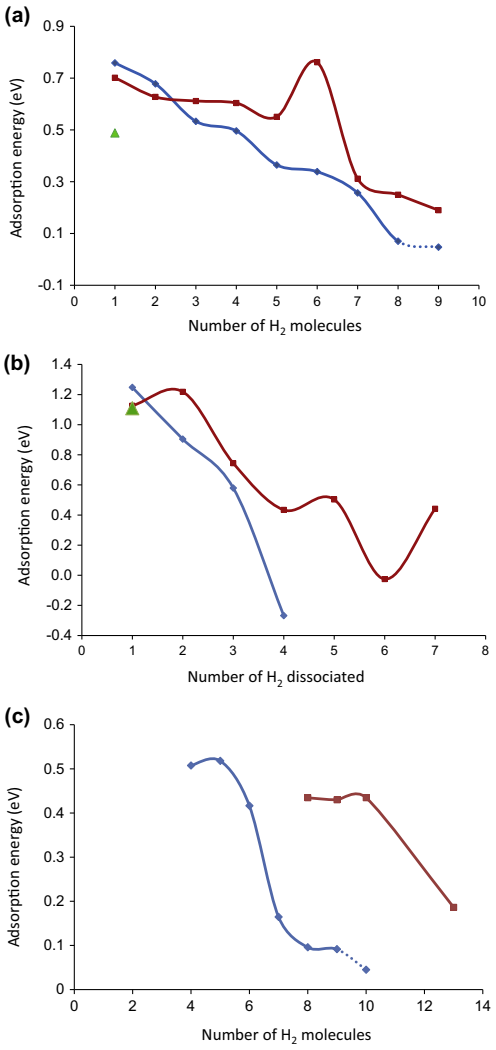

Fig. 3. Adsorption energies of (molecular or dissociated) hydrogen on free Pd_6 (red curves), Pd_6 supported on pristine graphene (green triangles) and Pd_6 anchored on a graphene vacancy (blue curves). (a) Adsorption energy of the nth hydrogen molecule adsorbed on Pd_6 preloaded with $(n-1)$ hydrogen molecules. The blue dotted line indicates that the ninth hydrogen molecule does not bind directly to Pd_6 anchored on a vacancy but begins to form a second hydrogen layer around the Pd cluster at a larger distance. (b) Dissociative chemisorption energy of the nth hydrogen molecule adsorbed on Pd_6 preloaded with $(n-1)$ dissociated hydrogen molecules. (c) Blue curve: Adsorption energy of the nth hydrogen molecule ($n = 4$–10) adsorbed in molecular form on Pd_6 anchored on a graphene vacancy preloaded with $(n-1)$ hydrogen molecules, three of them dissociated and $(n-4)$ molecular. The blue dotted line indicates that the tenth hydrogen molecule does not bind directly to Pd_6 but begins to form a second hydrogen layer around the Pd cluster at a larger distance. Red curve: Adsorption energy of the nth hydrogen molecule ($n = 8$–13) adsorbed on free Pd_6 preloaded with $(n-1)$ hydrogen molecules, seven of them dissociated and $(n-8)$ molecular. (For interpretation of the references to colour in this figure legend, the reader is referred to the web version of this article.)

orption of a hydrogen molecule. However, the free Pd_6 cluster is able to dissociate up to seven molecules. The successive chemisorption of hydrogen induces progressive structural transformations of the cluster (see Fig. 4). Starting with the OCT structure of the clean (without hydrogen) cluster, successive dissociative chemisorption of one to seven hydrogen molecules leads to OCT, iPB, iPB, decorated square pyramid, pentagonal pyramid, OCT, and OCT structures of Pd_6, respectively. Beginning with the sixth chemisorbed molecule, one H atom goes inside the octahedral cage of free Pd_6. It is interesting to notice that this small cluster already exhibits the tendency of bulk palladium to dissolve hydrogen. The seventh dissociated hydrogen molecule preserves the H atom inside the octahedral cage.

Fig. 3b shows the chemisorption energies of successive hydrogen molecules dissociated on free and supported Pd_6. The effect of the supporting layer on the dissociation energies of the first three hydrogen molecules is not large. However, the cluster anchored on the vacancy saturates with fewer (three) dissociated hydrogen molecules than the free cluster (seven). Similarly to the case of molecular adsorption, the effect of the supporting layer on the hydrogen saturation limit is two fold: (1) the steric effect, preventing hydrogen from being accomodated all around the Pd cluster, and (2) the chemical effect, preventing the attachment of hydrogen to Pd–Pd bonds or Pd faces involving the Pd atom that saturates the vacancy (see below for an analysis of the interaction between hydrogen and the Pd cluster).

Although dissociative chemisorption is the preferred channel for hydrogen adsorption on clean (without hydrogen) free and supported Pd clusters, there is a competition between the two channels as the Pd clusters are being loaded with hydrogen and, finally, the molecular adsorption becomes more stable. Thus, to identify the most stable situation, we have investigated both channels (molecular and dissociative) for adsorption of one additional hydrogen molecule (nth molecule) on a Pd cluster preloaded with $n-1$ molecules. On both free Pd_6 and Pd_6 anchored on a graphene vacancy the dissociative channel is more stable for adsorption of one and two hydrogen molecules, and the two channels are almost degenerate for adsorption of the third hydrogen molecule. But from the forth molecule onwards, the molecular channel is more stable. Actually, it becomes the only stable channel on Pd_6 anchored on a graphene vacancy, and six additional molecules can be adsorbed in the molecular form in this case. Thus, the cluster becomes saturated with nine hydrogen molecules, three dissociated and six in molecular form, as shown in Fig. 5. The successive adsorption energies in the molecular adsorption channel on Pd_6 anchored on a graphene vacancy and preloaded with three dissociated molecules are shown in Fig. 3c. On the other hand free Pd_6 can dissociate up to seven hydrogen molecules. Starting with the eighth molecule, the molecular adsorption is the only stable channel and the cluster can adsorb six additional molecules. Thus, the free Pd cluster becomes saturated with thirteen hydrogen molecules, seven dissociated and six in molecular form (see Fig. 5). Notice that the same number, six, of additional hydrogen molecules can be adsorbed in molecular form on free and supported Pd_6 clusters which have been previously fully saturated with dissociated hydrogen. The chemical and steric effects of the supporting layer are not so apparent in this case, although these effects are clearly present through the smaller saturation limit for dissociatively chemisorbed hydrogen and the smaller total saturation limit of the supported Pd clusters. The successive adsorption energies of molecular hydrogen on free Pd_6 preloaded with seven dissociated molecules are shown in Fig. 3c.

On the other hand, it is interesting to notice that free Pd_6 preloaded with one to six dissociated hydrogen molecules can also adsorb additional hydrogen in molecular form. The molecular adsorption energy of one H_2 on Pd_6 preloaded with n ($n = 1$–6) dissociated molecules is about 0.7 eV, almost independent of n.

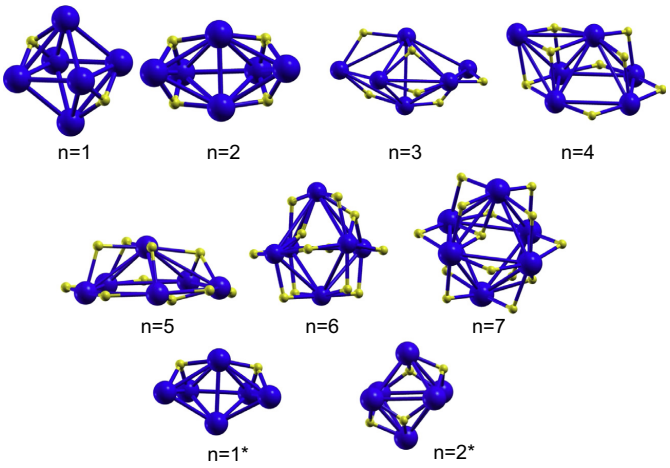

Fig. 4. Optimized structures of dissociated hydrogen adsorbed on free Pd_6 clusters. The lowest energy configurations are shown for one to seven dissociated molecules. Moreover, two higher energy configurations (marked with an asterisk) are also shown corresponding to the dissociation of one molecule on iPB and the dissociation of two molecules on the OCT structures of Pd_6, respectively. The Cartesian coordinates of all the structures are available in the Supplementary Material.

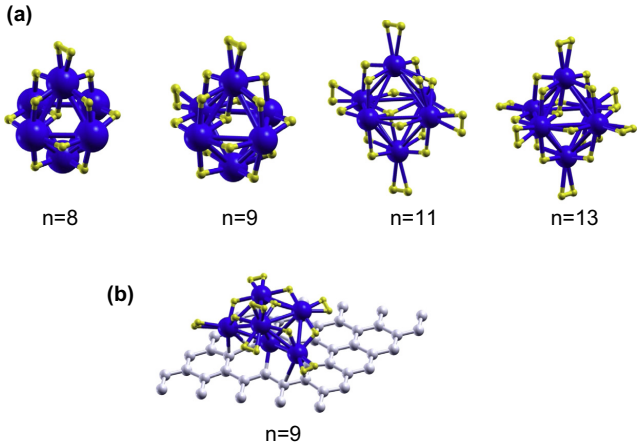

Fig. 5. (a) Optimized structures for n hydrogen molecules ($n = 8$–13) adsorbed on a free Pd_6 cluster. Seven molecules are dissociated and $(n - 7)$ are adsorbed in molecular form. (b) Optimized structure of Pd_6 anchored on a graphene vacancy fully saturated with nine adsorbed hydrogen molecules, three of them dissociated and six in molecular form. The Cartesian coordinates of all the structures are available in the Supplementary Material.

This value, however, is higher than the molecular adsorption energy of 0.4 eV (shown in Fig. 3c) of one H_2 molecule on the Pd cluster saturated with seven dissociated molecules.

The nature of the bonding between hydrogen and the Pd clusters can be investigated by calculating the electronic density difference $\Delta\rho$ between the system with adsorbed hydrogen and the two separated subsystems, formed by hydrogen on one hand and the free or supported Pd cluster on the other. $\Delta\rho$ for the adsorption of one hydrogen molecule on free Pd_6 is defined as

$$\Delta\rho = \rho(H_2 \text{ on } Pd_6) - \rho(H_2) - \rho(Pd_6) \quad (1)$$

where ρ is the electronic density. In the case of molecular adsorption of hydrogen on a free Pd_6 cluster, an increase (yellow surface in Fig. 6) of electronic density between the hydrogen molecule and the nearest Pd atom is observed, indicating a covalent type of bonding [23]; moreover some polarization is also apparent. The bond is localized and involves only one Pd atom. Additional adsorbed hydrogen molecules exhibit each of them a similar type of bonding localized around the attachment site (a Pd atom). However, in the case of dissociative chemisorption of hydrogen, each individual H atom sits in an environment of excess electronic density, characteristic of a metal-hydride type of bonding. The two types of bonding can coexist in the same cluster as it is shown in Fig. 6 for the case of two adsorbed molecules, one in the molecular form and the other dissociated. It is interesting to notice that we had found the same types of bonding [10] for the adsorption of hydrogen on Pd clusters anchored on graphene vacancies. This indicates that the supporting layer and the defects do not modify the

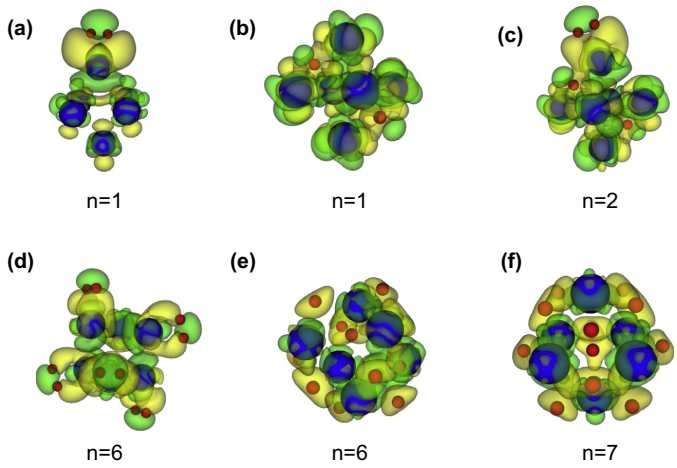

Fig. 6. Electronic density difference, $\Delta\rho$, between the system formed by hydrogen adsorbed on free Pd_6 and the two separated subsystems, hydrogen on one side and Pd_6 on the other side, for the cases of (a) molecular adsorption of one hydrogen molecule, (b) dissociative chemisorption of one molecule, (c) adsorption of two molecules, one dissociated and the other in molecular form. (d) Molecular adsorption of six hydrogen molecules, (e) dissociative chemisorption of six molecules, (f) dissociative chemisorption of seven molecules. The yellow isosurfaces correspond to positive values of the electronic density difference and the green isosurfaces to negative values. Red and blue balls represent H and Pd atoms, respectively. (For interpretation of the references to colour in this figure legend, the reader is referred to the web version of this article.)

type of bonding between palladium and hydrogen, because the interaction is local. Notice, however that some regions of the supported Pd clusters, those in direct contact with the vacancy and the graphene support, become inactive for hydrogen adsorption.

4. Conclusions

Doping with palladium has been proposed as a promising way to enhance the hydrogen storage capacity of nanoporous carbon materials. One of the enhancement mechanisms is the direct adsorption and/or dissociation of hydrogen on the Pd clusters doping the material. To better understand the role of the Pd dopant we have investigated, using the Density Functional formalism, the effect of the graphitic support and of the structural defects existing on the support on the adsorption and dissociation of hydrogen on palladium clusters. To this aim we have compared, as a case study, free Pd_6 clusters with Pd_6 supported on pristine graphene and with Pd_6 anchored on a graphene vacancy.

Two possible adsorption channels of hydrogen on Pd clusters, namely molecular adsorption and dissociative chemisorption, are found on both free and supported palladium clusters. The graphitic support does not modify the type of bonding corresponding to these two channels, weak covalent bond with some polarization for the molecular adsorption, and a hydride type of bonding between the dissociated hydrogen and the metal. The saturation limit for molecular adsorption of hydrogen is higher on free Pd_6 (twelve adsorbed hydrogen molecules) than on Pd_6 supported on pristine graphene (nine) and than on Pd_6 anchored on a graphene vacancy (eight). However, in all cases, the most stable adsorption channel is the dissociative chemisorption of hydrogen, and a competition between the two channels is stablished as additional hydrogen molecules are adsorbed onto the cluster. Pd_6 anchored to a graphene vacancy can dissociate three hydrogen molecules, whereas free Pd_6 is able to dissociate up to seven molecules. Six more molecules can be adsorbed in the molecular form in both cases. Clearly, more hydrogen can be adsorbed/dissociated in the free Pd clusters than in the supported ones. The supporting surface has two main effects on the adsorption of hydrogen on the Pd clusters: (1) a steric effect that does not allow hydrogen to fully surround the Pd cluster and (2) a chemical effect induced by the defect (vacancy) preventing hydrogen to be adsorbed on the Pd atom saturating the vacancy. In summary, although free and supported Pd clusters exhibit the same two channels for hydrogen adsorption, the effect of the supporting graphitic layer and of the defects have to be considered explicitly to asses the role of the Pd dopant on the storage capacity of nanoporous carbons. Another interesting observation from Fig. 3 is that most of the calculated adsorption energies fall in a range that makes possible the desorption step, required for using the stored hydrogen.

Acknowledgments

This work was supported by MICINN of Spain (Grant MAT2014-54378-R) and Junta de Castilla y León (Grant VA050U14). A.G. acknowledges a predoctoral fellowship from Junta de Castilla y León.

Appendix A. Supplementary material

Supplementary data associated with this article can be found, in the online version, at http://dx.doi.org/10.1016/j.comptc.2016.11.029.

References

[1] Y. Gogotsi, R.K. Dash, G. Yushin, T. Yildirim, G. Laudisio, J.E. Fischer, Tailoring of nanoscale porosity in carbide-derived carbons for hydrogen storage, J. Am. Chem. Soc. 127 (2005) 16006–16007.
[2] A. Linares-Solano, M. Jordá-Beneyto, D.L.-C.M. Kunowsky, F. Suárez-García, D. Cazorla-Amorós, Hydrogen storage in carbon materials, in: P.G.A.P. Terzyk, P. Kowalczyk (Eds.), Carbon Materials: Theory and Practice, Research Signpost, Kerala, India, 2008, pp. 245–281.
[3] P. Jena, Materials for hydrogen storage: past, present, and future, J. Phys. Chem. Lett. 2 (2011) 206–211.
[4] Multi-Year Research, Development and Demonstration Plan: Planned Program Activities for 2005–2015. Technical Plan–Storage. Updated april 2009, 2009.

<http://www1.eere.energy.gov/hydrogenandfuelcells/mypp/pdfs/storage.pdff>.

[5] C.I. Contescu, C.M. Brown, Y. Liu, V.V. Bhat, N.C. Gallego, Detection of hydrogen spillover in palladium-modified activated carbon fibers during hydrogen adsorption, J. Phys. Chem. C 113 (2009) 5886–5890.

[6] C.I. Contescu, K. van Benthem, S. Li, C.S. Bonifacio, S.J. Pennycook, P. Jena, N.C. Gallego, Single Pd atoms in activated carbon fibers and their contribution to hydrogen storage, Carbon 49 (2011) 4050–4058.

[7] B. Zielinska, B. Michalkiewicz, X. Chen, E. Mijowska, R.J. Kalenczuk, Pd supported ordered mesoporous hollow carbon spheres (OMHCS) for hydrogen storage, Chem. Phys. Lett. 647 (2016) 14–19.

[8] I. Cabria, M.J. López, S. Fraile, J.A. Alonso, Adsorption and dissociation of molecular hydrogen on palladium clusters supported on graphene, J. Phys. Chem. C 116 (2012) 21179–21189.

[9] M.J. López, I. Cabria, J.A. Alonso, Palladium clusters anchored on graphene vacancies and their effect on the reversible adsorption of hydrogen, J. Phys. Chem. C 118 (2014) 5081–5090.

[10] A. Granja, J.A. Alonso, I. Cabria, M.J. López, Competition between molecular and dissociative adsorption of hydrogen on palladium clusters deposited on defective graphene, RSC Adv. 5 (2015) 47945–47953.

[11] M.J. López, I. Cabria, J.A. Alonso, Simulated porosity and electronic structure of nanoporous carbons, J. Chem. Phys. 135 (2011) 104706.

[12] C. Zhou, S. Yao, J. Wu, R.C. Forrey, L. Chen, A. Tachibana, H. Cheng, Hydrogen dissociative chemisorption and desorption on saturated subnano palladium clusters (Pd_n, n = 29), Phys. Chem. Chem. Phys. 10 (2008) 5445–5451.

[13] A.W. Pelzer, J. Jellinek, K. Jackson, H_2 saturation on palladium clusters, J. Phys. Chem. A 119 (2015) 3594–3603.

[14] V. D'Anna, D. Duca, F. Ferrante, G.L. Manna, DFT studies on catalytic properties of isolated and carbon nanotube supported Pd_9 cluster – I: adsorption, fragmentation and diffusion of hydrogen, Phys. Chem. Chem. Phys. 11 (2009) 4077–4083.

[15] I. López-Corral, E. Germán, A. Juan, M.A. Volpe, G.P. Brizuela, DFT study of hydrogen adsorption on palladium decorated graphene, J. Phys. Chem. C 115 (2011) 4315–4323.

[16] C.M. Ramos-Castillo, J.U. Reveles, R.R. Zope, R. de Coss, Palladium clusters supported on graphene monovacancies for hydrogen storage, J. Phys. Chem. C 119 (2015) 8402–8409.

[17] DaCapo, See <https://wiki.fysik.dtu.dk/dacapo> For a Description of the Total Energy Code, Based on the Density Functional Theory, 2009.

[18] D. Vanderbilt, Soft self-consistent pseudopotentials in a generalized eigenvalue formalism, Phys. Rev. B 41 (1990) R7892.

[19] J.P. Perdew, Y. Wang, Accurate and simple analytic representation of the electron-gas correlation energy, Phys. Rev. B 45 (1992) 13244.

[20] H. Monkhorst, J. Pack, Special points for Brillouin-zone integration, Phys. Rev. B 13 (1976) 5188–5192.

[21] I. Cabria, M.J. López, J.A. Alonso, Theoretical study of the transition from planar to three-dimensional structures of palladium clusters supported on graphene, Phys. Rev. B 81 (2010) 035403.

[22] M. Moseler, H. Häkkinen, R.N. Barnett, U. Landman, Structure and magnetism of neutral and anionic palladium clusters, Phys. Rev. Lett. 86 (2001) 2545–2548.

[23] G.J. Kubas, Molecular hydrogen complexes: coordination of a sigma bond to transition metals, Acc. Chem. Res. 21 (1988) 120–128.

5.3 Additional Results

Energy barriers have been included in this section as unpublished additional results. These new results do not change the final conclusions about steric and chemical effects of adsorbing hydrogen on free and supported Pd nanoparticles.

Section 4.3.4 was devoted to investigate the energy barriers for several processes relevant for the adsorption of hydrogen on Pd_6 anchored on a graphene vacancy. In order to state the effect of the graphene support and of the defects on the activation barriers, we have studied the activation barriers for the corresponding processes on free Pd_6 clusters.

5.3.1 Energy Barriers

Energy barriers for (i) interconversion between OCT and iPB free structures in the absence of hydrogen, (ii) transition from OCT to iPB free structures with one dissociated hydrogen molecule adsorbed and (iii) the diffusion of one hydrogen atom on the unsupported Pd OCT structure are presented below. The Nudged Elastic Band (NEB) method in conjunction with Density Functional Theory (DFT) was used to find the saddle points and local minimum energy pathways for all the above mentioned processes. For the initial and final structures we have chosen the lowest energy configurations calculated from static structural relaxations.

The energy barrier for the transition between the OCT and the iPB structures of the free Pd_6 cluster is 0.29 eV. An edge on the OCT structure is broken and the two Pd atoms separate until the iPB structure is reached. The distance between these two Pd atoms in the iPB structure is 4.06 Å. Since the iPB structure of free Pd_6 is less stable than the OCT configuration, an up-hill energy barrier is found for this structural transformation (0.29 eV). Figure 5.1 shows the minimum energy path for the transformation from OCT to the iPB configuration.

The energy barrier for the interconversion between the OCT and iPB structures with one dissociated hydrogen molecule adsorbed on the free Pd_6 cluster is 0.20 eV. The two hydrogen atoms are adsorbed on faces which share a single vertex. The atoms remain in these positions relative to the Pd while one of the edges is breaking until reaching the iPB structure. In the final conformation, the two palladium atoms of the broken edge are separated 4.57 Å. This barrier is is only 0.05 eV lower than in the supported Pd_6 case (0.25 eV). Figure 5.2 shows the minimum energy path for the interconversion between OCT and iPB structures with one dissociated hydrogen molecule.

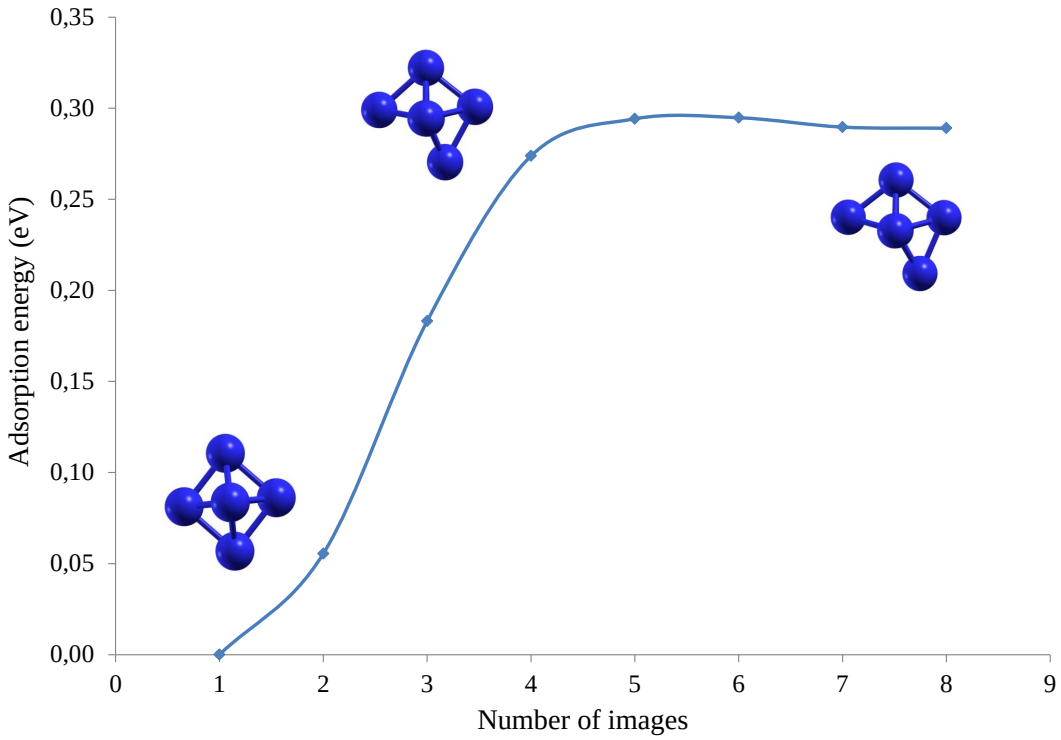

Figure 5.1: Minimum energy path for the structural change of a free Pd_6 cluster from the lowest energy OCT structure to the higher energy iPB configuration. There is an energy barrier of 0.29 eV. Pictures for images 1, 5 and 8 have been included in the chart.

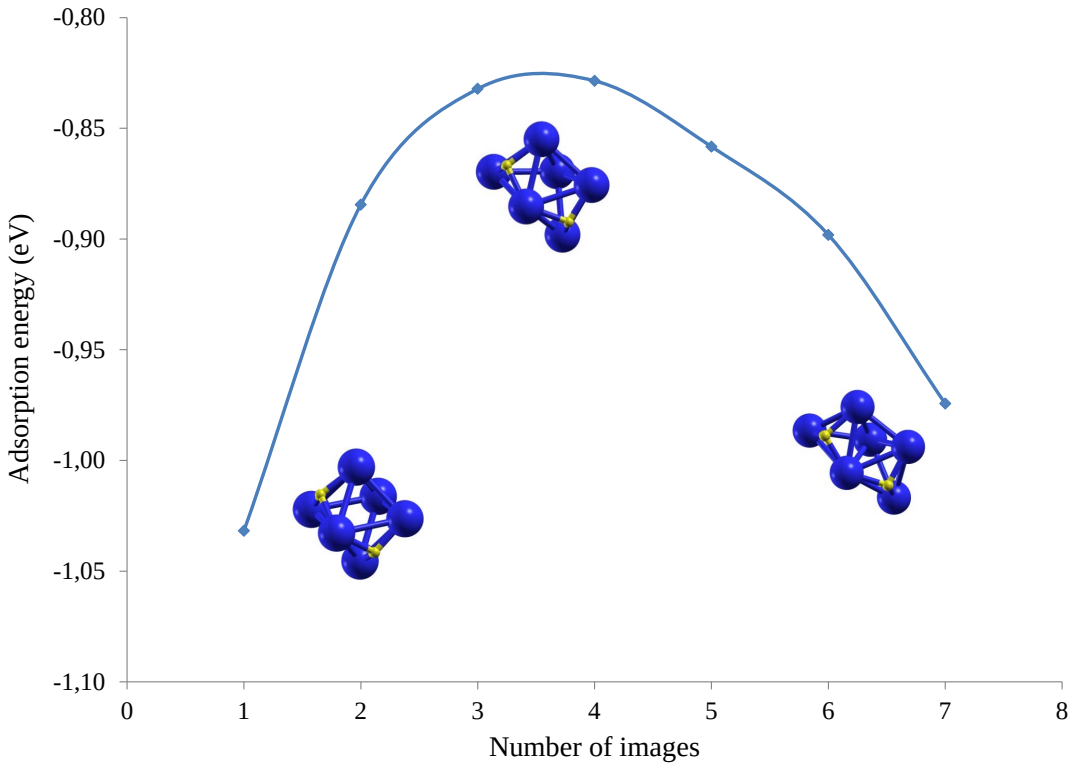

Figure 5.2: Minimum energy path for the structural change of free Pd_6 with one dissociatively adsorbed hydrogen molecule, from the lowest energy OCT structure to the higher energy iPB configuration. There is an energy barrier of 0.20 eV. The hydrogen atoms remain in the same configuration relative to the palladium. Pictures for images 1, 4 and 7 have been added to the chart.

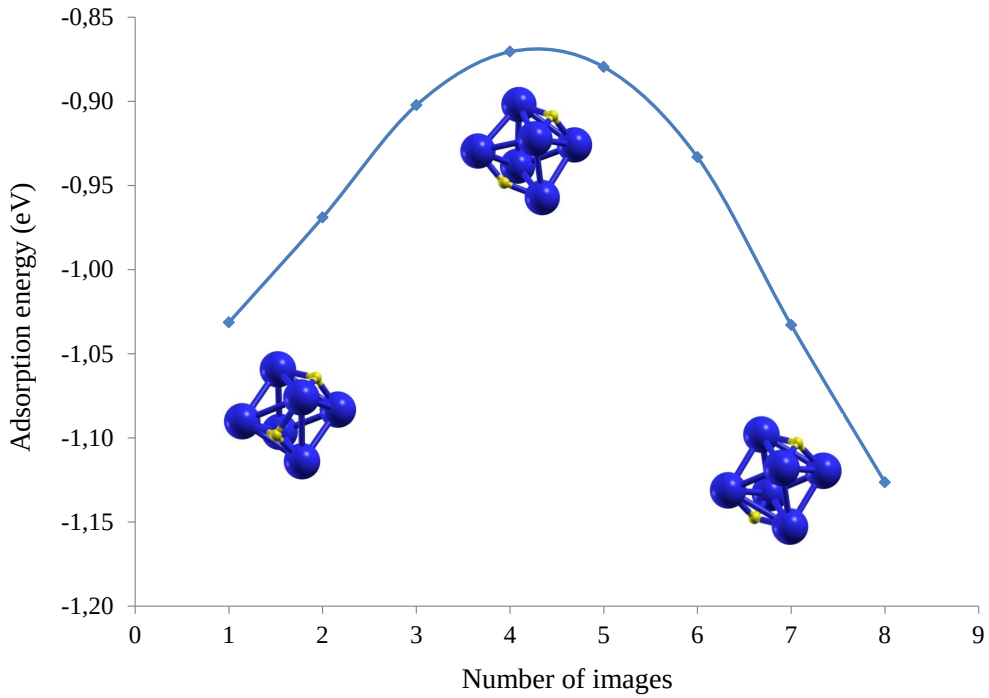

Figure 5.3: Minimum energy path for the diffusion of one H atom (of a dissociated hydrogen molecule adsorbed on free Pd_6 in the OCT structure) on the surface of the cluster. There is an energy barrier of 0.16 eV. In the initial state, two hydrogen atoms are adsorbed on two adjacent faces sharing a vertex of the octahedral structure. In the final state, the two hydrogen atoms are adsorbed on two opposed faces. Pictures for images 1, 4 and 8 have been added to the chart.

We have also calculated the minimum energy path for the diffusion of one H atom (of a dissociated hydrogen molecule adsorbed on free Pd_6 in the OCT structure) on the surface of the cluster. In the initial configuration the two hydrogen atoms are adsorbed on two adjacent faces sharing a single vertex of the octahedral structure. One hydrogen atom diffuses through an edge of the Pd nanoparticle. In the final state, the two hydrogen atoms are chemisorbed on the center of two opposed faces. The diffusion barrier is 0.16 eV. This value is larger than the one obtained for the diffusion of a single hydrogen atom within the Pd ICO cluster supported on a graphene mono-vacancy which is 0.04 eV (see Figure 4.7). Three effects that may account for this difference are: (i) the surface might play a role in the hydrogen atom diffusion, (ii) structure of free Pd_6 and Pd_6 supported on a graphene vacancy are different, OCT and iPB, respectively. Since the iPB structure is less compact than the OCT structure may facilitate the diffusion of H on the Pd surface, or (iii) the considered diffusion paths are very distinct, in the iPB structure the path which the H atom follows is more planar than in the OCT where the H atom has to turn around the edge. Figure 5.3 represents the energy barrier for the single hydrogen atom diffusion within the octahedral Pd structure.

5.4 Conclusions

Doping with Pd atoms and clusters enhances the hydrogen adsorption, dissociation and desorption processes in nanoporous carbons. To clarify the role of the Pd dopant we have studied the effect of the pristine and defective graphene support on the adsorption and the dissociation of hydrogen on the metal nanoparticle. To achieve this, we have compared free Pd_6 clusters with Pd_6 supported on pristine graphene and anchored on a graphene mono-vacancy.

Two adsorption channels (molecular and dissociative) are found on free and supported Pd clusters. The carbon support does not change the type of bonding of these two channels: weak covalent bond with a bit polarization for molecular adsorption and hydride type of bonding for dissociated hydrogen molecule and the metal. The saturation limit for molecular adsorption is higher on free Pd_6 cluster (twelve hydrogen moelcules) than on Pd_6 supported on pristine graphene (nine) and than on Pd_6 anchored on graphene mono-vacancy (eight). Nevertheless, dissociative chemisorption channel is the most stable in all cases. Pd_6 nanoparticles anchored to a vacancy can dissociate three hydrogen molecules whereas free Pd_6 clusters are able to dissociate up to seven molecules. The dissociative channel on free Pd clusters prompts several structural changes while adding the next dissociated hydrogen molecule. The minimum energy paths for structural transition from OCT to iPB

have been calculated for two systems: (i) bare free Pd_6 clusters (0.29 eV) and (ii) free Pd_6 aggregates with one dissociated hydrogen molecule (0.20 eV). These values are in concordance with the 0.25 eV of the minimum energy path for the structural transition from OCT to ICO structure supported on the graphene mono-vacancy. Six and seven additional hydrogen molecules can be adsorbed to the dissociative channel on free Pd_6 and on Pd_6 anchored on a graphene mono-vacancy, respectively. Obviously, more hydrogen can be adsorbed and dissociated on free clusters than on the supported ones.

Thus, the supporting surface has two main effects on the hydrogen adsorption on the Pd nanoparticles: (i) a steric effect that does not allow hydrogen to fully surround the metal aggregate and (ii) a chemical effect induced by the vacancy preventing hydrogen to be adsorbed on the saturating Pd atom.

Chapter 6

Competition between Pd and H_2 to saturate graphene vacancies

Physicists are made of atoms. A physicist is an attempt by an atom to understand itself.

Michio Kaku.

In the previous Chapters we have shown that the vacancies of the graphitic support play a key role in modulating hydrogen adsorption and desorption and the saturation limit of Pd_6 clusters supported on graphene. Although Pd clusters are strongly attached to graphene vacancies, the interaction of atomic hydrogen with the vacancies might affect the stability of the material since atomic hydrogen also binds strongly to the dangling bonds of defects and edges of graphitic carbon. Therefore, we have investigated the competition between hydrogen atoms, on one hand, and Pd atoms and clusters, on the other hand, to decorate the defects of the graphene layer. Our study also shows that the bonding capacity of the graphene vacancies is not exhausted through attachment of Pd atoms or clusters only on one side of the layer. The other side of the vacancy remains quite reactive and then additional Pd atoms or clusters can be attached on the other side of the layer.

In Section 6.1 we present a brief description of the theoretical model. In Section 6.2, the references and a more detailed explanation of the results can be found in the attached article. Finally, in Section 6.3 some conclusions are provided.

6.1 Theoretical Model

Computational simulations were performed to investigate the adhesion of hydrogen, atomic Pd and Pd_6 clusters to the graphene to the vacancy. As mentioned in former sections and in order to compare among systems, the computational details are identical to the ones which have been already described in Section 3.6.2 and have

been summarized in Table 3.1. Moreover, in this Chapter we have included dispersion interaction corrections which have been taken into account by using Grimme's DFT-D3 combined with the PBE functional for exchange-correlation. As a damping function we have used the modified version of BJ, the so-called BJM. Both energies, DFT-PW91 and DFT-PBE corrected for dispersion, are given in the accompanying article.

An extensive search for exploring several combinations and the interactions of hydrogen, Pd atom and Pd_6 clusters with one side and with both sides of the vacancy have been tested and fully optimized until the cohesive energies were converged within 10 meV. A more complete description of the theoretical model can be found in the accompanying article.

6.2 Publication: Competition between palladium clusters and hydrogen to saturate graphene vacancies

This Chapter provides the energies and structures for hydrogen and metal interactions with both sides of the graphene vacancy and the competition between hydrogen and Pd for saturating the defect.

THE JOURNAL OF PHYSICAL CHEMISTRY C

Article

Cite This: J. Phys. Chem. C 2017, 121, 10843-10850

pubs.acs.org/JPCC

Competition between Palladium Clusters and Hydrogen to Saturate Graphene Vacancies

Alejandra Granja-DelRío,[†] Julio A. Alonso,*[,†,‡] and María J. López*[,†]

[†]Departamento de Física Teórica, Atómica y Óptica, Universidad de Valladolid, 47011, Valladolid, Spain

[‡]Donostia International Physics Center, 20018 San Sebastian, Spain

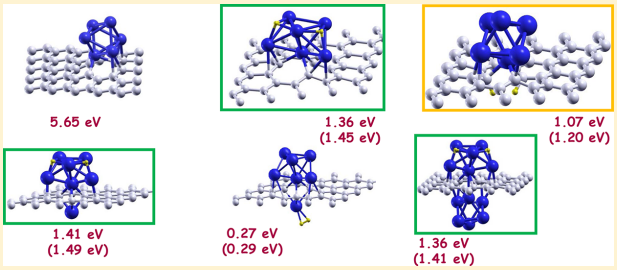

ABSTRACT: Doping with palladium has been proposed as a means to enhance the hydrogen storage capacity of nanoporous carbon materials. Palladium atoms and clusters attach strongly to defects on the walls of nanoporous carbons, which can be mimicked as graphene layers with vacancies. On the other hand, atomic hydrogen also binds strongly to the dangling bonds of defects and edges of graphitic carbon. Therefore, hydrogen adsorbed on Pd-doped nanoporous carbons could compete with the Pd dopant to saturate the vacancies. In this work we have performed density functional calculations to investigate the competition between palladium atoms and clusters, on one hand, and hydrogen, on the other hand, to saturate graphene vacancies. We find that palladium binds stronger than hydrogen to graphene vacancies and, therefore, hydrogen can not replace the palladium atoms or clusters attached to the vacancies. Instead, hydrogen adsorbs on the palladium. Thus, hydrogen adsorption on Pd-doped carbons does not destroy the stability of the material. Moreover, our study shows that graphene vacancies decorated with Pd just on one side of the graphene layer are not fully saturated. The other side of the vacancy remains quite reactive and therefore Pd atoms and clusters can be attached, simultaneously, to both sides of the vacancy. Interestingly, the hydrogen adsorption mechanisms and energies do not depend on whether Pd atoms and clusters are decorating one side or both sides of the vacancies.

1. INTRODUCTION

Nowadays, the threats from global warming due to the consumption of fossil fuels have increased. This problem requires adopting new strategies to find other sources of energy that could replace fossil fuels, and hydrogen is considered a good candidate.[1,2] Hydrogen is an energy carrier that holds tremendous promise as a new renewable and clean energy option. The basic mechanism of this fuel is the reaction of hydrogen with atmospheric oxygen in a hydrogen fuel cell, producing an electric current, and the only emission is water. However, hydrogen is a gas, and the problem with this technology is to find an efficient way to store hydrogen in a tank at room temperature and moderate pressures, to be able to run the car for about 600−700 km.[3] For those reasons, the USA Department of Energy established three main targets for an efficient hydrogen storage as (a) a gravimetric density of at least 7.5%, (b) a volumetric density of 0.07 kg of hydrogen per liter, and (c) a reversible operation at ambient temperature and moderates pressures.[4] A promising method to store hydrogen is to adsorb it in light porous solid materials like porous carbon structures, because these have a lightweight and a large surface area. Those materials have a reasonable storage capacity of hydrogen at low temperatures (about 77 K), but their capacity diminishes drastically at room temperature and normal pressure[5,6] Thermodynamic estimations indicate that the adsorption energies that would lead to an efficient cyclic adsorption/desorption operation at room temperature and moderate pressures are in the range of 0.2−0.6 eV per hydrogen molecule, which is a narrow energy window intermediate between typical physisorption (less than 0.2 eV) and chemisorption (more than 0.6 eV).[7,8]

Experimental work by Contescu et al.[9,10] indicated that doping the carbon materials with metallic species is a promising

Special Issue: ISSPIC XVIII: International Symposium on Small Particles and Inorganic Clusters 2016

Received: November 29, 2016
Revised: February 1, 2017
Published: February 16, 2017

DOI: 10.1021/acs.jpcc.6b12018
J. Phys. Chem. C 2017, 121, 10843−10850

strategy to enhance the hydrogen adsorption because these metal species have the effect of increasing the binding energies of molecular hydrogen to the pore walls.[11−17] In addition, the deposited metallic atoms and small clusters also can bind several hydrogen molecules, and this increases the hydrogen storage capacity of the material.[10,18] The binding of molecular hydrogen to transition metals has been explained using the Kubas model as a donation of electronic charge to the unfilled d orbitals of transition metals such as Pd, followed by back-donation from the transition metal to the antibonding orbital of H_2.[19] However, there are some difficulties with the metal doping of graphitic materials. The first one is that aggregation of the adsorbed dopant atoms and small clusters may occur, because metal−metal bonding is usually stronger than the metal−carbon bonding.[20−22] Theoretical studies based on density functional theory reported that transition metal adatoms on pristine graphene have binding energies ranging from 0.2 to 1.5 eV, and their calculated migration barriers proved to be low, in the range of 0.2−0.8 eV, indicating that those adatoms should be mobile even at room temperature when deposited on pristine graphene. These results reveal a tendency of adsorbed transition metal atoms to form large clusters on the graphene surface, leading to a reduction in the potential hydrogen storage capacity of the doped material. The second problem is that desorption of metal−hydrogen complexes often competes with desorption of H_2. Both problems will be reduced by increasing the binding energy of the metal atoms or small metal clusters to the supporting carbon substrate, and this is achieved by anchoring the metal atoms and small clusters to the abundant existing defects in the carbon networks of the graphitic pore walls. In fact, it has been found that defects in graphene, such as mono- and divacancies, increase the adsorption energies of metal atoms and small metal clusters significantly, to the point of exceeding the cohesive energy of the metal.[23−26]

Hydrogen adsorption energies are dependent on both the size of the Pd cluster and the adsorption site on the cluster.[18,27,28] A comparison between adsorption on free Pd clusters,[29,30] adsorption on Pd clusters supported on pristine graphene,[27] and adsorption on Pd clusters anchored on vacancies[18,26,30] reveals that the vacancies play a role in modulating hydrogen adsorption through their interaction with the Pd clusters. One of the effects is steric, that is, the Pd atoms bonded to the vacancy are less exposed to hydrogen. The second, and equally important effect is chemical, that is, the Pd atoms bonded to the vacancy lose part of their affinity toward hydrogen. For instance, we have reported[26] that the adsorption binding energy of molecular hydrogen on a single Pd atom anchored on a graphene vacancy is 0.21 eV. This value contrasts with the adsorption energies of 0.96 eV on Pd-doped pristine graphene and 1.12 eV on a free Pd atom. That is, the Pd atom utilizes a part of its bonding capacity by interacting with the dangling bonds of the graphene vacancy, and consequently its bonding with the H_2 molecule is weaker compared to the bonding of H_2 with Pd adsorbed on pristine graphene or with free Pd.

Other workers have also investigated the interaction of hydrogen with metal atoms and clusters (lithium,[31] aluminum,[32] nickel[33]) anchored on graphene vacancies, and their consequences for hydrogen storage. Very recently, Rangel and co-workers[34] investigated the effect of having more complex vacancy defects, namely, vacancies in which some of the surrounding carbon atoms have been replaced by nitrogen. Their calculations show that the presence of the nitrogen atoms lowers the formation energies of those vacancies.

Although palladium clusters attach strongly to graphene vacancies,[26] atomic hydrogen produced by the dissociation of H_2 on the Pd clusters[18,27] could also interact strongly with the dangling bonds of those vacancies, affecting perhaps the stability of the material. In order to unravel the competition between hydrogen and the metal to decorate vacancies in the inner walls of porous carbons we have performed density functional calculations for different configurations relevant to that competition. The result is that Pd atoms and clusters attach to graphene vacancies with higher binding energies than hydrogen and, therefore, hydrogen adsorption and dissociation on Pd-doped carbons does not affect the stability of the doped material. In addition, our study shows that the bonding capacity of graphene vacancies does not saturate through Pd attachment on only one side of the layer, and that additional Pd atoms or clusters can also be attached on the other side of the layer. Both are favorable conclusions for the technology of hydrogen storage in doped porous carbons. In Section 2 we present the key features of the Density Functional Formalism used in the calculations, Section 3 presents the results and the conclusions are reported in Section 4.

2. THEORETICAL MODEL

We have investigated the mechanisms of saturation of graphene single-vacancies by hydrogen, a palladium atom and Pd_6 clusters using the density functional theory (DFT). Attaching those species on one side and on both sides of the vacancy is investigated. The graphene layer is a good model often used to simulate the graphitic walls of nanoporous carbon materials, and vacancies are representative defects of those walls. Palladium deposited on graphene tends to aggregate and form three-dimensional clusters,[20] especially near vacancies, where they become strongly attached.[26] The DFT calculations have been performed with the DACAPO[35] code, using the supercell method and a plane wave basis set. The graphene layer is represented by a supercell containing 5 × 5 hexagonal unit cells, each of which contains two C atoms. The total supercell has 50 carbon atoms (included the one that is removed to create the vacancy). The supercell size in the x direction is 12.33 Å, and in the z direction the supercell is taken to be large enough (14 Å) to avoid interactions between the images of the graphene layer in different supercells. The interactions of the valence electrons with the ionic cores are described with Vanderbilt ultrasoft pseudopotentials.[36] An energy cutoff of 350 eV was taken for the plane wave expansion of the wave functions, and a cutoff of 1000 eV for the electron density, for good convergence. The Monkhorst-Pack[37] k-point set was [2,2,1], and because the supercells used in the calculations are quite large, this selection is sufficient to guarantee convergence in the binding energies better than 10 meV. Electronic exchange and correlation effects are treated by the generalized gradient approximation of Perdew and Wang (GGA-PW91).[38] The DFT-PW91 calculations do not incorporate dispersion interactions but based in other studies one would expect a small contribution (less than 0.2 eV) to the adsorption energies. However, to assess that, indeed, the effect of the dispersion interactions is small, we have also performed dispersion corrected density functional theory calculations using Grimme's DFT-D3[39] combined with the PBE[40] functional for exchange-correlation. The reason for using PBE is that the DFT-D3 method has not been implemented for the

DOI: 10.1021/acs.jpcc.6b12018
J. Phys. Chem. C 2017, 121, 10843−10850

PW91 functional. We have used the modified version[41] of the so-called BJ-damping.[42] Both DFT-PW91 and DFT-PBE corrected for dispersion (DFT-D3) energies are given in the manuscript. Our calculations confirm that the contribution of the dispersion interactions to the adsorption energies of hydrogen is lower than 0.2 eV. An extensive search of the possible combinations and interactions between hydrogen, Pd and both sides of the vacancy has been performed. The search also included the adsorption of a second hydrogen molecule. Then, the structures of all the systems explored were fully optimized until the forces acting on the atoms were smaller than 0.05 eV/Å.

3. RESULTS AND DISCUSSION

Hydrogen adsorbs readily on palladium atoms and clusters supported on graphene vacancies.[18] However, atomic hydrogen, produced by the dissociation of H_2 either on the Pd clusters or on the vacancy, can also saturate the dangling bonds of the C atoms around the vacancy. Moreover, adsorption of palladium and/or hydrogen may take place at a graphene vacancy on both sides of the graphene layer. Therefore, we have first investigated the saturation of the vacancies with palladium and hydrogen on both sides of the graphene layer, and then the competition between palladium and hydrogen for the vacant site. Atomic palladium and Pd_6 clusters are considered as case studies.

Palladium on Graphene Vacancies. Palladium atoms attach strongly to graphene vacancies with an adsorption energy of 5.25 eV[26] (see Figure 1). The Pd atom sits above the center of the vacancy, interacting with the dangling bonds of the three C atoms around the vacant site. The graphene layer deforms a little near the vacancy; the C atoms in direct contact with the Pd atom move out of plane toward Pd by 0.3−0.4 Å, and the next neighboring C atoms (counted from the vacancy) move by 0.1−0.2 Å. The adsorption binding energy given above was calculated as

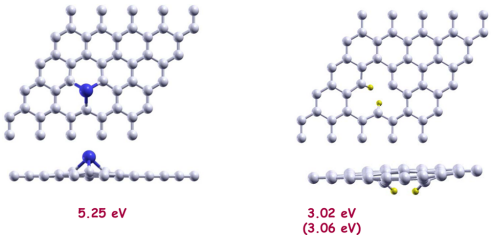

Figure 1. Top and side views of the optimized structures of one Pd atom and one dissociated hydrogen molecule adsorbed on a graphene vacancy, respectively. The corresponding adsorption energies are given in the figure. The PBE+DFT-D3 dispersion corrected adsorption energy of hydrogen is given in parentheses.

$$E_{ad}(\mathrm{Pd}) = E(G) + E(\mathrm{Pd}) - E(\mathrm{Pd\ on\ G}) \quad (1)$$

where E(G) is the total energy of graphene with a vacancy, E(Pd) is the energy of the Pd atom, and E(Pd on G) is the energy of the system formed by Pd adsorbed on the graphene vacancy. Other adsorption binding energies will appear below, and for all of them the definition is analogous, that is, the adsorption energy is obtained by first adding the energies of the two separated systems, substrate and adsorbate, and then subtracting the energy of the composite system after adsorption.

Pd atoms exhibit a strong tendency to form three-dimensional clusters around the graphene vacancies and the clusters attach to the vacancies with substantial adsorption energies[26] of 5.2−5.9 eV. For instance, the lowest energy, octahedral (OCT) structure of Pd_6, binds to the vacancy with an adsorption energy of 5.65 eV (see Figure 3). The cluster structure experiences only a minor distortion upon deposition on the graphene layer. Pd_6 rests on one of its triangular faces. One of the Pd atoms of that face sits above the center of the vacancy and the other two Pd atoms are above two C−C bonds around the vacancy. The C atoms in direct contact with the cluster move out of plane (in the direction of the Pd atoms) by 0.5−0.7 Å and the next shell of C atoms (counted from the vacancy) move by 0.3−0.4 Å. The magnetic moment of 2 μ_B of the free Pd_6 cluster is quenched down to zero upon adsorption on the vacancy due to the strong interaction between the cluster and the vacancy. Similarly, the first isomeric structure of Pd_6 (an incomplete pentagonal bipyramid, IPB) binds to the vacancy with an adsorption energy of 5.79 eV, evaluated with respect to free Pd_6 in the same IPB configuration (see Figure 3). The IPB structure rests on a lateral face of one of the pyramids with the apex atom sitting above the center of the vacancy.

However, graphene vacancies do not become fully saturated by attaching palladium atoms or clusters on one side on the graphene layer only. Pd atoms and clusters can be attached to the vacancy from both sides of the graphene layer (see Figures 2 and 3). Thus, a vacancy already doped with one Pd atom admits a second Pd atom from the other side of the graphene layer with an adsorption energy of 3.31 eV. This energy is higher than the adsorption energy of 1.98 eV for the second Pd atom on the same side of the graphene layer. In this case, the two Pd atoms form a Pd_2 dimer bound to the graphene layer. Thus, saturating the vacancy with two Pd atoms, one on each side of the graphene layer, leads to a configuration more stable than that obtained by attaching the two atoms on the same side. Moreover, the adsorption energies of one Pd atom on the other side of a vacancy having an OCT, or an IPB Pd_6 cluster already attached are 2.72 and 2.79 eV, respectively. Those adsorption energies are a little lower compared to the adsorption of Pd on the other side of a vacancy with a single Pd atom attached, 3.31 eV). This indicates that the other side of vacancies having Pd clusters on one side are less reactive than those having single Pd atoms. This fact becomes also evident when adsorbing a second Pd_6 (OCT) cluster on the other side of a vacancy with one Pd_6 (either in the OCT or in the IPB structure) already attached. The adsorption energy of the second cluster drops to 2.5 and 2.77 eV, respectively, about half of the adsorption energy of the

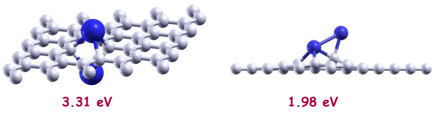

Figure 2. Optimized structures of graphene vacancies doped with one Pd atom on each side of the graphene layer and with a Pd_2 dimer on one side. The adsorption energies of the second Pd atom with respect to the vacancy doped with one Pd atom are also included in the figure.

DOI: 10.1021/acs.jpcc.6b12018
J. Phys. Chem. C 2017, 121, 10843−10850

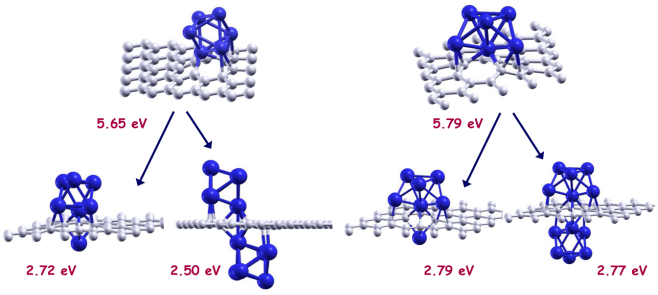

Figure 3. Optimized structures of graphene vacancies doped with a Pd_6 cluster on one side of the graphe layer, and clean or doped with a Pd atom or a Pd_6 cluster on the other side. The following adsorption energies are also included in the figure: for the vacancies doped on one side only, the adsorption energy with respect to the free cluster in the same configuration; for the vacancies doped on both sides, the adsorption energy of the atom, or cluster, on the second side. In the latter case, the reactions are indicated by the arrows.

first one. In spite of the drop, it is worth noticing that the bonding capacity of the vacancy still remains strong.

Competition between Hydrogen and Palladium to Saturate Graphene Vacancies. Graphene vacancies can be also saturated with hydrogen. Similarly to hydrogen adsorption on the edges of graphene nanoribbons,[43] hydrogen molecules adsorb dissociatively on a vacancy, that is, the H−H bond breaks up, and each individual hydrogen atom binds to one of the C atoms that form the vacancy (see Figure 1). Those two C atoms move out of plane by 0.3−0.4 Å in the direction of the H atoms. The activation barriers in the dissociation process are expected to be small. In a previous study[43] we found that the barriers for the dissociation of H_2 on the clean edges of graphene nanoribbons are smaller than 0.2 eV, and Jiang et al.[44] have obtained barriers of 0.8 eV for the dissociation of H_2 on graphene vacancies; in all these cases, the dissociation reaction can proceed at room temperature. The adsorption energy of the dissociated molecule is 3.02 eV; although lower than the adsorption energies of Pd atoms and clusters on the vacancy, it is quite substantial. Therefore, hydrogen might compete with the Pd atoms or clusters to decorate the vacancy.

First we consider the adsorption of hydrogen on vacancies with one Pd atom attached on one side (the upper side in Figure 4). The relevant configurations are shown in Figure 4. Molecular hydrogen adsorbs on top of the Pd atom with an adsorption energy of 0.25 eV. The Pd atom is not able to dissociate the hydrogen molecule. However, the molecule dissociates directly on the vacancy from the other side (botton side) of the graphene layer with an adsorption energy of 1.49 eV. Each H atom interacts with the dangling bond of one C atom of the vacancy, and this arrangement, with the Pd atom and the (dissociated) hydrogen molecule on opposite sides of the vacancy, is the most stable configuration.

A second hydrogen molecule can be added into this configuration, attached to the Pd atom with an adsorption energy of 0.39 eV. This is the most stable configuration, which can be also viewed as the dissociative adsorption of a hydrogen molecule directly on the lower side of vacancy having a PdH_2 complex on the upper side. The corresponding adsorption energy is 1.63 eV. Evidently, the two sums of successive adsorption energies, 1.49 eV + 0.39 eV, and 0.25 eV + 1.63 eV, give the same result. By contrast, if the second hydrogen molecule is added on the same side of the layer occupied by the Pd dopant, that molecule becomes attached to the PdH_2

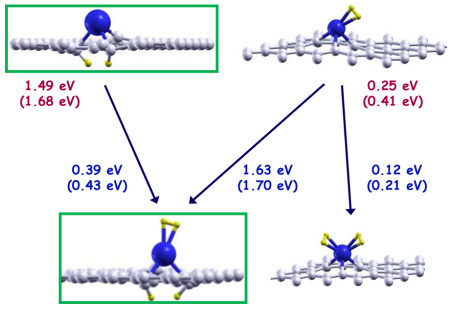

Figure 4. Optimized structures of hydrogen adsorbed on a graphene vacancy doped with one Pd atom. The adsorption energies for the first and second hydrogen molecules are shown in the picture. The starting point of the arrows indicate the reference system for adsorption of the second hydrogen molecule. Values in parentheses give the PBE+DFT-D3 dispersion corrected adsorption energies.

complex with a small adsorption energy of 0.12 eV. Configurations with a dissociated hydrogen molecule adsorbed directly on the vacancy from the same side of the Pd atom are highly unstable. Our results show that graphene vacancies are not fully saturated by adsorption of Pd on one side of the layer. Hydrogen can adsorb dissociatively on the other side of the vacancy. On the other hand, if molecular hydrogen is supplied from the same side of the layer as the Pd dopant, it does not displace the Pd atom from the vacant site, but instead the molecules get adsorbed on top of the Pd atom forming $Pd(H_2)$ and $Pd(H_2)_2$ complexes.

The structural configurations and adsorption energies for hydrogen adsorption on a graphene vacancy doped with two Pd atoms, one on each side of the layer, are shown on Figure 5. A first hydrogen molecule adsorbs on the doubly decorated vacancies on top of one of the Pd atoms (the Pd atom on the upper side of the layer) with an adsorption energy of 0.31 eV. This value is slightly larger than the molecular adsortion energy (0.25 eV) when the vacancy is decorated by only one Pd atom. The small increase can be explained by the reduced Pd-vacancy bonding strength occurring when two Pd atoms (instead of one Pd) decorate the vacancy; that reduced bonding strength allows for a stronger bonding between Pd and the hydrogen molecule. A second hydrogen molecule is adsorbed on the second Pd

DOI: 10.1021/acs.jpcc.6b12018
J. Phys. Chem. C 2017, 121, 10843−10850

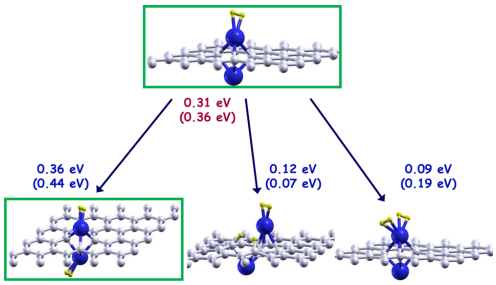

Figure 5. Optimized structures of hydrogen adsorbed on a graphene vacancy doped with two Pd atoms, one on each side of the layer. The adsorption energies for the first and second hydrogen molecules are shown in the picture. The starting point of the arrows indicate the reference system for adsorption of the second hydrogen molecule. The PBE+DFT-D3 dispersion-corrected adsorption energies are given in parentheses.

atom (the one on the lower side of the vacancy) with an adsorption energy of 0.36 eV (this configuration is the ground state of the system), while the adsorption energy of that molecule on the first Pd atom is only 0.09 eV. The first adsorbed hydrogen molecule can not dissociate directly on the vacancy decoraded on both sides with Pd atoms. However, a second hydrogen molecule adsorbed from the same side as the first one can dissociate and attach directly to the vacancy with a small adsorption energy of 0.12 eV, displacing the PdH_2 complex from the center of the vacant site. This dissociation on the same side of the Pd atom was not possible for a single hydrogen molecule. The reason has again to do with the bonding capacity of the Pd atom. When an H_2 molecule is adsorbed on the Pd atom, the bonding capacity of this Pd atom for a second H_2 molecule becomes a bit reduced, and the dissociative channel of H_2 directly on the vacancy becomes competitive. However, it is worth stressing that the most stable configuration corresponds to the molecular adsorption of the two molecules, one on each Pd atom, respectively. Thus, our results show that the adsorption energy of a hydrogen molecule on a Pd atom attached to a vacancy fits within a narrow interval of energies of 0.25−0.39 eV, then it is independent of whether the other side of the vacancy is clean or it is decorated with a dissociated hydrogen molecule, with a Pd atom or with a PdH_2 complex. On the other hand, the adsorption energy of a second hydrogen molecule on a Pd atom doping the vacancy is similar (0.12 and 0.09 eV, respectively) for clean vacancies and vacancies decorated with one Pd atom on the other side.

It was found in previous work[18,27] that hydrogen can be adsorbed on supported Pd clusters following two channels: the molecular and the dissociative channels. For low hydrogen loading, the dissociative channel leads to more stable states than the molecular channel. Moreover, the dissociative adsorption of hydrogen on Pd_6 anchored on a graphene vacancy induces a structural change in the cluster from the OCT to the IPB structure. The calculated activation barrier[27] for the dissociation of H_2 on Pd_6 supported on pristine graphene is 0.3 eV, and estimations for the dissociation on Pd_6 anchored to a vacancy give a similar value. Figure 6 shows the most relevant configurations for hydrogen adsorption on a system formed by a graphene vacancy decorated on one side with a Pd_6 cluster in the IPB structure. For comparison, the results for adsorption when the Pd_6 cluster is in the OCT structure are given in Figure 7. If we start with adsorbed OCT Pd_6, which is the lowest energy structure in the absence of hydrogen, the dissociative adsorption of a hydrogen molecule on the other (lower) side of the vacancy does not change the structure of the Pd cluster (see Figure 7). Moreover, for both OCT Pd_6 and IPB Pd_6 the adsorption energies of a hydrogen molecule dissociated on the other side of the vacancy, 1.07 and 1.01 eV respectively, are quite similar. Even more, this similarity of the adsorption energies holds not only for the case of clean OCT Pd_6 and IPB Pd_6 supported clusters. In fact, starting with clusters already decorated with a dissociated hydrogen molecule, the dissociative adsorption energies of a second molecule on the opposite (lower) side of the vacancy are 1.04

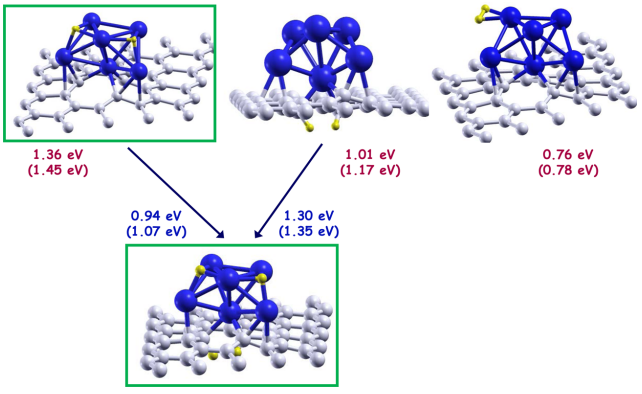

Figure 6. Optimized structures of hydrogen adsorbed on a graphene vacancy doped with IPB Pd_6 on one side of the layer. The adsorption energy of the first adsorbed hydrogen molecule is given with respect to the clean system having the Pd cluster in the IPB configuration. The starting point of the arrows indicate the reference system used to calculate the adsorption energy of the second hydrogen molecule. The green color frames enclose the lowest energy configurations of the system with one and two adsorbed hydrogen molecules, respectively. The PBE+DFT-D3 dispersion corrected adsorption energies are given in parentheses.

DOI: 10.1021/acs.jpcc.6b12018
J. Phys. Chem. C 2017, 121, 10843−10850

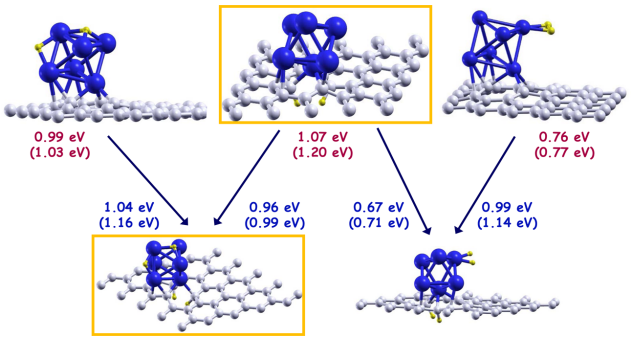

Figure 7. Optimized structures of hydrogen adsorbed on a graphene vacancy doped with OCT Pd_6 on one side of the layer. The adsorption energy of the first adsorbed hydrogen molecule is given with respect to the clean system having the Pd cluster in the OCT configuration. The starting point of the arrows indicate the reference system used to calculate the adsorption energy of the second hydrogen molecule. The orange color frames enclose the corresponding lowest energy configurations restricted to the OCT structure of the Pd_6 cluster. The PBE+DFT-D3 dispersion-corrected adsorption energies are given in parentheses.

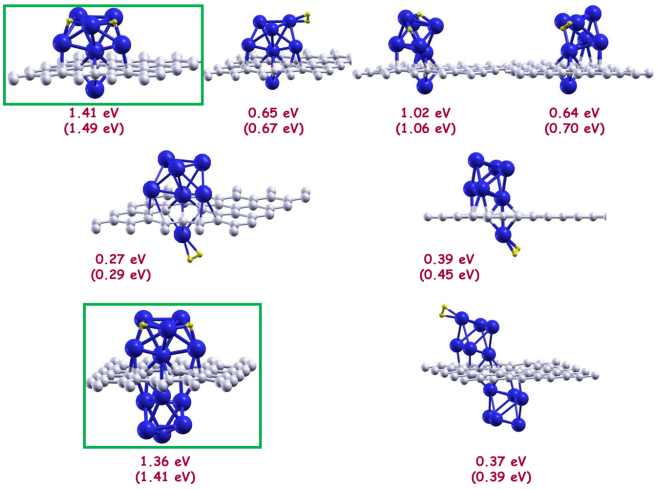

Figure 8. Optimized structures of hydrogen adsorbed on a graphene vacancy doped with Pd_6 (OCT and IPB structures are shown) on one side of the layer and with either a Pd atom or another Pd_6 cluster on the other side. The adsorption energies are given with respect to the clean system (before hydrogen adsorption) with the adsorbed Pd_6 cluster(s) in the same configuration. The frames in green color mark the lowest energy configurations of one adsorbed hydrogen molecule on Pd_6 when the opposite side of the layer is decorated with one Pd atom or Pd_6, respectively. The PBE+DFT-D3 dispersion corrected adsorption energies are given in parentheses.

and 0.94 eV, respectively. Those energies are, however, lower compared to the case of the vacancy doped with a single Pd atom (1.49 and 1.63 eV for clean Pd and Pd decorated with an adsorbed H_2 molecule, respectively). This indicates that the lower side of the graphene vacancy is less reactive when the upper side is decorated with Pd clusters as compared to the decoration with single Pd atoms.

Another interesting observation is that the adsorption of hydrogen on the Pd cluster is not affected by the presence of hydrogen on the opposite (lower) side of the vacancy. For instance, the dissociative hydrogen chemisorption energies on the IPB cluster are 1.30 and 1.36 eV whether or not the lower side of the vacancy holds hydrogen. Those two energies are quite similar. The corresponding chemisorption energies on OCT Pd_6 are 0.96 and 0.99 eV, respectively, quite similar again. Finally, the binding energies for molecular adsorption on OCT Pd_6 are 0.67 and 0.76 eV whether or not the lower side of the vacancy holds hydrogen. In conclusion, the same hydrogen adsorption mechanisms on Pd_6 anchored on a vacancy and similar adsoption energies are found independently of whether the opposite side of the vacancy holds hydrogen.

A behavior similar to the one just described above is observed for adsorption of hydrogen on Pd_6 anchored on a vacancy that holds on the opposite side either a single Pd atom or another Pd_6 cluster (see Figure 8), and we illustrate this feature with some examples. First, we find adsorption energies of 1.41 and 1.36 eV for the dissociative chemisorption on IPB Pd_6 when the opposite side of the vacancy is decorated with Pd

DOI: 10.1021/acs.jpcc.6b12018
J. Phys. Chem. C 2017, 121, 10843−10850

or OCT Pd_6, respectively. Considering next the molecular adsorption on OCT Pd_6, the binding energies in those two cases are 0.64 eV (Pd on the opposite side), and 0.37 eV (OCT Pd_6 on the opposite side). It should be noticed that, in each of the two examples presented, the hydrogen adsorption energies are quite similar to those obtained for adsorption on Pd_6 when the opposite side of the vacancy is either clean or doped with hydrogen. On the other hand, the energy for the molecular adsorption of H_2 on one Pd atom anchored on a vacancy is similar for all the cases studied: when the other side of the vacancy is decorated with OCT Pd_6, with IPB Pd_6, with a dissociated hydrogen molecule, with a single Pd atom or even clean (non decorated). For those various situations, the molecular adsorption energies are between 0.39 and 0.25 eV, a rather small variation.

The competition between palladium and hydrogen to saturate the vacancies is settled in favor of palladium. If palladium and hydrogen are present on the same side of the graphene layer, then the most stable configurations are those with palladium attached to the vacancy and hydrogen adsorbed on the Pd dopant. Configurations in which a dissociated hydrogen molecule displaces the Pd or Pd_6 dopants to adsorb directly on the vacancy from the same side of palladium are highly unstable. The only exception we have found is for the vacancy doped with one Pd atom on each side. In this case, a second hydrogen molecule displaces the preformed PdH_2 complex from the vacancy and attaches directly on the vacancy as a dissociated molecule with a moderate energy of 0.12 eV. On the other hand, if hydrogen is supplied from the other side of a Pd-doped vacancy, it chemisorbs dissociatively on the vacancy with substantial adsorption energies of 1.5−1.6 eV for the vacancy doped with a Pd atom, and 1.0 eV for the vacancy doped with a Pd_6 cluster (see Figures 4, 6, and 7). However, doping the two sides of the graphene vacancies with palladium are the preferred configurations (see Figures 5 and 8). It is interesting to note that very close adsorption energies are obtained based on DFT-PW91 calculations and based on DFT-PBE with the dispersion corrections given by DFT-D3. The dispersion corrected energies are about 0.1 eV higher than the pure DFT energies. This small difference does not affect the discussions and the conclusions throughout the manuscript.

4. CONCLUSIONS

Palladium-doped nanoporous carbon materials are good candidates for hydrogen storage. The Pd atoms and clusters attach preferentially to the defects, e.g., vacancies, of the graphitic walls of the nanopores. It has been found that palladium doping enhances the adsorption of hydrogen on the nanoporous carbons. However, the adsorbed hydrogen might compete with palladium to decorate the vacancies, compromising the stability of the material. We have performed density functional calculations to investigate the competition between palladium and hydrogen to saturate graphene vacancies. Graphene with vacancies is used here as an appropriate model for the walls of nanoporosus carbons and their defects. To assess the contribution of the dispersion interactions, we have compared the results obtained with DFT-PW91 and with DFT-PBE corrected for dispersion using DFT-D3. We found that dispersion interactions are small and therefore do not modify the conclusions of the present study.

Graphene vacancies are very reactive, and Pd atoms, Pd clusters, and hydrogen bind strongly to those defects. Moreover, the vacancies are not fully saturated by attachment of Pd atoms, Pd clusters, or hydrogen only on one side of the graphene layer, and those species can decorate both sides of the vacancy simultaneously. It is fair to notice that vacancies already predoped with palladium on one side are less reactive than clean vacancies; however, the adsorption energies of Pd atoms, Pd clusters, and hydrogen on the other side of those vacancies are still quite substantial. When hydrogen is present on the other side of a vacancy predoped on one side with a Pd atom or a Pd cluster, it becomes adsorbed on the vacancy as a dissociated molecule, similarly to its adsorption on undoped vacancies. However, because palladium attaches stronger than hydrogen to graphene vacancies, when palladium and hydrogen are both present on the same side of a vacancy, the Pd atom (or the Pd cluster) is the species binding directly to the vacancy, and hydrogen adsorbs on palladium. This behavior has been found on vacancies doped with Pd on one side only and on vacancies doped with palladium on both sides. Comparing the adsorption of hydrogen on Pd-doped graphene vacancies for vacancies decorated on one side and vacancies decorated on two sides, we have found: (a) the same adsorption mechanism (molecular adsorption) and similar binding energies for adsorption of hydrogen on Pd atoms decorating the vacancies, independently of whether the vacancy was decorated on one side or two sides, and (b) the same two adsorption mechanisms (molecular and dissociative adsorption) and similar corresponding adsorption energies for adsorption of hydrogen on Pd clusters anchored on the vacancies, independently of whether the vacancy was decorated on one side or two sides. In summary, hydrogen is not a successful competitor of palladium to saturate vacancies in the walls of porous carbon materials and therefore the adsorption of hydrogen does not destroy the stability of the palladium doped material. This is important for future hydrogen storage technologies on doped porous carbons.

AUTHOR INFORMATION

Corresponding Authors

*E-mail: jaalonso@fta.uva.es; Phone: +34 983 423142. Fax: +34 983 423013.
*E-mail: maria.lopez@fta.uva.es

ORCID

María J. López: 0000-0001-7698-9327

Notes

The authors declare no competing financial interest.

ACKNOWLEDGMENTS

This work was supported by MINECO of Spain (Grant MAT2014-54378-R) and Junta de Castilla y León (Grant VA050U14). A.G. acknowledges a predoctoral fellowship from Junta de Castilla y León.

REFERENCES

(1) Satyapal, S.; Petrovic, J.; Thomas, G. Gassing up with Hydrogen. *Sci. Am.* **2007**, *296* (4), 80−87.
(2) Dresselhaus, M. S.; Thomas, I. L. Alternative Energy Technologies. *Nature* **2001**, *414*, 332−337.
(3) Jena, P. Materials for Hydrogen Storage: Past, Present, and Future. *J. Phys. Chem. Lett.* **2011**, *2*, 206−211.
(4) Targets for Onboard Hydrogen Storage Systems for Light-Duty Vehicles September 2009, http://energy.gov/sites/prod/files/2014/03/f11/targets_onboard_hydro_storage_explanation.pdf (2009). Last accessed on January 2017.

DOI: 10.1021/acs.jpcc.6b12018
J. Phys. Chem. C 2017, 121, 10843−10850

(5) Liu, C.; Fan, Y.; Liu, M.; Cong, H.; Cheng, H.; Dresselhaus, M. Hydrogen Storage in Single-Walled Carbon Nanotubes at Room Temperature. *Science* **1999**, *286*, 1127−1129.
(6) Chen, P.; Wu, X.; Lin, J.; Tan, K. L. High H_2 Uptake by Alkali-Doped Carbon Nanotubes Under Ambient Pressure and Moderate Temperatures. *Science* **1999**, *285*, 91−93.
(7) Li, J.; Furuta, T.; Goto, H.; Ohashi, T.; Fujiwara, Y.; Yip, S. Theoretical Evaluation of Hydrogen Storage Capacity in Pure Carbon Nanostructures. *J. Chem. Phys.* **2003**, *119*, 2376−2385.
(8) Bhatia, S. K.; Myers, A. L. Optimum Conditions for Adsorptive Storage. *Langmuir* **2006**, *22*, 1688−1670.
(9) Contescu, C. I.; Brown, C. M.; Liu, Y.; Bhat, V. V.; Gallego, N. C. Detection of Hydrogen Spillover in Palladium-Modified Activated Carbon Fibers during Hydrogen Adsorption. *J. Phys. Chem. C* **2009**, *113*, 5886−5890.
(10) Contescu, C. I.; van Benthem, K.; Li, S.; Bonifacio, C. S.; Pennycook, S. J.; Jena, P.; Gallego, N. C. Single Pd Atoms in Activated Carbon Fibers and their Contribution to Hydrogen Storage. *Carbon* **2011**, *49*, 4050−4058.
(11) Yang, R. T. Hydrogen Storage by Alkali-Doped Carbon Nanotubes-Revisited. *Carbon* **2000**, *38*, 623−626.
(12) Bhat, V. V.; Contescu, C. I.; Gallego, N. C.; Baker, F. S. Atypical Hydrogen Uptake on Chemically-Activated, Ultramicroporous Carbon. *Carbon* **2010**, *48*, 1331−1340.
(13) Cabria, I.; López, M. J.; Alonso, J. A. Enhancement of Hydrogen Physisorption on Graphene and Carbon Nanotubes by Li Doping. *J. Chem. Phys.* **2005**, *123*, 204721.
(14) Cabria, I.; López, M. J.; Alonso, J. A. Hydrogen Storage in Pure and Li-doped Carbon Nanopores: Combined Effects of Concavity and Doping. *J. Chem. Phys.* **2008**, *128*, 144704.
(15) Tozzini, V.; Pellegrini, V. Prospects for Hydrogen Storage in Graphene. *Phys. Chem. Chem. Phys.* **2013**, *15*, 80−89.
(16) Parambhath, V. B.; Nagar, R.; Sethupathi, K.; Ramaprabhu, S. Investigation of Spillover Mechanism in Palladium Decorated Hydrogen Exfoliated Functionalized Graphene. *J. Phys. Chem. C* **2011**, *115*, 15679−15685.
(17) Lee, H.; Ihm, J.; Cohen, M.; Louie, S. Calcium-Decorated Graphene-Based Nanostructures for Hydrogen Storage. *Nano Lett.* **2010**, *10*, 793−798.
(18) Granja, A.; Alonso, J. A.; Cabria, I.; López, M. J. Competition between Molecular and Dissociative Adsorption of Hydrogen on Palladium Clusters Deposited on Defective Graphene. *RSC Adv.* **2015**, *5*, 47945−47953.
(19) Kubas, G. J. Molecular Hydrogen Complexes: Coordination of a Sigma Bond to Transition Metals. *Acc. Chem. Res.* **1988**, *21*, 120−128.
(20) Cabria, I.; López, M. J.; Alonso, J. A. Theoretical Study of the Transition from Planar to Three-Dimensional Structures of Palladium Clusters Supported on Graphene. *Phys. Rev. B: Condens. Matter Mater. Phys.* **2010**, *81*, 035403.
(21) Sun, Q.; Wang, Q.; Jena, P.; Kawazoe, Y. Clustering of Ti on a C_{60} Surface and its Effect on Hydrogen Storage. *J. Am. Chem. Soc.* **2005**, *127*, 14582−14583.
(22) Krasnov, P. O.; Ding, F.; Singh, A. K.; Yakobson, B. I. Clustering of Sc on SWNT and Reduction of Hydrogen Uptake: Ab-initio All Electron Calculations. *J. Phys. Chem. C* **2007**, *111*, 17977−17980.
(23) Kim, G.; Jhi, S. H.; Lim, S.; Park, N. Effect of Vacancy Defects in Graphene on Metal Anchoring and Hydrogen Adsorption. *Appl. Phys. Lett.* **2009**, *94*, 173102.
(24) Lim, D. H.; Negreira, A. S.; Wilcox, J. DFT Studies on the Interaction of Defective Graphene-Supported Fe and Al Nanoparticles. *J. Phys. Chem. C* **2011**, *115*, 8961−8970.
(25) Fair, K. M.; Cui, X. Y.; Li, L.; Shieh, C. C.; Zheng, R. K.; Liu, Z. W.; Delley, B.; Ford, M. J.; Ringer, S. P.; Stampfl, C. Hydrogen Adsorption Capacity of Adatoms on Double Carbon Vacancies of Graphene: A Trend Study from First Principles. *Phys. Rev. B: Condens. Matter Mater. Phys.* **2013**, *87*, 014102.
(26) López, M. J.; Cabria, I.; Alonso, J. A. Palladium Clusters Anchored on Graphene Vacancies and Their Effect on the Reversible Adsorption of Hydrogen. *J. Phys. Chem. C* **2014**, *118*, 5081−5090.
(27) Cabria, I.; López, M. J.; Fraile, S.; Alonso, J. A. Adsorption and Dissociation of Molecular Hydrogen on Palladium Clusters Supported on Graphene. *J. Phys. Chem. C* **2012**, *116*, 21179−21189.
(28) Ramos-Castillo, C. M.; Reveles, J. U.; Zope, R. R.; de Coss, R. Palladium Clusters Supported on Graphene Monovacancies for Hydrogen Storage. *J. Phys. Chem. C* **2015**, *119*, 8402−8409.
(29) Pelzer, A. W.; Jellinek, J.; Jackson, K. H_2 Saturation on Palladium Clusters. *J. Phys. Chem. A* **2015**, *119*, 3594−3603.
(30) Granja-DelRío, A.; Alonso, J. A.; López, M. J. Steric and Chemical Effects on the Hydrogen Adsorption and Dissociation on Free and Graphene-Supported Palladium Clusters. *Computational and Theoretical Chemistry* **2016**, DOI: 10.1016/j.comptc.2016.11.029.
(31) Seenithurai, S.; Pandyan, R. K.; Kumar, S. V.; Saranya, C.; Mahendran, M. Li-Decorated Double Vacancy Graphene for Hydrogen Storage Application: A First Principles Study. *Int. J. Hydrogen Energy* **2014**, *39*, 11016−11026.
(32) Ao, Z.; Dou, S.; Xu, Z.; Jiang, Q.; Wang, G. Hydrogen Storage in Porous Graphene with Al Decoration. *Int. J. Hydrogen Energy* **2014**, *39*, 16244−16251.
(33) Yadav, S.; Zhu, Z.; Singh, C. V. Defect Engineering of Graphene for Effective Hydrogen Storage. *Int. J. Hydrogen Energy* **2014**, *39*, 4981−4995.
(34) Rangel, E.; Sansores, E.; Vallejo, E.; Hernández-Hernández, A.; López-Pérez, P. A. Study of the Interplay Between N-Graphene Defects and Small Pd Clusters for Enhanced Hydrogen Storage Via a Spill-over Mechanism. *Phys. Chem. Chem. Phys.* **2016**, *18*, 33158−33170.
(35) dacapo, dacapo: See https://wiki.fysik.dtu.dk/dacapo for a description of the total energy code, based on the density functional theory (2009). Last accessed on January 2017.
(36) Vanderbilt, D. Soft Self-Consistent Pseudopotentials in a Generalized Eigenvalue Formalism. *Phys. Rev. B: Condens. Matter Mater. Phys.* **1990**, *41*, R7892−7895.
(37) Monkhorst, H.; Pack, J. Special Points for Brillouin-Zone Integration. *Phys. Rev. B* **1976**, *13*, 5188−5192.
(38) Perdew, J. P.; Wang, Y. Accurate and Simple Analytic Representation of the Electron-Gas Correlation Energy. *Phys. Rev. B: Condens. Matter Mater. Phys.* **1992**, *45*, 13244−13249.
(39) Grimme, S.; Antony, J.; Ehrlich, S.; Krieg, H. A consistent and Accurate ab Initio Parametrization of Density Functional Dispersion Correction (DFT-D) for the 94 Elements H-Pu. *J. Chem. Phys.* **2010**, *132*, 154104.
(40) Perdew, J. P.; Burke, K.; Ernzerhof, M. Generalized Gradient Approximation Made Simple. *Phys. Rev. Lett.* **1996**, *77*, 3865−3868.
(41) Smith, D. G. A.; Burns, L. A.; Patkowski, K.; Sherrill, C. D. Revised Damping Parameters for the D3 Dispersion Correction to Density Functional Theory. *J. Phys. Chem. Lett.* **2016**, *7*, 2197−2203.
(42) Grimme, S.; Ehrlich, S.; Goerigk, L. Effect of the Damping Function in Dispersion Corrected Density Functional Theory. *J. Comput. Chem.* **2011**, *32*, 1456−1465.
(43) Bores, C.; Cabria, I.; Alonso, J. A.; López, M. J. Adsorption and Dissociation of Molecular Hydrogen on the Edges of Graphene Nanoribbons. *J. Nanopart. Res.* **2012**, *14*, 1263.
(44) Jiang, Q. G.; Ao, Z. M.; Zheng, W. T.; Li, S.; Jiang, Q. Enhanced Hydrogen Sensing Properties of Graphene by Introducing a Mono-Atom-Vacancy. *Phys. Chem. Chem. Phys.* **2013**, *15*, 21016−21022.

DOI: 10.1021/acs.jpcc.6b12018
J. Phys. Chem. C 2017, 121, 10843−10850

6.3 Conclusions

Graphene vacancies are very reactive and they are not fully saturated by the attachment of Pd atoms, Pd_6 clusters or H_2 only on one side of the graphene mono-layer, so both sides of the vacancy can be decorated at the same time. A pre-doped vacancy is less reactive than non-doped vacancies. However, pre-doped vacancies are able to adsorb Pd atoms, Pd_6 clusters and H_2 on the other side with significant adsorption energies.

Palladium binds more strongly than hydrogen to graphene vacancies. Therefore, hydrogen can not remove and replace the Pd atoms or aggregates anchored to vacancies. As an alternative, hydrogen is asorbed on the metal and thus, it does not spoil the stability of the material. Finally, hydrogen adsorption mechanisms and energies do not depend on whether Pd atoms and clusters are anchored on one side or both sides of the graphene mono-vacancies.

Chapter 7

H_2 spillover from Pd clusters onto the graphene support

If fifty-million people say a foolish thing, it is still a foolish thing.

Anatole France.

In previous chapters we have shown that hydrogen adsorbs strongly on palladium nanoparticles supported on graphene. This direct adsorption of several hydrogen molecules on the palladium nanoparticles contributes to the enhancement of the hydrogen storage capacity of Pd-doped nanoporous carbons that has been found experimentally. However, the main hypothesis used in the literature to justify the enhancement of the storage capacity has been the spillover mechanism [85,86,89]. This mechanism consists on the following steps: i) adsorption of molecular hydrogen on the metal nanoparticle, ii) dissociation of hydrogen, iii) diffusion of the individual H atoms to the edge of the nanoparticle, iv) spill of the H atom from the metal nanoparticle onto the substrate, v) diffusion of H on the substrate were it is stored. Although invoked by several authors, the spillover mechanism has not been demonstrated in the context of hydrogen storage. [Here we do not refer to the spillover mechanism in the contexts of heterogeneous catalysis on metal catalysts supported on metal-oxide surfaces where this mechanisms has been extensively proven]. Blanco et al. have shown that hydrogen spillover mechanism in Pd_6 and Pd_{13} clusters supported on pristine graphene is a endothermic process with very high activation barriers [109]. Nonetheless, vacancies and defects of the graphene layer might facilitate the spillover mechanism. In our case, a mon-vacancy might promote the spillover mechanism from the Pd_6 cluster anchored on that mono-vacancy to the graphene layer. For this reason, this Chapter is devoted to investigate the last steps of the spillover mechanism on palladium clusters supported of graphene vacancies, namely the transfer of H atoms from the Pd cluster to the graphitic substrate and the subsequent diffusion

of H on the graphene surface away from the Pd cluster. We have considered the spillover of hydrogen from Pd clusters in two different conditions: a) Pd clusters having a low (one molecule) content of hydrogen and b) Pd clusters fully saturated with hydrogen (high hydrogen content).

This Chapter includes four sections. In the first one, we describe briefly the computational details. In the second Section, we report the spillover results obtained for unsaturated and hydrogen saturated palladium clusters. In the third, section we investigate the diffusion of one hydrogen atom on the graphene layer away from the palladium cluster for the case of hydrogen saturated Pd clusters. In the last Section, we discuss the contribution of dispersion interactions to the spillover and diffusion of hydrogen on the Pd-graphene systems. All the systems are based on the most stable structures obtained from Chapter 4, for the adsorption of hydrogen on Pd_6 supported on a graphene vacancy.

7.1 Theoretical model

To investigate the spillover mechanism we have attached a iPB Pd_6 cluster on a graphene mono-vacancy. The reason is that iPB supported structure is the most stable system when hydrogen molecules are dissociated on the metal nanoparticle (see Chapter 4). This is a good model to simulate hydrogen spillover mechanism on defective nanoporous carbon walls. As mentioned in former sections and in order to compare among systems, the computational details are identical to the ones which have been already described in Section 3.6.2 and have been summarized in Table 3.1. In addition, in this Chapter an analysis of the dispersion interaction corrections has been included, using Grimme's DFT-D3 combined with the PBE functional for exchange-correlation. For this analysis, we have utilized BJ, BJM, zero and zerom damping functions.

An extensive search for exploring the spillover mechanism and the diffusion of a single-hydrogen atom through the graphene layer, have been tested and fully optimized until the cohesive energies were converged within 10 meV.

7.2 Results

We have investigated the last steps of the hydrogen spillover mechanism, that is, the possibility of H atoms being transferred from a Pd cluster anchored on a graphene vacancy onto the substrate. We have considered Pd_6 clusters loaded with different amounts of hydrogen corresponding to hydrogen-saturated and unsaturated Pd clusters. We have taken structures with one, three and four hydrogen molecules ($n = 1, 3, 4$) as representatives for unsaturated systems and with nine and ten hydrogen molecules ($n = 9, 10$) as models for saturated systems. We have also

studied the diffusion of one hydrogen atom on the graphene layer in the $n = 10$ saturated case.

7.2.1 Hydrogen atom spillover in unsaturated and hydrogen saturated conditions

To model the spillover process, we have considered the lowest energy structures obtained in Chapter 4 for $n = 1, 3, 4, 9, 10$ as initial configurations to transfer one hydrogen atom from Pd_6 onto the defective graphene layer. The aim of this study is to asses whether the presence of the vacancy facilitates the spill over of the hydrogen atom from the nanoparticle onto the carbonaceous surface. Therefore, we have explored the transfer of one H atom from the Pd cluster to one of the C atoms around the graphene vacancy (labelled as site C in Fig 7.1)

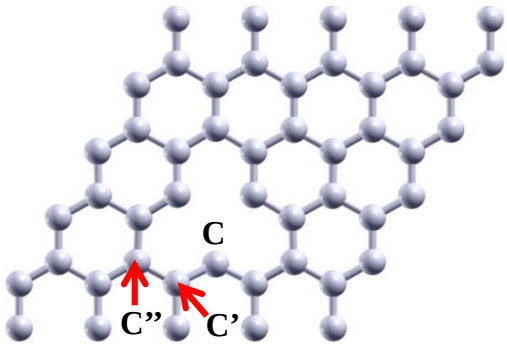

Figure 7.1: Defective graphene layer. Carbon atoms around the vacancy are labelled with C. The C atoms of the next shell of atoms counting from the vacancy are labelled with C’ and the third shell of atoms from the centre of the vacancy is labelled as C”.

The graphene layer deforms around the vacancy due to the removal of one C atom, the adsorption of the Pd cluster and the transfer of one H atom from the Pd cluster to the graphene surface. After the spillover of one H atom, the C-carbon atom in direct contact with the Pd atom that saturates the vacancy and with the transferred hydrogen atom, moves out of plane in direction towards to the Pd cluster about 0.9 Å. The two remaining C atoms in direct contact with the Pd atom that saturates the vacancy get out of plane about 0.5-0.8 Å. The C’ carbon atoms (next shell of atoms counted from the centre of the vacancy), move by about 0.3 Å. Spillover energies have been calculated as:

$$E(\mathrm{H_S}) = E_{original} - E_{spillover} \tag{7.1}$$

where $\mathrm{H_S}$ represents the hydrogen atom that has been transferred to the substrate, $E_{original}$ is the energy of the ground-state of the system with all the hydrogen atoms

and molecules adsorbed on the Pd_6 (obtained from Chapter 4) and $E_{spillover}$ is the energy of the system when one hydrogen atom has been transferred from the Pd cluster to the substrate where attaches on top of a carbon atom around the vacancy (labelled with C). $E(H_S)$ is positive when the transfer of a hydrogen atom from the metal to the substrate is a favourable process and negative when the transfer is unfavourable. This definition is valid for hydrogen saturated and unsaturated Pd clusters.

Unsaturated systems are now discussed starting with one dissociated H_2 molecule ($n = 1$) on the Pd_6 cluster anchored on a graphene vacancy. The most stable configuration for one dissociated hydrogen molecule was obtained in Chapter 4. The two hydrogen atoms are adsorbed on different faces of the Pd iPB structure. From that configuration, one of the hydrogen atoms is transferred onto the graphene layer and it is attached on top of a carbon atom closest to the centre of the vacancy, labelled atom C in Fig. 7.1. The H_S-C distance is 1.15 Å. The Pd cluster becomes distorted and the Pd atom attached to the C-carbon where the H atom is transferred, moves a little to bind to a C" carbon. The hydrogen spillover energy is $E(H_S) = -1.57$ eV (see Fig. 7.2). This negative value indicates that the spillover process is not favourable under these conditions.

Palladium clusters loaded with a total of $n = 3$ and $n = 4$ hydrogen molecules have been also considered. The reason for choosing these amounts of hydrogen molecules is that they represent special cases: (i) $n = 3$ is maximum number of hydrogen molecules that can be dissociatively adsorbed on Pd_6 supported on a graphene vacancy and (ii) $n = 4$ corresponds to the adsorption of one hydrogen molecule in the molecular form on Pd_6 pre-saturated with three dissociated hydrogen molecules. In both cases, one hydrogen atom initially on an edge of the iPB structure, was transferred to a position on top of a carbon atom closest to the vacancy centre with an energy of $E(H_S) = -0.76$ eV for $n = 3$ and $E(H_S) = -0.71$ eV for $n = 4$. The H_S-C distance is 1.12 Å for $n = 3$ and 1.13 Å for $n = 4$. The structures for $n = 3, 4$ are shown in Figure 7.2.

From these results we can conclude that the spillover mechanism is unfavourable for unsaturated Pd_6 iPB clusters anchored on a graphene mono-vacancy. However, we found that in moderately saturated systems ($n = 3, 4$), the spillover energies drop significantly (from -1.57 eV to -0.76 eV) with respect to the unsaturated case.
The above results suggest that the presence of pre-adsorbed hydrogen on the metal nanoparticle reaching saturation limits, might promote the spillover mechanism. Therefore, we have studied spillover mechanism in systems saturated with hydrogen.

The saturation limit for Pd_6 is reached with nine and ten total hydrogen molecules ($n = 9, 10$). These systems have three dissociated hydrogen molecules and six and seven molecules adsorbed in molecular form for $n = 9$ and $n = 10$, respectively.

Pd_6 with nine or ten adsorbed hydrogen molecules is lifted up from the graphene layer, and therefore, in those configurations the hydrogen atoms have more space to interact with the surface. This might favour the spillover mechanism.

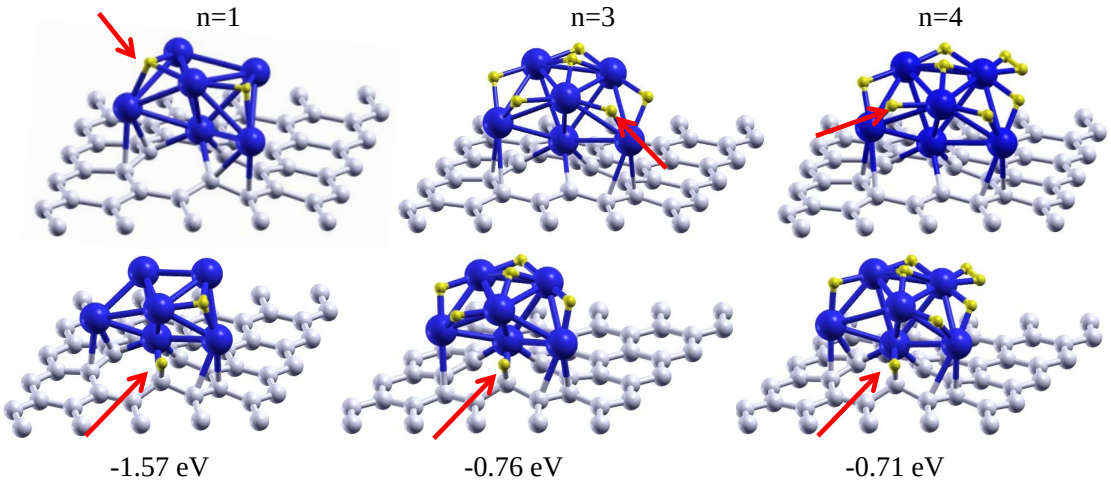

Figure 7.2: Upper panels show the lowest energy configurations of Pd_6 anchored on a graphene vacancy with one, three and four dissociated hydrogen molecules, respectively. These structures are the same as those shown in Figure 3 and in Figure 4 of the article 4.2 and are included here to help with the visualization of the spill over of hydrogen. Red arrows indicate the hydrogen atom which is going to be transferred onto the graphene layer. $n = 1, 3, 4$ indicate the total number of hydrogen molecules. Lower panels show the configurations for $n = 1$, $n = 3$ and $n = 4$, respectively, in which one hydrogen atom has been transferred from the Pd_6 cluster to one of the C atoms around the vacancy. The transferred H atom is marked by a red arrow. Spillover energies ($E(H_S)$) are calculated using Equation 7.1.

For the $n = 9$ case shown in Fig. 7.3, one of the hydrogen atoms is transferred on top of one of the carbon atoms next to the vacancy centre. In this case, the C atom on which the H_S atom is attached, is different from the C atom of the other cases $n = 1, 3, 4, 10$. The H_S-C distance is 1.13 Å. The transferred hydrogen atom was initially on one of the edges of the Pd iPB structure. After spillover, one hydrogen molecule and one hydrogen atom that were close to the initial position of the transferred hydrogen atom (H_S) are rearranged on the Pd nanoparticle. The hydrogen spillover energy for $n = 9$ is $E(H_S) = -0.33$ eV. The negative value indicates that the spillover is unfavourable although the energy cost is pretty much reduced with respect to the unsaturated case.

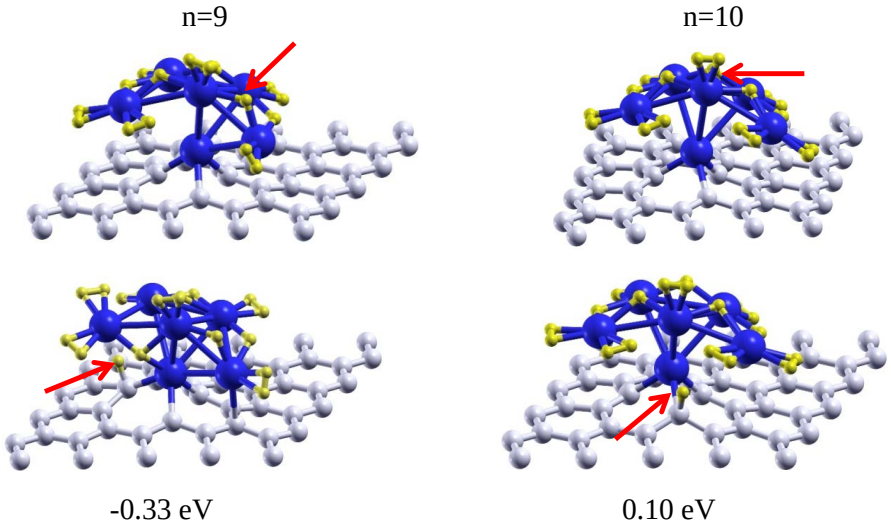

Figure 7.3: Upper panels show the lowest energy configurations of Pd_6 anchored on a graphene vacancy, saturated with nine and ten hydrogen molecules, respectively (three of them dissociated and the rest in the molecular form). These structures are the same as those shown in Figure 4.4 and are included here to help with the visualization of the spill over of hydrogen. Red arrows indicate the hydrogen atom which is going to be transferred onto the graphene layer. $n = 9, 10$ indicate the total number of hydrogen molecules. Lower panels show the configurations for $n = 9$ and $n = 10$, respectively, in which one hydrogen atom has been transferred from the Pd_6 cluster to one of the C atoms around the vacancy. The transferred H atom is marked by a red arrow. Spillover energies ($E(H_S)$) are calculated using Equation 7.1.

In the $n = 10$ case, the hydrogen atom which is placed in one of the faces of the Pd_6 iPB, moves to a position on top of C atom closest to the vacancy centre. The H_S-C distance is 1.12 Å. After spillover, the rest of the hydrogen atoms and molecules remained at the same original positions. The spillover energy is $E_{spillover}(H_S) = 0.10$ eV. The positive number indicates that the spillover process is favourable. This is the only case in which the spillover is found to be energetically favourable. These results indicate that hydrogen saturation of Pd_6 anchored on a graphene defect might facilitate hydrogen spillover mechanism. Table 7.1 summarises the spillover energies ($E(H_S)$) for all the systems described above.

7.2.2 Hydrogen atom diffusion through graphene layer

Since the only case for which we find the possibility of hydrogen spillover is for $n = 10$, we have investigated for this system the diffusion of atomic hydrogen on the surface of the graphitic substrate, away from the Pd cluster. The starting point is the configuration with one hydrogen atom transferred onto the C atom closest to the vacancy centre. Then, we have investigated the diffusion of the hydrogen atom

Table 7.1: Hydrogen spillover energies for saturated and unsaturated systems.

Number of total hydrogen molecules n	$E(\mathrm{H_S})$ (eV)
1	-1.57
3	-0.76
4	-0.71
9	-0.33
10	0.10

towards two different carbon atoms of the layer in order to find the preferred site to diffuse through the graphene layer. The two sites considered for hydrogen diffusion are the carbon atom labelled as C' in Fig. 7.1, and the carbon labelled as C". The graphene layer is also distorted in these cases due to the presence of the vacancy, the adsorbed Pd_6 and the hydrogen atom attached to the graphene layer. After the diffusion of the hydrogen atom to C' or C" positions, the three C atoms closest to the vacancy centre protrude out of the plane, towards the Pd cluster by about 0.5 Å. The next shell of carbon atoms, counted from the vacancy get out about 0.3 Å, except for the carbon atom (C' or C") bound to the hydrogen atom, which is moved out of plane 0.5 Å. Diffusion energies have been calculated as:

$$E(\mathrm{H_D}) = E_{spillover} - E_{diffusion}. \tag{7.2}$$

$\mathrm{H_D}$ is the hydrogen atom diffusing on the carbon substrate. $E_{diffusion}$ is energy of the system with the hydrogen atom placed on the C' or C" carbon atom and $E(\mathrm{H_D})$ is the energy for moving one hydrogen atom from C to C' or from C to C".

First, we have investigated the hydrogen diffusion from C to C' (to a nearest neighbour). The distance C-C' is 1.46 Å. The energy for this process, that is, the difference in energy between the initial and final states, is $E(\mathrm{H_D}) = -1.26$ eV and the $\mathrm{H_D}$-C' distance is 1.14 Å.

Second, we have calculated the energy to diffuse the hydrogen atom ($\mathrm{H_D}$) from C to C" (to a second neighbour), which is -0.16 eV. It is eight times lower than the value obtained to diffuse to the first neighbouring C'. The C-C" distance is 2.51 Å and the $\mathrm{H_D}$-C" distance is 1.14 Å. From these results we can conclude that diffusing to C" atom is less unfavourable than diffusing to C' atom. Nonetheless, both energies are negative which indicates that hydrogen diffusion is not favourable, at least in these conditions. Moreover, diffusion barriers will make diffusion even less probable.

Borodin et al. reported that the diffusion barrier on pristine graphene from C to C' is about 0.99 eV which competes with the desorption barrier (1.1 eV) and a direct leap from C to C" atom is less probable than two nearest-neighbour jumps [185, 186].

We have calculated the diffusion barriers for the migration of one hydrogen atom from C to C' and from C to C". The estimated value for the diffusion of one hydrogen atom from C to a nearest-neighbour carbon atom (C') is about 1.38 eV and for diffusing from C to a second nearest-neighbour carbon atom (C") is approximately 1.89 eV. The value of the diffusion barrier from C to C" is higher than diffusing the hydrogen atom from C to C'.

Therefore, spillover of one hydrogen atom from the Pd cluster to the supporting surface, close to the metal cluster, might take place under hydrogen saturating conditions. However, once the hydrogen atom is transferred onto the graphene layer, the diffusion process is not favourable. Therefore, it is more favourable for the H atom to be re-adsorbed on the Pd cluster than diffusing through the graphene layer.

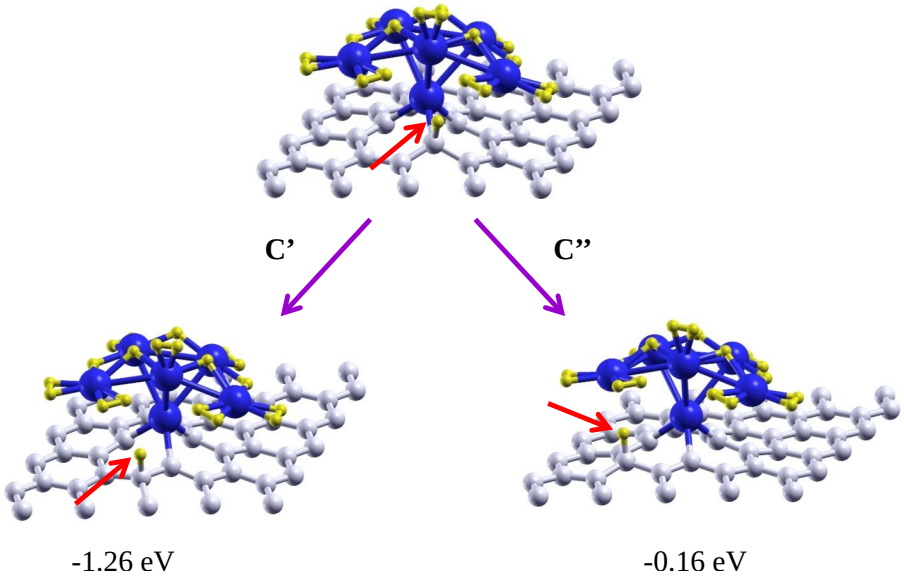

Figure 7.4: Upper panel shows the configuration of Pd_6 anchored on a graphene vacancy saturated with ten hydrogen molecules (three of them dissociated and the rest in the molecular form) and with one hydrogen atom transferred from the Pd_6 onto the graphene layer (hydrogen spillover). This structure is the same as the one shown in Figure 7.3 and is included here to help with the visualization of the diffusion of hydrogen. Red arrows indicate the hydrogen atom which is going to diffuse through the graphene layer. Lower panels show the configurations for $n = 10$ for one hydrogen atom diffusion. Left panel shows one hydrogen atom diffusion from C to C'. Right panel, shows the diffusion of one hydrogen atom from C to C". The H atom which have diffused is marked by a red arrow. Hydrogen diffusion energies ($E(H_D)$) are calculated using Equation 7.2.

7.2.3 Dispersion interaction corrections

To evaluate contribution of the dispersion interactions to the spillover mechanism and to the diffusion of one hydrogen atom through the graphene layer, we have performed Grimme DFT-PBE-D3 calculations for both cases.

We have investigated the dispersion interaction contributions for the spillover mechanism for unsaturated systems with one, three and four hydrogen molecules ($n = 1, 3, 4$) and for saturated systems with nine and ten hydrogen molecules ($n = 9, 10$). These configurations are the same as those defined in Section 7.2.1 for $n = 1, 3, 4, 9, 10$. In the case for which hydrogen spillover is favourable, this is for $n = 10$, we have evaluated the dispersion interaction contributions for the diffusion of one hydrogen atom from C to C' and from C to C". The configurations are the same as those described in Section 7.2.2.

To analyse in detail the dispersion interaction contributions for hydrogen spillover cases and for the hydrogen diffusion case (defined above), we have tested the different damping function options included in Grimme DFT-PBE-D3 dispersion correction package described in Section 2.5. BJ, CHG or zero, BJM and zerom damping functions have been evaluated for hydrogen spillover cases $n = 1, 3, 4, 9, 10$ and for hydrogen atom diffusion case. DFT-PW91, DFT-PBE and DFT-PBE-D3 energy values for each damping function have been collated in Table 7.2 and in Table 7.3 for spillover and diffusion cases, respectively.

First and second rows in Table 7.2 show the DFT-PW91 and the DFT-PBE energy values for one hydrogen atom spillover for $n = 1, 3, 4, 9, 10$ cases described in Section 7.2.1. The next rows show the dispersion-corrected energy values for each damping function option (BJ, BJM, CHG or zero and zerom, respectively). Each one of these values have to be added to the energy value given by DFT-PBE in order to obtain the dispersion corrected spillover energies for each system and for each damping function.

From Table 7.2 we can conclude that, in all cases, the dispersion interaction does not contribute to one hydrogen atom spillover except for the cases (i) $n = 1$ and zero damping function, (ii) $n = 10$ and BJM damping function and (iii) $n = 10$ and zero damping function. In these cases, the dispersion interaction contribution promotes the spillover mechanism.

First and second rows in Table 7.3 show the DFT-PW91 and the DFT-PBE energy values for one hydrogen atom diffusion cases (from C to C' and from C to C") described in Section 7.2.2. The next rows show the dispersion-corrected energy values for each damping function option (BJ, BJM, CHG or zero and zerom, respectively). Each one of these values have to be added to the energy value given by DFT-PBE in order to obtain the dispersion corrected diffusion energies for each system and for each damping function.

From Table 7.3, we can conclude that the dispersion interaction contribution

Table 7.2: Dispersion interaction contribution to the spillover mechanism. The first row shows the DFT-PW91 energy values for one hydrogen atom spillover (these values are the same as those given in Section 7.2.1 and we have included them here to help with the comparison between PW91 energy values and PBE energy values). The second row is the DFT-PBE energy values for one hydrogen atom spillover. The next rows are the dispersion interaction corrections for each damping function (BJ, BJM, CHG or zero and zerom, respectively) which have to be added to the energy values given by DFT-PBE in order to obtain the dispersion corrected spillover energies. $E(H_S)$ is the hydrogen spillover energy (as defined in Section 7.2.1). n indicates the total hydrogen molecules. Positive values for PW91 and for PBE indicate that the spillover process is favourable. Positive values for BJ, BJM, CHG or zero and zerom represent that the dispersion contribution promotes the spillover mechanism.

DFT	$E(H_S)$ $n=1$	$E(H_S)$ $n=3$	$E(H_S)$ $n=4$	$E(H_S)$ $n=9$	$E(H_S)$ $n=10$
PW91	-1.5711	-0.7621	-0.7065	-0.3315	0.0979
PBE	-1.5744	-0.7279	-0.6958	-0.3317	0.0771
BJ	-0.0183	-0.0036	-0.0545	-0.0788	-0.0091
BJM	-0.0914	-0.0121	-0.1936	-0.0196	0.0006
zero	0.0170	-0.0067	-0.0051	-0.0853	0.0137
zerom	-0.1668	-0.0831	-0.2480	-0.0570	-0.0324

Table 7.3: Dispersion interaction contribution to the diffusion of a single hydrogen atom through the graphene layer. The first row shows the DFT-PW91 energy values for one hydrogen atom diffusion (these values are the same as those given in Section 7.2.2 and we have included them here to help with the comparison between PW91 energy values and PBE energy values). The second row is the DFT-PBE energy values for one hydrogen atom diffusion. The next rows are the dispersion interaction corrections for each damping function (BJ, BJM, CHG or zero and zerom, respectively) which have to be added to the energy values given by DFT-PBE in order to obtain the dispersion corrected diffusion energies. $E(\mathrm{H_D})$ is the hydrogen diffusion energy (as defined in Section 7.2.2). First column shows the hydrogen atom diffusion from C to C' and the second column shows the hydrogen atom diffusion from C to C". Negative values for PW91 and for PBE indicate that the diffusion process is unfavourable. Positive values for BJ, CHG or zero, BJM and zerom represent that the dispersion contribution promotes the hydrogen atom diffusion from C to C' or from C to C".

DFT	$E(\mathrm{H_D})$ C'	$E(\mathrm{H_D})$ C"
PW91	-1.2558	-0.1633
PBE	-1.2501	-0.1631
BJ	0.0189	0.0179
BJM	0.0331	0.0378
zero	0.0133	0.0043
zerom	0.0386	0.0597

promotes the hydrogen diffusion for both cases: from C to C' and from C to C" and for all the damping functions options. However, as we have seen in the former section, hydrogen diffusion under our system conditions, is not favourable. In addition, dispersion interaction contributions are not big enough to transform diffusion into a suitable process.

7.3 Future Perspectives

From the work performed in this thesis, four future prospects can further be addressed to study and improve the hydrogen adsorption, desorption and storage on carbon surfaces. Firstly, studying other defects, this is, generating divacancies, replacing one or two carbon atoms with impurities such as, nitrogen, boron or oxygen or mixing impurities and vacancies, instead of using a mono-vacancy. The second one concerns the surface: the graphene layer might not be plane and it might be corrugated. The third one consists in considering different temperature and pressure, this is, different environmental conditions. Finally, focussing on the nanoparticle nature: (i) increasing the number of palladium atoms of the metal cluster, (ii) changing the transition metal or (iii) mixing different metal atoms, for example, palladium and nickel.

Conclusions

This thesis investigates the interaction and adsorption mechanisms of hydrogen on palladium nanoparticles supported on graphene with the aim to assess the effect that doping with metal nanoparticles has on the hydrogen storage capacity of nanoporous carbon materials. The most advanced, "state of the art", quantum-mechanical calculations within the Desnsity Functional formlism have been performed in this study. The most relevant conclusions are:

1) Pd_6 anchored on the graphene mono-vacancy was considered to model hydrogen adsorption, dissociation and desorption on defective pore walls of nanoporous carbons. We have found that, **eight** hydrogen molecules can be adsorbed directly on Pd_6 OCT cluster. However, the **dissociative** adsorption channel **is preferred over** the molecular channel for hydrogen adsorption. The system can adsorb up to three dissociated hydrogen molecules and the first dissociated hydrogen molecule prompts an structural transition in the palladium cluster from an octahedral (OCT) structure to an incomplete pentagonal bypiramid, refered as **ICO structure**. The saturation limit is reached with the addition of seven additional non-dissociated hydrogen molecules. This saturation limit is higher for the dissociative hydrogen adsorption mode than for the molecular adsorption channel. Finally, anchoring Pd clusters on the graphene mono-vacancy retains their capacity for adsorbing hydrogen and it prevents the desorption of the Pd-H complexes that competed with the hydrogen release.

2) Free Pd clusters were compared with Pd_6 nanoparticles supported on pristine graphene and with Pd_6 anchored on a graphene vacancy to study the effect of the carbonaceous support on hydrogen adsorption and dissociation. We have found that twelve hydrogen molecules can be adsorbed on the free Pd_6, while only eight and nine can be adsorbed on the Pd cluster supported on the defective and on the pristine graphene layer, respectively. However, the dissociative adsorption is the most stable channel in all cases. Free Pd_6 clusters are able to dissociate up to seven molecules but Pd_6 anchored on the graphene vacancy only dissociates up to three. Six more molecules can be adsorbed on free Pd clusters in the molecular form. Thus, we can conclude that free and supported clusters show the same two hydrogen adsorption channel. Nevertheless, more hydrogen can be adsorbed in

free Pd clusters than in the supported ones. Thus, the surface has a **steric** effect which does not allow hydrogen to surround the Pd cluster and a **chemical** effect induced by the vacancy that prevents hydrogen to interact with the Pd atom that saturates the defect.

3) The energies and structures for hydrogen and metal interactions with both sides of the graphene vacancy and the competition between hydrogen and Pd for saturating the defect were explored. We found that, graphene vacancies are very reactive and they are not fully saturated by the attachment of Pd atoms, Pd clusters or hydrogen on only one side of the graphene mono-layer. Thus, they can decorate both sides of the vacancy at the same time. **Palladium** is bonded **more strongly** than hydrogen to graphene vacancies. Therefore, hydrogen can not replace the Pd atoms or aggregates anchored to vacancies. Finally, we can conclude that hydrogen adsorption mechanisms and energies do not depend on whether the vacancy was decorated on one or two sides with Pd atoms and clusters.

4) The transfer of one hydrogen atom from the nanoparticle onto the supporting carbon surface and its diffusion were studied for saturated and unsaturated systems. The relevant outcome has been that for the limit of hydrogen saturation system, one hydrogen atom was transferred onto the Pd-graphene interface, but it might not be consider as hydrogen spillover. In addition, there is not evidence of hydrogen diffusion through the surface for unsaturated nor saturated systems, hydrogen atom prefers to be adsorbed again on the Pd cluster.

   Therefore, we might conclude that **there is not** evidence of the **hydrogen spillover mechanism** and **there are not hydrogen diffusion** events under the conditions studied in this thesis.

In summary this thesis contributes to unravel the hydrogen storage mechanisms on palladium doped nanoporous carbon materials. The effects of the palladium nanoparticles and of the graphitic substrate on the adsorption of hydrogen are clarified. Our study shows that the direct adsorption of hydrogen on the metal nanoparticles leads to a small to moderate enhancement of the storage capacity of the doped materials in agreement with the experimental observations. In contrast, the spillover mechanism proposed in the literature is not supported by our results under the conditions of this study.

Appendix A

Publications

Prediction is very difficult, especially if it's about the future.

Niels Bohr.

I. Thesis Publications

- **Competition between molecular and dissociative adsorption of hydrogen on palladium clusters deposited on defective graphene.** A. Granja, J. A. Alonso, I. Cabria and M. J. López; RSC Advances, **5**, *59*, 47945-47953, 2015. Cites from Web of Science (WoS) database: 20.
- **Competition between Palladium Clusters and Hydrogen to Saturate Graphene Vacancies.** A. Granja-DelRío, J. A. Alonso and M. J. López;
  The Journal of Physical Chemistry C, **121**, *20*, 10843-10850, 2017.
- **Steric and chemical effects on the hydrogen adsorption and dissociation on free and graphene-supported palladium clusters.** A. Granja-DelRío, J. A. Alonso and M. J. López;
  Computational and Theoretical Chemistry, **1107**, 23-29, 2017. Cites from WoS database: 6.

II. Publications not included in thesis

- **Adsorption and Growth of Palladium Clusters on Graphdiyne.** A. Seif, M. J. López, A. Granja-DelRío, K. Azizi and J. A. Alonso;
  Physical Chemistry Chemical Physics, **19**, *29*, 19094-19102, 2017. Cites from WoS database: 3.

Proceedings

- **Interaction of hydrogen with palladium clusters deposited on graphene.** J. A. Alonso, A. Granja, I. Cabria and M. J. López;
  AIP Conference Proceedings, **1702**, 050002, 2015.

Appendix B

Short stays and conferences

Whatever you are, be a good one.

Abraham Lincoln.

I. Short Stays

- **Visiting PhD Student University of Birmingham** (United Kingdom). School of Chemistry. 3 months, September-December 2017.
- **Visiting PhD Student Donostia International Physics Center (DIPC)** (San Sebastián). 1 month, October-November 2018.

II. Conferences

- Oral contribution. ***Bimetallic clusters to enhance hydrogen adsorption on graphene sheets***. Alejandra Granja Del Río, Roy L. Johnston, María J. López Santodomingo, Julio A. Alonso Martín. X Jornadas de Jóvenes Investigadores en Física Atómica y Molecular. (Barcelona, Spain). 3-6 April 2018.
- Oral contribution. ***Clusters metálicos para la adsorción de hidrógeno en láminas de grafeno***. Alejandra Granja Del Río, Julio A. Alonso Martín, María J. López Santodomingo. Ciclo de Conferencias Día Internacional de la Mujer. (Valladolid, Spain). 2 March 2018.
- Oral contribution. ***Competición entre hidrógeno y paladio para saturar vacantes de grafeno***. Alejandra Granja Del Río, María J. López Santodomingo, Julio A. Alonso Martín. IX Jornadas de Jóvenes Investigadores en Física Atómica y Molecular. (Sevilla, Spain). 22-24 March 2017.

- Poster contribution. ***Competition between palladium and hydrogen to saturate graphene vacancies***. Alejandra Granja Del Río, Julio A. Alonso Martín, María J. López Santodomingo. XIII Simposio de Investigadores Jóvenes de la RSEQ. (Logroño, Spain). 8-11 November 2016.
- Oral contribution. ***Adsorción de hidrógeno en agregados de paladio libres y soportados en grafeno***. Alejandra Granja Del Río, María J. López Santodomingo, Julio A. Alonso Martín. Ciclo de Conferencias Día Internacional de la Mujer. (Valladolid, Spain). 4 March 2016.
- Oral contribution. ***Adsorción de hidrógeno en agregados de paladio libres y soportados en grafeno***. Alejandra Granja Del Río, María J. López Santodomingo, Julio A. Alonso Martín. VIII Jornadas de Jóvenes Investigadores en Física Atómica y Molecular. (Valladolid, Spain). 24-26 February 2016.
- Oral contribution. ***Disociación y adsorción molecular de hidrógeno en agregados de Paladio soportados sobre vacantes de grafeno***. Alejandra Granja Del Río, María J. López Santodomingo, Julio A. Alonso Martín, Iván Cabria. VII Jornadas de Jóvenes Investigadores en Física Atómica y Molecular. (Jaén, Spain). 18-20 March 2015.

Bibliography

[1] The World Bank. https://data.worldbank.org/indicator/EG.USE.COMM.FO.ZS/, Last accessed 04-09-2018. (Cited in page 2.)

[2] CIA Fuel Consumption. https://www.cia.gov/library/publications/the-world-factbook/rankorder/2246rank.html, Last accessed 04-09-2018. (Cited in page 2.)

[3] Institute for Energy Research. https://instituteforenergyresearch.org/topics/encyclopedia/petroleum/, Last accessed 04-09-2018. (Cited in page 2.)

[4] Environmental and Energy Study Institute. http://www.eesi.org/topics/fossil-fuels/description, Last accessed 04-09-2018. (Cited in page 2.)

[5] US Energy Information Administration. https://www.eia.gov/energyexplained/index.php?page=oil_use, Last accessed 04-09-2018. (Cited in pages 2 and 4.)

[6] BP Energy Outlook Regions. https://www.bp.com/content/dam/bp/en/corporate/pdf/energy-economics/energy-outlook/bp-energy-outlook-2018-global-insights.pdf, Last accessed 04-09-2018. (Cited in page 2.)

[7] CIA Fuel Production. https://www.cia.gov/library/publications/the-world-factbook/rankorder/2241rank.html, Last accessed 04-09-2018. (Cited in page 2.)

[8] T. S. Ahlbrandt. Future petroleum energy resources of the world. *International Geology Review*, 44(12):1092–1104, 2010. (Cited in page 2.)

[9] M. S. Dresselhaus and I. L. Thomas. Alternative energy technologies. *Nature*, 414:332–337, 2001. (Cited in page 2.)

[10] N. Demirdöven and J. Deutch. Hybrid cars now, fuel cell cars later. *Science*, 305(5686):974–976, 2004. (Cited in page 2.)

[11] S. Satyapal, J. Petrovic, and G. Thomas. Gassing up with hydrogen. *Scientific American*, 296(4):80–87, 2007. (Cited in page 2.)

[12] Hydrogen Council. http://hydrogencouncil.com/, Last accessed 04-09-2018. (Cited in page 2.)

[13] F. Zhang, P. Zhao, M. Niu, and J. Maddy. The survey of key technologies in hydrogen energy storage. *International Journal of Hydrogen Energy*, 41(33):14535–14552, 2016. (Cited in page 3.)

[14] C-J. Winter. Hydrogen energy - abundant, efficient, clean: A debate over the energy-system-of-change. *International Journal of Hydrogen Energy*, 34(14, Supplement 1):S1–S52, 2009. (Cited in page 3.)

[15] A. Verméglio and J-C. Fontecilla-Camps. Primary energies and their transformation, hydrogen, the energy vector of the future. *CELFS CEA*, (44), 2000. (Cited in page 3.)

[16] 5 innovaciones que cambiarán para siempre el paisaje renovable. http://eoliccat.net/innovaciones-cambiaran-paisaje-renovables/?lang=es, Last accessed 04-09-2018. (Cited in page 3.)

[17] Global Renewable Energy Consumption Over the Long-run. https://ourworldindata.org/renewables, Last accessed 04-09-2018. (Cited in page 3.)

[18] Electricity Storage. https://www.imnovation-hub.com/es/energia/almacenes-de-electricidad-segunda-revolucion/, Last accessed 04-09-2018. (Cited in page 3.)

[19] Hydrogen Storage and Production. https://www.iea.org/publications/freepublications/publication/hydrogen.pdf, Last accessed 04-09-2018. (Cited in page 3.)

[20] P. Jena. Materials for hydrogen storage: Past, present, and future. *J. Phys. Chem. Lett.*, 2:206–211, 2011. (Cited in page 4.)

[21] Tecnologías del hidrógeno y pilas de combustible. http://www.aeh2.org/index.php?option=com_content&view=category&layout=blog&id=44&Itemid=41&lang=es, Last accessed 04-09-2018. (Cited in page 4.)

[22] U.S.A. Energy. https://www.energy.gov/energy-economy, Last accessed 04-09-2018. (Cited in page 4.)

[23] H. T. Hwang and A. Varma. Hydrogen storage for fuel cell vehicles. *Current Opinion in Chemical Engineering*, 5:42–48, 2014. (Cited in page 4.)

[24] A. Züttel. Hydrogen storage methods. *International Journal of Hydrogen Energy*, 91(4):157–172, 2004. (Cited in page 4.)

[25] V. Tozzini and V. Pellegrini. Prospects for hydrogen storage in graphene. *Physical Chemistry Chemical Physics*, 15:80–89, 2013. (Cited in pages 4, 8, 10, 11, 12, and 13.)

[26] Department of Energy U.S.A. `https://www.energy.gov/eere/fuelcells/doe-technical-targets-onboard-hydrogen-storage-light-duty-vehicles`, Last accessed 04-09-2018. (Cited in pages 4 and 5.)

[27] Hydrogen Storage Overview. `https://www.hydrogen.energy.gov/pdfs/progress17/iv_0_stetson_2017.pdf`, Last accessed 04-09-2018. (Cited in pages 4 and 5.)

[28] J. A. Alonso, I. Cabria, and M. J. López. The storage of hydrogen in nanoporous carbons. *Journal of the Mexican Chemical Society*, 56:261–269, 2012. (Cited in pages 5, 8, and 9.)

[29] J. Kleperis, P. Lesnicenoks, L. Grinberga, G. Chikvaidze, and J. Klavins. Zeolite as material for hydrogen storage in transport applications. *Latvian Journal of Physics and Technical Sciences*, 50(3):59 – 64, 2013. (Cited in page 5.)

[30] J. Dong, X. Wang, H. Xu, Q. Zhao, and J. Li. Hydrogen storage in several microporous zeolites. *International Journal of Hydrogen Energy*, 32(18):4998 – 5004, 2007. (Cited in page 5.)

[31] M. H. Alkordi, Y. Belmabkhout, A. Cairns, and M. Eddaoudi. Metal-organic frameworks for H_2 and CH_4 storage: insights on the pore geometry-sorption energetics relationship. *IUCrJ*, 4(2):131–135, 2017. (Cited in page 5.)

[32] D. Gygi, E. D. Bloch, J. A. Mason, M. R. Hudson, M. I. Gonzalez, R. L. Siegelman, T. A. Darwish, W. L. Queen, C. M. Brown, and J. R. Long. Hydrogen storage in the expanded pore Metal-Organic Frameworks M2(dobpdc) (M = Mg, Mn, Fe, Co, Ni, Zn). *Chemistry of Materials*, 28(4):1128–1138, 2016. (Cited in page 5.)

[33] V. P. Ting, A. J. Ramirez-Cuesta, N. Bimbo, J. E. Sharpe, A. Noguera-Diaz, V. Presser, S. Rudic, and T. J. Mays. Direct evidence for solid-like hydrogen in a nanoporous carbon hydrogen storage material at supercritical temperatures. *ACS Nano*, 9(8):8249–8254, 2015. (Cited in pages 5, 9, and 51.)

[34] I. Cabria, M. J. López, and J. A. Alonso. Hydrogen storage in nanoporous carbon. In *Handbook of Nanophysics*, chapter 41. CRC Press, Boca Raton,, 2010. (Cited in page 5.)

[35] R. Ferrando, J. Jellinek, and R. L. Johnston. Nanoalloys: From theory to applications of alloy clusters and nanoparticles. *Chemical Reviews*, 108(3):845–910, 2008. (Cited in page 7.)

[36] J. J. Requejo-Isidro, R. del Coso, J. Solis, J. Gonzalo, and C. N. Afonso. Role of surface-to-volume ratio of metal nanoparticles in optical properties of Cu:Al_2O_3 nanocomposite films. *Applied Physics Letters*, 86(19):194104, 2005. (Cited in page 7.)

[37] C-C. Yang, W-L. Huang, Y-H. Lin, C-Y. Weng, Z-Y. Mo, and Y-Y. Chen. Quantum size effects on vanadium nanoparticles. *IEEE Transactions on magnetics*, 47(10):3535–3537, 2011. (Cited in page 8.)

[38] P.M. Paulus, A. Goossens, R. C. Thiel, A. M. van der Kraan, G. Schmid, and L. J. de Jongh. Surface and quantum-size effects in pt and au nanoparticles probed by ^{197}Au Mössbauer spectroscopy. *Physical Review B*, 64:205418, 2001. (Cited in page 8.)

[39] A. Ramírez. Anisotropic diffusion of hydrogen in nanoporous carbons. *Journal of Materials Science*, 49(20):7087–7098, 2014. (Cited in page 8.)

[40] J. A. Alonso, I. Cabria, and M. J. López. Simulation of hydrogen storage in porous carbons. *Journal of Materials Research*, 28(4):589–604, 2013. (Cited in pages 8 and 51.)

[41] I. Cabria, M. J. López, and J. A. Alonso. The optimum average nanopore size for hydrogen storage in carbon nanoporous materials. *Carbon*, 45:2649–2658, 2007. (Cited in page 9.)

[42] I. Cabria, M. J. López, and J. A. Alonso. Hydrogen storage capacities of nanoporous carbon calculated by density functional and Møller-Plesset methods. *Physical Review B*, 78:075415, 2008. (Cited in page 9.)

[43] P. Pfeifer, A. Gillespie, D. Stalla, and E. Dohnke. Multiply surface-functionalized nanoporous carbon for vehicular hydrogen storage. `https://www.osti.gov/biblio/1344383`, 2017. (Cited in page 9.)

[44] B. Panella, M. Hirscher, and S. Roth. Hydrogen adsorption in different carbon nanostructures. *Carbon*, 43(10):2209 – 2214, 2005. (Cited in pages 9 and 51.)

[45] Y. Gogotsi, R. K. Dash, G. Yushin, T. Yildirim, G. Laudisio, and J. E. Fischer. Tailoring of nanoscale porosity in carbide-derived carbons for hydrogen storage. *Journal of the American Chemical Society*, 127(46):16006–16007, 2005. (Cited in page 9.)

[46] I. Cabria, M.J. López, and J.A. Alonso. Simulation of the hydrogen storage in nanoporous carbons with different pore shapes. *International Journal of Hydrogen Energy*, 36(17):10748–10759, 2011. (Cited in page 9.)

[47] M. Sevilla, A. B. Fuertes, and R. Mokaya. High density hydrogen storage in superactivated carbons from hydrothermally carbonized renewable organic materials. *Energy Environment Science*, 4:1400–1410, 2011. (Cited in pages 9 and 51.)

[48] S. J. Yang, H. J., T. Kim, and C. R. Park. Recent advances in hydrogen storage technologies based on nanoporous carbon materials. *Progress in Natural Science: Materials International*, 22(6):631 – 638, 2012. (Cited in page 9.)

[49] C. Liu, Y. Y. Fan, M. Liu, H. T. Cong, H. M. Cheng, and M. S. Dresselhaus. Hydrogen storage in single-walled carbon nanotubes at room temperature. *Science*, 286(5442):1127–1129, 1999. (Cited in page 9.)

[50] B. K. Pradhan, G. U. Sumanasekera, K. W. Adu, H. E. Romero, K. A. Williams, and P. C. Eklund. Experimental probes of the molecular hydrogen-carbon nanotube interaction. *Physica B: Condensed Matter*, 323(1):115 – 121, 2002. (Cited in pages 9 and 51.)

[51] G. E. Froudakis. Hydrogen interaction with carbon nanotubes: a review of ab initio studies. *Journal of Physics: Condensed Matter*, 14(17):R453, 2002. (Cited in page 9.)

[52] G. E. Froudakis. Hydrogen storage in nanotubes & nanostructures. *Materials Today*, 14(7):324 – 328, 2011. (Cited in page 9.)

[53] D. C. Elias, R. R. Nair, T. M. G. Mohiuddin, S. V. Morozov, P. Blake, M. P. Halsall, A. C. Ferrari, D. W. Boukhvalov, M. I. Katsnelson, A. K. Geim, and K. S. Novoselov. Control of graphene's properties by reversible hydrogenation: Evidence for graphane. *Science*, 323(5914):610–613, 2009. (Cited in page 9.)

[54] A. K. Geim and K. S. Novoselov. The rise of graphene. *Nature materials*, 6:183–191, 2007. (Cited in page 9.)

[55] K. V. Kumar, A. Salih, L. Lu, E. A. Müller, and F. Rodrǵuez-Reinoso. Molecular simulation of hydrogen physisorption and chemisorption in nanoporous carbon structures. *Adsorption Science & Technology*, 29(8):799, 2011. (Cited in page 10.)

[56] Y. Miura, H. Kasai, W. Di no, H. Nakanishi, and T. Sugimoto. First principles studies for the dissociative adsorption of H2 on graphene. *Journal of Applied Physics*, 93(6):3395–3400, 2003. (Cited in page 10.)

[57] A. Züttel, P. Sudan, Ph. Mauron, T. Kiyobayashi, Ch. Emmenegger, and L. Schlapbach. Hydrogen storage in carbon nanostructures. *International Journal of Hydrogen Energy*, 27(2):203–212, 2002. (Cited in page 10.)

[58] I. Cabria, M.J. López, and J. A. Alonso. Searching for DFT-based methods that include dispersion interactions to calculate the physisorption of H2 on benzene and graphene. *The Journal of Chemical Physics*, 146(21):214104, 2017. (Cited in page 10.)

[59] L. Zhou, Y. P. Zhou, and Y. Sun. A comparative study of hydrogen adsorption on superactivated carbon versus carbon nanotubes. *Internation Journal of Hydrogen Energy*, 29(5):475–479, 2004. (Cited in page 10.)

[60] P. Kowalczyk, R. Holyst, M. Terrones, and H. Terrones. Hydrogen storage in nanoporous carbon materials: myth and facts. *Physical Chemistry Chemical Physics*, 9:1786–1792, 2007. (Cited in page 10.)

[61] R. T. Yang. Hydrogen storage by alkali-doped carbon nanotubes-revisited. *Carbon*, 38(4):623–626, 2000. (Cited in page 11.)

[62] Y. Chen, H. Zhu, and Y. Liu. Preparation of activated rectangular polyaniline-based carbon tubes and their application in hydrogen adsorption. *International Journal of Hydrogen Energy*, 36(18):11738–11745, 2011. (Cited in page 11.)

[63] V. D. Camiola, R. Farchioni, T. Cavallucci, A. Rossi, V. Pellegrini, and V. Tozzini. Hydrogen storage in rippled graphene: Perspectives from multi-scale simulations. *Frontiers in Materials*, 2:3, 2015. (Cited in page 11.)

[64] K.S Spyrou, D. Gournis, and P. Rudolf. Hydrogen storage in graphene-based materials: Efforts towards enhanced hydrogen absorption. *ECS Journal of Solid State Science and Technology*, 2:M3160–M3169, 2013. (Cited in pages 11 and 12.)

[65] V. B. Parambhath, R. Nagar, K. Sethupathi, and S. Ramaprabhu. Investigation of spillover mechanism in palladium decorated hydrogen exfoliated functionalized graphene. *The Journal of Physical Chemistry C*, 115(31):15679–15685, 2011. (Cited in pages 11, 12, and 13.)

[66] V. Tozzini and V. Pellegrini. Reversible hydrogen storage by controlled buckling of graphene layers. *The Journal of Physical Chemistry C*, 115(51):25523–25528, 2011. (Cited in pages 11 and 12.)

[67] El grafeno aplicado a la inyección y extrusión de plásticos. `http://plasfur.com/en/espanol-grafeno-inyeccion-extrusion/`, Last accessed 04-09-2018. (Cited in page 11.)

[68] I. Cabria, M. J. López, and J. A. Alonso. Enhancement of hydrogen physisorption on graphene and carbon nanotubes by Li doping. *The Journal of Chemical Physics*, 123(20):204721, 2005. (Cited in page 12.)

[69] C. Ataca, E. Aktürk, S. Ciraci, and H. Ustunel. High-capacity hydrogen storage by metallized graphene. *Applied Physics Letters*, 93(4):043123, 2008. (Cited in page 12.)

[70] G. J. Kubas, R. R. Ryan, B. I. Swanson, P. J. Vergamini, and H. J. Wasserman. Characterization of the first examples of isolable molecular hydrogen complexes, M(CO)3(PR3)2(H2) (M = molybdenum or tungsten; R = Cy or isopropyl). evidence for a side-on bonded dihydrogen ligand. *Journal of the American Chemical Society*, 106(2):451–452, 1984. (Cited in page 12.)

[71] G. J. Kubas. Molecular hydrogen complexes: Coordination of a sigma bond to transition metals. *Accounts of Chemical Research*, 21:120–128, 1988. (Cited in page 12.)

[72] G. J. Kubas. Metal-dihydrogen and σ-bond coordination: The consummate extension of the dewar-chatt duncanson model for metal-olefin π bonding. *Journal Organometallic Chemistry*, 635:37–68, 2001. (Cited in page 12.)

[73] G. J. Kubas. Fundamentals of H2 binding and reactivity on transition metals underlying hydrogenase function and H2 production and storage. *Chemical Reviews*, 107(10):4152–4205, 2007. (Cited in page 12.)

[74] Y. Liu, L. Ren, Y. He, and H-P. Cheng. Titanium-decorated graphene for high-capacity hydrogen storage studied by density functional simulations. *Journal of Physics: Condensed Matter*, 22(44):445301, 2010. (Cited in page 12.)

[75] E. Durgun, S. Dag, V. M. K. Bagci, O. Gülseren, T. Yildirim, and S. Ciraci. Systematic study of adsorption of single atoms on a carbon nanotube. *Physical Review B*, 67:201401, 2003. (Cited in page 12.)

[76] C. I. Contescu, C. M. Brown, Y. Liu, V. V. Bhat, and N. C. Gallego. Detection of hydrogen spillover in palladium-modified activated carbon fibers during hydrogen adsorption. *Journal of Physical Chemistry C*, 113:5886–5890, 2009. (Cited in pages 12, 14, and 51.)

[77] V. V. Bhat, C. I. Contescu, and N. C. Gallego. The role of destabilization of palladium hydride in the hydrogen uptake of pd-containing activated carbons. *Nanotechnology*, 20(20):204011, 2009. (Cited in pages 12 and 51.)

[78] J. Wu, S. W. Ong, H. C. Kang, and E. S. Tok. Hydrogen adsorption on mixed platinum and nickel nanoclusters: The influence of cluster composition and

graphene support. *The Journal of Physical Chemistry C*, 114(49):21252–21261, 2010. (Cited in page 12.)

[79] S. Cui, N. Zhao, C. Shi, C. Feng, C. He, J. Li, and E. Liu. Effect of hydrogen molecule dissociation on hydrogen storage capacity of graphene with metal atom decorated. *The Journal of Physical Chemistry C*, 118(2):839–844, 2014. (Cited in page 12.)

[80] I. Cabria, M. J. López, S. Fraile, and J. A. Alonso. Adsorption and dissociation of molecular hydrogen on palladium clusters supported on graphene. *The Journal of Physical Chemistry C*, 116(40):21179–21189, 2012. (Cited in pages 12, 13, 14, 16, and 51.)

[81] M. J. López, I. Cabria, and J. A. Alonso. Palladium clusters anchored on graphene vacancies and their effect on the reversible adsorption of hydrogen. *The Journal of Physical Chemistry C*, 118(10):5081–5090, 2014. (Cited in pages 12, 16, and 51.)

[82] Divya P. and S. Ramaprabhu. Hydrogen storage in platinum decorated hydrogen exfoliated graphene sheets by spillover mechanism. *Physical Chemistry Chemical Physics*, 16:26725–26729, 2014. (Cited in page 12.)

[83] L. Wang and R. T. Yang. Hydrogen storage properties of carbons doped with ruthenium, platinum, and nickel nanoparticles. *The Journal of Physical Chemistry C*, 112(32):12486–12494, 2008. (Cited in page 12.)

[84] X-Y. Liu, J-X. Yu, X-D. Li, G-C. Liu, X-F. Li, and J-K. Lee. Effect of metal catalyst on the mechanism of hydrogen spillover in three-dimensional covalent-organic frameworks. *Chinese Physics B*, 26(2):027302, 2017. (Cited in page 12.)

[85] R. Juarez-Mosqueda, A. Mavrandonakis, A. B. Kuc, L. G. M. Pettersson, and T. Heine. Theoretical analysis of hydrogen spillover mechanism on carbon nanotubes. *Frontiers in Chemistry*, 3:2, 2015. (Cited in pages 12, 17, and 101.)

[86] A. K. Singh, M. A. Ribas, and B. I. Yakobson. H-spillover through the catalyst saturation: An ab initio thermodynamics study. *ACS Nano*, 3(7):1657–1662, 2009. (Cited in pages 12 and 101.)

[87] S. K. Konda and A. Chen. Palladium based nanomaterials for enhanced hydrogen spillover and storage. *Materials Today*, 19(2):100 – 108, 2016. (Cited in page 12.)

[88] A. Dahal and M. Batzill. Graphene-nickel interfaces: a review. *Nanoscale*, 6:2548–2562, 2014. (Cited in page 12.)

[89] W. C. Conner and J. L. Falconer. Spillover in heterogeneous catalysis. *Chemical Reviews*, 95(3):759–788, 1995. (Cited in pages 12 and 101.)

[90] L. Wang and R. T. Yang. New sorbents for hydrogen storage by hydrogen spillover - a review. *Energy Environmental Science*, 1:268–279, 2008. (Cited in page 12.)

[91] A. J. Lachawiec, G. Qi, and R. T. Yang. Hydrogen storage in nanostructured carbons by spillover: Bridge-building enhancement. *Langmuir*, 21(24):11418–11424, 2005. (Cited in page 12.)

[92] A. Reyhani, S. Z. Mortazavi, S. Mirershadi, A. Z. Moshfegh, P. Parvin, and A. N. Golikand. Hydrogen storage in decorated multiwalled carbon nanotubes by Ca, Co, Fe, Ni, and Pd nanoparticles under ambient conditions. *The Journal of Physical Chemistry C*, 115(14):6994–7001, 2011. (Cited in page 13.)

[93] C. I. Contescu, K. van Benthem, S. Li, C. S. Bonifacio, S. J. Pennycook, P. Jena, and N. C. Gallego. Single Pd atoms in activated carbon fibers and their contribution to hydrogen storage. *Carbon*, 49:4050–4058, 2011. (Cited in pages 13, 14, and 51.)

[94] Q. Sun, Q. Wang, P. Jena, and Y. Kawazoe. Clustering of ti on a C60 surface and its effect on hydrogen storage. *Journal of the American Chemical Society*, 127(42):14582–14583, 2005. (Cited in page 13.)

[95] I. Cabria, M. J. López, and J. A. Alonso. Theoretical study of the transition from planar to three-dimensional structures of palladium clusters supported on graphene. *Physical Review B*, 81:035403, 2010. (Cited in pages 13 and 14.)

[96] Y. Tang, H. Zhang, Z. Shen, M. Zhao, Y. Li, and X. Dai. The electronic and diffusion properties of metal adatoms on graphene sheets: a first-principles study. *RSC Advances*, 7:33208–33218, 2017. (Cited in page 14.)

[97] F. Ruffino and F. Giannazzo. A review on metal nanoparticles nucleation and growth on/in graphene. *Crystals*, 7(7):219, 2017. (Cited in page 14.)

[98] B. F. Habenicht, D. Teng, L. Semidey-Flecha, D. S. Sholl, and Y. Xu. Adsorption and Diffusion of 4d and 5d Transition Metal Adatoms on Graphene/Ru(0001) and the Implications for Cluster Nucleation. *Crystals*, 57:69–79, 2014. (Cited in page 14.)

[99] A. Ishii, M. Yamamoto, H. Asano, and K. Fujiwara. DFT calculation for adatom adsorption on graphene sheet as a prototype of carbon nanotube functionalization. *Journal of Physics: Conference Series*, 100(5):052087, 2008. (Cited in page 14.)

[100] K. T. Chan, J. B. Neaton, and M. L. Cohen. First-principles study of metal adatom adsorption on graphene. *Physical Review B*, 77:235430, 2008. (Cited in page 14.)

[101] C. M. Ramos-Castillo, J. U. Reveles, R. R. Zope, and R. de Coss. Palladium clusters supported on graphene monovacancies for hydrogen storage. *The Journal of Physical Chemistry C*, 119(15):8402–8409, 2015. (Cited in page 14.)

[102] C. Zlotea, F. Cuevas, V. Paul-Boncour, E. Leroy, P. Dibandjo, R. Gadiou, C. Vix-Guterl, and M. Latroche. Size-Dependent Hydrogen Sorption in Ultrasmall Pd Clusters Embedded in a Mesoporous Carbon Template. *Journal of the American Chemical Society*, 132(22):7720–7729, 2010. (Cited in page 14.)

[103] L. Fen, J. Xue, Z. Jijun, and Z. Shengbai. Graphene oxide: A promising nanomaterial for energy and environmental applications. *Nano Energy*, 16:488–515, 2015. (Cited in page 14.)

[104] R. Nagar, B. P. Vinayan, S. S. Samantaray, and S. Ramaprabhu. Recent advances in hydrogen storage using catalytically and chemically modified graphene nanocomposites. *Journal of Materials Chemistry A*, 5:22897–22912, 2017. (Cited in page 14.)

[105] S. Nachimuthu, P-J. La, E. G. Leggesse, and J-C. Jiang. A first principles study on boron-doped graphene decorated by Ni-Ti-Mg atoms for enhanced hydrogen storage performance. *Scientific Reports*, 5(16797):1–8, 2015. (Cited in page 14.)

[106] H-Y. Wu, X. Fan, J-L. Kuo, and W-Q. Deng. DFT study of hydrogen storage by spillover on graphene with boron substitution. *The Journal of Physical Chemistry C*, 115(18):9241–9249, 2011. (Cited in page 14.)

[107] G. Kim, S-H. Jhi, S. Lim, and N. Park. Effect of vacancy defects in graphene on metal anchoring and hydrogen adsorption. *Applied Physics Letters*, 94(17):173102, 2009. (Cited in page 14.)

[108] W. Gao, J. E. Mueller, J. Anton, Q. Jiang, and T. Jacob. Nickel cluster growth on defect sites of graphene: A computational study. *Angewandte Chemie International Edition*, 52(52):14237–14241, 2013. (Cited in page 14.)

[109] M. Blanco-Rey, J. I. Juaristi, M. Alducin, M. J. López, and J. A. Alonso. Is spillover relevant for hydrogen adsorption and storage in porous carbons doped with palladium nanoparticles? *The Journal of Physical Chemistry C*, 120(31):17357–17364, 2016. (Cited in pages 17 and 101.)

[110] T. Young. I. the bakerian lecture. experiments and calculations relative to physical optics. *Philosophical Transactions of the Royal Society of London*, 94:1–16, 1804. (Cited in page 21.)

[111] C. Davisson and L. H. Germer. Diffraction of electrons by a crystal of nickel. *Physical Review*, 30:705–740, 1927. (Cited in page 21.)

[112] R. M. Dreizler and E. K. U. Gross. *Density Functional Theory: An Approach to the Quantum Many-Body Problem*. Springer, Berlin, 1990. (Cited in page 21.)

[113] C. Fiolhais, F. Nogueira, and M. A. L. Marques. *A primer in Density Functional Theory*. Springer-Verlag Berlin Heidelberg, New York, 2003. (Cited in pages 21, 22, and 34.)

[114] D. S. Sholl and J. K. A. Steckel. *Density Functional Theory: a practical introduction*. Wiley, Hoboken, New Jersey, 2009. (Cited in pages 21 and 22.)

[115] R. M. Eisberg and R. Resnick. *Quantum Physics of Atoms, Molecules, Solids, Nuclei and Particles*. Wiley, Santa Barbara, 1985. (Cited in page 23.)

[116] M. Born and R. Oppenheimer. Zur quantentheorie der molekeln. *Annalen der Physik*, 389(20):57–484, 1927. (Cited in page 23.)

[117] P. W. Atkins and R. S. Friedman. *Molecular Quantum Mechanics*. Oxford University Press Inc., New York, 1997. (Cited in pages 23, 24, 25, 26, 27, 30, 32, and 34.)

[118] K. Burke. Perspective on density functional theory. *Journal of Chemical Physics*, 136(15):150901, 2012. (Cited in page 25.)

[119] P. Geerlings, F. De Proft, and W. Langenaeker. Conceptual Density Functional Theory. *Chemical Reviews*, 103(5):1793–1874, 2003. (Cited in page 25.)

[120] N. Mardirossian and M. Head-Gordon. Thirty years of density functional theory in computational chemistry: an overview and extensive assessment of 200 density functionals. *Molecular Physics*, 115(19):2315–2372, 2017. (Cited in pages 25 and 38.)

[121] A. D. Becke. Perspective: Fifty years of density-functional theory in chemical physics. *The Journal of Chemical Physics*, 140(18):18A301, 2014. (Cited in page 25.)

[122] N. Argaman and G. Makov. Density functional theory: An introduction. *American Journal of Physics*, 68(1):69–79, 2000. (Cited in page 25.)

[123] W. Kohn. Nobel lecture: Electronic structure of matter-wave functions and density functionals. *Review of Modern Physics*, 71:1253–1266, 1999. (Cited in pages 25 and 27.)

[124] F. Jensen. *Introduction to computational chemistry*. Wiley, Chichester, 2007. (Cited in pages 25, 32, 34, and 35.)

[125] L. H. Thomas. The calculation of atomic fields. *Mathematical Proceedings of the Cambridge Philosophical Society*, 23(5):542–548, 1927. (Cited in pages 25 and 26.)

[126] E. Fermi. Un metodo statistico per la determinazione di alcune prioprietà dell'Atomo. Endiconti: Accademia Nazionale dei Lincei. *Accademia Nazionale dei Lincei*, 6(5):602–607, 1927. (Cited in pages 25 and 26.)

[127] P. A. M. Dirac. Quantum mechanics of many-electron systems. *Proceedings of the Royal Society of London A: Mathematical, Physical and Engineering Sciences*, 123(792):714–733, 1929. (Cited in pages 25 and 27.)

[128] R. G. Parr and W. Yang. *MapReduce: Simplified Data Processing on Large Clusters*. Oxford University Press; Clarendon Press, New York, 1989. (Cited in pages 26 and 34.)

[129] S. Lundqvist and N. H. March. *Theory of the Inhomogeneous Electron Gas*. Springer US, New York, 1983. (Cited in pages 27, 28, 31, and 34.)

[130] T. Ziegler. Approximate density functional theory as a practical tool in molecular energetics and dynamics. *Chemical Reviews*, 91(5):651–667, 1991. (Cited in page 27.)

[131] P. Hohenberg and W. Kohn. Inhomogeneous electron gas. *Physical Review*, 136:B864–B871, 1964. (Cited in pages 27 and 28.)

[132] W. Koch and M. C. Holthausen. *A Chemist's Guide to Density Functional Theory*. Wiley-VCH, Weinheim, Germany, 2001. (Cited in page 29.)

[133] W. Kohn and L. J. Sham. Self-consistent equations including exchange and correlation effects. *Physical Reveview*, 140:A1133–A1138, 1965. (Cited in pages 30, 31, and 34.)

[134] P. A. M. Dirac. Note on exchange phenomena in the Thomas atom. *Mathematical Proceedings of the Cambridge Philosophical Society*, 26(3):376–385, 1930. (Cited in page 34.)

[135] S. H. Vosko, L. Wilk, and M. Nusair. Accurate spin-dependent electron liquid correlation energies for local spin density calculations: a critical analysis. *Canadian Journal of Physics*, 58(8):1200–1211, 1980. (Cited in page 34.)

[136] J. P. Perdew and A. Zunger. Self-interaction correction to density-functional approximations for many-electron systems. *Physical Review B*, 23:5048–5079, 1981. (Cited in page 34.)

[137] R. O. Jones and O. Gunnarsson. The density functional formalism, its applications and prospects. *Reviews of Modern Physics*, 61:689–746, 1989. (Cited in page 34.)

[138] J. P. Perdew and Y. Wang. Correlation hole of the spin-polarized electron gas, with exact small-wave-vector and high-density scaling. *Physical Review B*, 44:13298–13307, 1991. (Cited in pages 35 and 36.)

[139] J. P. Perdew and Y. Wang. Accurate and simple analytic representation of the electron-gas correlation energy. *Physical Review B*, 45:13244–13249, 1992. (Cited in pages 35 and 36.)

[140] J. P. Perdew, K. Burke, and M. Ernzerhof. Generalized Gradient Approximation made simple. *Physical Review Letters*, 77:3865–3868, 1996. (Cited in pages 35 and 36.)

[141] C. Lee, W.Yang, and R. G. Parr. Development of the Colle-Salvetti correlation-energy formula into a functional of the electron density. *Physical Review B*, 37:785–789, 1988. (Cited in page 36.)

[142] A. D. Becke. Density-functional exchange-energy approximation with correct asymptotic behavior. *Physical Review A*, 38:3098–3100, 1988. (Cited in page 36.)

[143] J. P. Perdew and K. Schmidt. Jacob's ladder of density functional approximations for the exchange-correlation energy. *AIP Conference Proceedings*, 577(1):1–20, 2001. (Cited in page 36.)

[144] J. Tao, J. P. Perdew, V. N. Staroverov, and G. E. Scuseria. Climbing the Density Functional Ladder: Nonempirical Meta-Generalized Gradient Approximation Designed for Molecules and Solids. *Physical Review Letters*, 91:146401, 2003. (Cited in page 36.)

[145] A. D. Becke. Density-functional thermochemistry. III. The role of exact exchange. *The Journal of Chemical Physics*, 98(7):5648–5652, 1993. (Cited in page 36.)

[146] R. O. Jones. Density Functional Theory: Its origins, rise to prominence, and future. *Reviews Modern Physics*, 87:897–923, 2015. (Cited in page 36.)

[147] P. J. Stephens, F. J. Devlin, C. F. Chabalowski, and M. J. Frisch. Ab Initio Calculation of Vibrational Absorption and Circular Dichroism Spectra Using Density Functional Force Fields. *The Journal of Physical Chemistry*, 98(45):11623–11627, 1994. (Cited in page 36.)

[148] J. P. Perdew, M. Ernzerhof, and K. Burke. Rationale for mixing exact exchange with density functional approximations. *The Journal of Chemical Physics*, 105(22):9982–9985, 1996. (Cited in page 36.)

[149] J. Heyd, G. E. Scuseria, and M. Ernzerhof. Hybrid functionals based on a screened Coulomb potential. *The Journal of Chemical Physics*, 118(18):8207–8215, 2003. (Cited in page 36.)

[150] S. Grimme. Semiempirical GGA-type density functional constructed with a long-range dispersion correction. *Journal of Computational Chemistry*, 27(15):1787–1799, 2006. (Cited in page 37.)

[151] S. Grimme, J. Antony, S. Ehrlich, and H.Krieg. A consistent and accurate ab initio parametrization of density functional dispersion correction DFT-D for the 94 elements H-Pu. *The Journal of Chemical Physics*, 132(15):154104, 2010. (Cited in pages 37 and 38.)

[152] S. Grimme, S. Ehrlich, and L. Goerigk. Effect of the damping function in dispersion corrected density functional theory. *Journal of Computational Chemistry*, 32(7):1456–1465, 2011. (Cited in pages 37 and 38.)

[153] D. G. A. Smith, L. A. Burns, K. Patkowski, and C. D. Sherrill. Revised damping parameters for the D3 dispersion correction to Density Functional Theory. *The Journal of Physical Chemistry Letters*, 7(12):2197–2203, 2016. (Cited in pages 37 and 38.)

[154] C. Kittel. *Introduction to solid state physics*. Wiley, Hoboken, New Jersey, 2005. (Cited in pages 39, 41, and 42.)

[155] N. W. Ashcroft and N. D. Mermin. *Solid state physics*. New York Holt, New York, 1976. (Cited in pages 41 and 42.)

[156] F. Z. Bloch. Über die Quantenmechanik der Elektronen in Kristallgittern. *Zeitschrift für Physik*, 52(7-8):555–600, 1929. (Cited in page 42.)

[157] G. H. Wannier. The structure of electronic excitation levels in insulating crystals. *Physical Review*, 52:191–197, 1937. (Cited in page 42.)

[158] J. Ihm, A. Zunger, and M. L. Cohen. Momentum-space formalism for the total energy of solids. *Journal of Physics C: Solid State Physics*, 13(16):3095, 1980. (Cited in page 42.)

[159] J. Ihm. Total energy calculations in solid state physics. *Reports on Progress in Physics*, 51(1):105, 1988. (Cited in page 42.)

[160] H. J. Monkhorst and J. D. Pack. Special points for brillouin-zone integrations. *Physical Review B*, 13:5188–5192, 1976. (Cited in page 44.)

[161] J. Rath and A. J Freeman. Generalized magnetic susceptibilities in metals: Application of the analytic tetrahedron linear energy method to Sc. *Physical Review B*, 11:2109–2117, 1975. (Cited in page 44.)

[162] R. A. Evarestov and V. P. Smirnov. Modification of the Monkhorst-Pack special points meshes in the brillouin zone for Density Functional Theory and Hartree-Fock calculations. *Physical Review B*, 70:233101, 2004. (Cited in page 44.)

[163] D. J. Chadi and M. L. Cohen. Special points in the brillouin zone. *Physical Review B*, 8:5747–5753, 1973. (Cited in page 44.)

[164] J. C. Phillips and L. Kleinman. New Method for Calculating Wave Functions in Crystals and Molecules. *Physical Review*, 116:287–294, 1959. (Cited in page 45.)

[165] J. C. Phillips. Energy-Band Interpolation Scheme Based on a Pseudopotential. *Physical Review*, 112:685–695, 1958. (Cited in page 45.)

[166] E. Fermi. Motion of neutrons in hydrogenous substances. *Ricerca Scientifica*, 7(1):13–52, 1934. (Cited in page 45.)

[167] H. Hellmann. A New Approximation Method in the Problem of Many Electrons. *The Journal of Chemical Physics*, 3(1):61–61, 1935. (Cited in page 45.)

[168] L. Kleinman and J. C. Phillips. Crystal Potential and Energy Bands of Semiconductors. III. Self-Consistent Calculations for Silicon. *Physical Review*, 118:1153–1167, 1960. (Cited in page 45.)

[169] D. Vanderbilt. Soft self-consistent pseudopotentials in a generalized eigenvalue formalism. *Physical Review B*, 41:7892–7895, 1990. (Cited in page 45.)

[170] K. Schwarz, P. Blaha, and G. K. H. Madsen. Electronic structure calculations of solids using the WIEN2k package for material sciences. *Computer Physics Communications*, 147(1):71–76, 2002. (Cited in page 46.)

[171] W. J. Hehre, R. Ditchfield, and J. A. Pople. Self-consistent molecular orbital methods. XII. Further extensions of gaussian-type basis sets for use in molecular orbital studies of organic molecules. *The Journal of Chemical Physics*, 56(5):2257–2261, 1972. (Cited in page 46.)

[172] M. D. Newton, W. A. Lathan, W. J. Hehre, and J. A. Pople. Self-consistent molecular orbital methods. V. Ab initio calculation of equilibrium geometries and quadratic force constants. *The Journal of Chemical Physics*, 52(8):4064–4072, 1970. (Cited in page 46.)

[173] DACAPO. `https://wiki.fysik.dtu.dk/dacapo`, Last accessed 04-09-2018. (Cited in page 46.)

[174] H. Jürgen. Ab-initio simulations of materials using VASP: Density-functional theory and beyond. *Journal of Computational Chemistry*, 29(13):2044–2078, 2008. (Cited in page 46.)

[175] G. Kresse and J. Furthmüller. Efficiency of ab-initio total energy calculations for metals and semiconductors using a plane-wave basis set. *Computational Materials Science*, 6(1):15–50, 1996. (Cited in page 46.)

[176] G. Kresse and J. Furthmüller. Efficient iterative schemes for ab initio total-energy calculations using a plane-wave basis set. *Physical Review B*, 54:11169–11186, 1996. (Cited in page 46.)

[177] G. Kresse and J. Hafner. Ab initio molecular dynamics for liquid metals. *Physical Review B*, 47:558–561, 1993. (Cited in page 46.)

[178] X. Gonze, B. Amadon, P.-M. Anglade, J.-M. Beuken, F. Bottin, P. Boulanger, F. Bruneval, D. Caliste, R. Caracas, M. Côté, T. Deutsch, L. Genovese, Ph. Ghosez, M. Giantomassi, S. Goedecker, D.R. Hamann, P. Hermet, F. Jollet, G. Jomard, S. Leroux, M. Mancini, S. Mazevet, M.J.T. Oliveira, G. Onida, Y. Pouillon, T. Rangel, G.-M. Rignanese, D. Sangalli, R. Shaltaf, M. Torrent, M.J. Verstraete, G. Zerah, and J.W. Zwanziger. ABINIT: First-principles approach to material and nanosystem properties. *Computer Physics Communications*, 180(12):2582–2615, 2009. (Cited in page 46.)

[179] P.Giannozzi, S. Baroni, N. Bonini, M. Calandra, R. Car, C. Cavazzoni, D. Ceresoli, G. L. Chiarotti, M. Cococcioni, I. Dabo, A. Dal Corso, S. de Gironcoli, S. Fabris, G. Fratesi, R. Gebauer, U. Gerstmann, C. Gougoussis, A. Kokalj, M. Lazzeri, L. Martin-Samos, N. Marzari, F. Mauri, R. Mazzarello, S. Paolini, A. Pasquarello, L. Paulatto, C. Sbraccia, S. Scandolo, G. Sclauzero, A. P. Seitsonen, A. Smogunov, P. Umari, and R. M. Wentzcovitch. Quantum espresso:

a modular and open-source software project for quantum simulations of materials. *Journal of Physics: Condensed Matter*, 21(39):395502, 2009. (Cited in page 46.)

[180] J. M. Soler, E. Artacho, J. D. Gale, A. García, J. Junquera, P. Ordejón, and D. Sánchez-Portal. The SIESTA method for ab initio order- n materials simulation. *Journal of Physics: Condensed Matter*, 14(11):2745, 2002. (Cited in page 46.)

[181] ASE. `https://wiki.fysik.dtu.dk/ase/`, Last accessed 04-09-2018. (Cited in page 47.)

[182] M. J. López, I. Cabria, and J. A. Alonso. Simulated porosity and electronic structure of nanoporous carbons. *The Journal of Chemical Physics*, 135(10):104706, 2011. (Cited in page 51.)

[183] I. López-Corral, E. Germán, A. Juan, M.A. Volpe, and G.P. Brizuela. DFT Study of Hydrogen Adsorption on Palladium Decorated Graphene. *The Journal of Physical Chemistry C*, 115(10):4315–4323, 2011. (Cited in page 51.)

[184] I. López-Corral, E. Germán, M.A. Volpe, G.P. Brizuela, and A. Juan. Tight-binding study of hydrogen adsorption on palladium decorated graphene and carbon nanotubes. *International Journal of Hydrogen Energy*, 35(6):2377 – 2384, 2010. (Cited in page 51.)

[185] V. A. Borodin, T. T. Vehviläinen, M. G. Ganchenkova, and R. M. Nieminen. Hydrogen transport on graphene: Competition of mobility and desorption. *Physical Review B*, 84:075486, 2011. (Cited in page 107.)

[186] J. A. Alonso and M. J. López. Interaction of hydrogen with graphitic surfaces, clean and doped with metal clusters. In W. Andreoni and S. Yip, editors, *Handbook of Materials Modeling: Applications: Current and Emerging Materials*, pages 1–22. Springer International Publishing, Cham, 2018. (Cited in page 107.)

If you want different results than what you are getting, you have to try different approaches.

Albert Einstein.